Study of Co-optimization Stochastic SuperOPF Application in the CAISO System

Final Report

Prepared for

Prepared by
Bigwood Systems, Inc.
Ithaca, NY

September 10, 2015

Executive Summary

Objectives

The focus of this project is to study the impact of co-optimization in improving key challenges in the CAISO system. The work will include evaluations of co-optimization at CAISO using the commercial-grade SuperOPF tool for the following applications.

- Co-optimize the objective function and the updated worst scenario for voltage stability.
- Co-optimize the objective function, operational reserve and the renewable energies. In addition, the ramp rate of renewable energy should be included.
- Handling of ramp constraints of generation.
- Handling of constraints needed for LMP calculations and outputs needed for the power market.

The current commercial-grade SuperOPF package is equipped with a commercial power flow solver and a homotopy-based interior point based solver and supports various industrial-grade static power system models such as 13,000-bus EMS models. Standard data formats are supported including the Common Information Model (CIM) and Siemens's PSS/E data formats. The current commercial-grade SuperOPF-VS package is equipped with a commercial voltage stability solver capable of handling the voltage stability constraint of a large set of contingencies, such as, 2,500 contingencies. Both SuperOPF and SuperOPF-VS have been extensively evaluated on practical PJM models and California ISO models with promising results.

The current release of SuperOPF is comprehensive in its modeling capability and able to handle the following components.

1. Generators that are modeled as active and reactive power sources which also provide voltage control. The MVAR output of each on-line generator is adjusted during power flow solutions in order to control the voltage of the local bus (the bus where the generator is connected) or a remote bus. The generator's MW output has fixed limit. And the generator's MVAR output is limited by fixed limits defined by the so-called capability curves.
2. Loads that are modeled as constant power (P-Q), constant current (I), constant impedance (Z), or any linear combination of them. The tool must also accept nonlinear load models that are expressed as nonlinear functions of voltage.
3. Control Devices: The following control devices are modeled: (i) Switchable shunts and static VAR compensators, (ii) ULTC Transformers, (iii) ULTC phase shifters, and (iv) Static tap changers and phase shifters.

4. DC Transmission Lines

Deliverables

This project will have the following deliverables:

1. SuperOPF version which can co-optimize the objective function and the updated worst scenario for voltage stability (requested by CAISO).
2. Demonstrate Deliverable 1 on CAISO system data.
3. SuperOPF version which can co-optimize the objective function, operational reserve and the renewable energies. In addition, the ramp rate of renewable energy should be included.
4. Demonstrate Deliverable 3 on CAISO system data.
5. Commercial-grade Co-optimization SuperOPF software equipped with the ramp constraints of generations (requested by CAISO).
6. Demonstrate the Super-OPF with ramping constraints, deliverable 5 on CAISO system data.
7. Super-OPF software which can handle constraints needed for LMP calculations and outputs needed for the power market (requested by CAISO).
8. Demonstrate Deliverable 7 on CAISO system data.
9. Regular meetings with CAISO for progress report (including 2 face-to-face meetings).
10. Compile feedback reports from CAISO.
11. Users' manual for the commercial-grade core Co-optimization SuperOPF software.
12. Design manual for the commercial-grade core Co-optimization SuperOPF software.
13. A final report detailing the relevant results developed in this phase.

Project Status

Date	Scheduled Deliverable	Status
July 1– August 31, 2014	Deliverables 1 & 2	Delivered as scheduled.
September 1 – October 31, 2014	Deliverables 3 & 4	Delivered as scheduled.
November 15, 2014	Deliverable 9, part 1	Delivered as scheduled.

November 1 – December 31, 2014	Deliverables 5 & 6	Delivered as scheduled.
January 1 – February 15, 2015	Deliverables 7 & 8	Delivered as scheduled.
March 15, 2015	Deliverable 9, part 2	Delivered as scheduled.
February 16 – March 30, 2015 **September 10, 2015**	Deliverables 10, 11, 12 & 13 Revised Final Report (13)	Delivered as scheduled. Delivered
July 6, 2015	Supplemental Report	Delivered

Note: CAISO legal department was not able to approve disclosure of power market data even in a highly "sanitized" form for evaluation. Since a good market case could not be provided, BSI gathered publically available sources of market data in the state of California and applied this data to a recent on-line CAISO power flow case to create an OPF case with representative data. Input for this case was based on the date request we compiled by working with CAISO to produce detailed requirements. A new set of simulations was carried out and a supplementary report regarding the new simulation results was submitted.

Table of Contents

List of Figures

List of Tables

1. Introduction

The optimal power flow (OPF) is relevant in power system operations, scheduling, and planning. The main objective of the OPF problem is to determine the optimal operation of an electric power system while satisfying technical and economic constraints. OPF is a cost-effective way to forecast snapshots of locational marginal prices (LMPs) under various conditions of load and generation patterns and generator bidding strategies. With the structural deregulation of electric power systems and prevalence of power markets, OPF is becoming a basic tool for planning and operations of the power network.

A commercial OPF should have the capability to adjust control variables for both real and reactive power, including SC, ULTC and phase shifters. Moreover, a commercial OPF package should be comprehensive in its modeling capability and be able to handle the following components:

- Generators: modeled as active and reactive power sources which also provide voltage control. The MVAR output of each on-line generator is adjusted during power flow solutions in order to control the voltage of the local bus (the bus where the generator is connected to) or a remote bus. The generator's MW output has fixed limit. And the generator's MVAR output is limited by fixed limits the so-called capability curves.
- Loads: modeled as constant power (P-Q), constant current (I), or constant impedance (Z), or any linear combination of them. The tool can also accept nonlinear load models as long as they are expressed as nonlinear functions of voltage.
- Control devices: The following control devices are modeled: (i) switchable shunts and static VAR compensators, (ii) ULTC Transformers, (iii) ULTC phase shifters, and (iv) static tap changer and phase shifters.
- DC transmission lines.
- Interchange schedules.

For many utilities around the world, there has been considerable pressure to increase power flows over existing transmission corridors, partly due to economic incentives (a trend towards deregulation and competition) and partly due to practical difficulties in obtaining authorization to build power plants and transmission lines (environmental concerns). Therefore, it is crucial for the OPF solutions to be not only economic and but also secure. A power system is secure if it is able to maintain a normal and stable operation when encountering contingencies, which are discrete events such as failure of devices (e.g., lines, generators, shunts, etc.). The "N-1 security" contingency standard has been established by the North American Electric Reliability Corporation (NERC) and is required to be complied by utilities.

In the meantime, the drive for cleaner sources of energy has led to the proliferation of renewable energy sources, such as wind and solar energy, in today's power systems. However, most of

these renewable energy sources are inherently stochastic and as a result introduce more uncertainty into the power system. Forecasters, which are constructed based on different disciplines, are used by power utilities to predict most probable renewable energy outputs in the planning horizon. These forecasters are never perfect due to the inherent variability of the renewable energy. On the other hand, power system operations need to be planned to accommodate various possible scenarios, such that the power system can still operate securely and economically should any considered scenario occur within the planning horizon. Therefore, power system computation and analysis, such as voltage stability analysis (VSA), dynamic stability analysis (DSA) and optimal power flow (OPF) computation, involving probabilistic scenarios become more and more common because of the increasing penetration of renewable energies into the power grid.

The stochastic contingency-constrained and renewable energy-constrained AC optimal power flow (OPF) formulation behind the SuperOPF makes it applicable to a variety of problems arising in power system planning and operations under deregulation and the power market. The focus of this project is to study the impact of co-optimization in improving key challenges in the CAISO system. The work will include evaluations of co-optimization at CAISO using the commercial-grade SuperOPF tool for the following applications.

- Co-optimize the objective function and the updated worst scenario for voltage stability.
- Co-optimize the objective function, operational reserve and the renewable energies. In addition, the ramp rate of renewable energy should be included.
- Handling of ramp constraints of generation.
- Handling of constraints needed for LMP calculations and outputs needed for the power market.

This project will have the following key deliverables:

1. SuperOPF version which can co-optimize the objective function and the updated worst scenario for voltage stability (requested by CAISO).
2. Demonstrate Deliverable 1 on CAISO system data.
3. SuperOPF version which can co-optimize the objective function, operational reserve and the renewable energies. In addition, the ramp rate of renewable energy should be included.
4. Demonstrate Deliverable 3 on CAISO system data.
5. Commercial-grade Co-optimization SuperOPF software equipped with the ramp constraints of generations (requested by CAISO).
6. Demonstrate the Super-OPF with ramping constraints, deliverable 5 on CAISO system data.

7. Super-OPF software which can handle constraints needed for LMP calculations and outputs needed for the power market (requested by CAISO).
8. Demonstrate Deliverable 7 on CAISO system data.
9. Regular meetings with CAISO for progress report (including 2 face-to-face meetings).
10. Compile feedback reports from CAISO.
11. Users' manual for the commercial-grade core Co-optimization SuperOPF software.
12. Design manual for the commercial-grade core Co-optimization SuperOPF software.
13. A final report detailing the relevant results developed in this phase.

2. Co-optimized OPF Analysis

Existing solvers and programs for optimal power flow (OPF) computation are mostly focused on achieving an optimal solution to the study objective for a single scenario, namely, the base case system, without considering any uncertainties that might arise during the planning horizon. In fact, with more and more penetrations of renewable energy, whose output is stochastic in nature, in the power networks and requests for regulatory compliance (such as compliance to FERC regulations), these uncertainties cannot be neglected any longer. It is crucial for the OPF solutions to not only be economic for the base-case system, but also maintain economic and secure for the whole planning horizon even if one or more uncertain scenarios (with the largest probabilities) occur. This motivates the development of the multi-scenario SuperOPF co-optimization solver and program, considering a comprehensive set of physical and operation constraints, to address the need of computing OPF solutions involving uncertain scenarios for power networks nowadays that are operated in a more and more dynamic environment.

2.1 Problem Formulations

Mathematically, OPF is modeled as a nonlinear programming (NLP) problem of the generic form (2-1),

$$\begin{array}{ll} min_x & f(x) \\ s.t & h(x) = 0 \\ & g(x) \le 0 \\ & x^l \le x \le x^u \end{array} \tag{2-1}$$

which usually minimizes the total generation dispatch cost, transmission loss, or their combination subject to a set of equality and inequality constraints. From a computational viewpoint, the OPF problem is a large-scale non-convex NLP problem, in which both the objective function and constraint functions can be nonlinear.

More specifically, the conventional OPF formulation is presented with the following notations:

- n_B: the number of buses in the system;
- n_G: the number of generators in the system;
- L: the set of lines or branches in the system;
- n_T: the number of tap-changing transformers in the system;
- n_P: the number of phase-shifting transformers in the system; and

- n_S: the number of switchable shunt devices in the system.

The overall formulation for an OPF problem can be stated as the following nonlinear optimization problem (2-2):

$$\begin{aligned} min \quad & f(V,\theta,t,\phi,b,P^G,Q^G) \\ s.t. \quad & P_i(V,\theta,t,\phi,b)+P_i^L-P_i^G=0, i=1,\cdots,n_B \\ & Q_i(V,\theta,t,\phi,b)+Q_i^L-Q_i^G=0, i=1,\cdots,n_B \\ & S_{ij}(V,\theta,t,\phi,b)\le(1+\lambda)\bar{S}_{ij},(i,j)\in L \\ & S_{ji}(V,\theta,t,\phi,b)\le(1+\lambda)\bar{S}_{ij},(i,j)\in L \\ & \underline{V_i}\le V_i\le\bar{V_i}, i=1,\cdots,n_B \\ & \underline{t_i}\le t_i\le\bar{t_i}, i=1,\cdots,n_T \\ & \underline{\phi_i}\le\phi_i\le\bar{\phi}_i, i=1,\cdots,n_P \\ & \underline{b_i}\le b_i\le\bar{b_i}, i=1,\cdots,n_S \\ & \underline{P_j^G}\le P_j^G\le\bar{P}_j^G, j=1,\cdots,n_G \\ & \underline{Q_j^G}\le Q_j^G\le\bar{Q}_j^G, j=1,\cdots,n_G \end{aligned} \tag{2-2}$$

In this formulation,

- $V=\left[V_1,\cdots,V_{n_B}\right]^T$ is the vector of bus voltage amplitudes with lower bounds $\underline{V}$ and upper bounds $\bar{V}$,
- $\theta=\left[\theta_1,\cdots,\theta_{n_B}\right]^T$ the vector of bus voltage phase angles with lower bounds $\underline{\theta}$ and upper bounds $\bar{\theta}$,
- $t=\left[t_1,\cdots,t_{n_T}\right]^T$ is the vector of tap positions for tap-changing transformers with lower bounds $\underline{t}$ and upper bounds $\bar{t}$, and
- $\phi=\left[\phi_1,\cdots,\phi_{n_P}\right]^T$ the vector positions for phase-shifting transformers with lower bounds $\underline{\phi}$ and upper bounds $\bar{\phi}$,
- $b=\left[b_1,\cdots,b_{n_S}\right]^T$ is the vector of positions for switchable shunts with lower bounds $\underline{b}$ and upper bounds $\bar{b}$, and
- $P^G=\left[P_{g1},\cdots,P_{gn_G}\right]$ is the vector of real power outputs of generators with lower bounds $\underline{P^G}$ and upper bounds $\bar{P}^G$ and
- $Q^G=\left[Q_{g1},\cdots,Q_{gn_G}\right]$ is the vector of reactive power outputs of generators with lower bounds $\underline{Q^G}$ and upper bounds $\bar{Q}^G$.
- $P_i(V,\theta,t,\phi,b)$ and $Q_i(V,\theta,t,\phi,b)$ are the real and reactive power injections at the i-th bus in the system, respectively.

- $S_{ij}(V,\theta,t,\phi,b)$ and $S_{ji}(V,\theta,t,\phi,b)$ are the power flows transmitted through the branch connecting i-th and j-th buses, measured at the from-end (i-th bus) and the to-end (j-th) bus, respectively. $\bar{S}$ is vector of thermal limit imposed on the transmission lines (branches) in the system.

The central task for the multi-scenario SuperOPF (SuperOPF-MS) solver is to solve the OPF problem that will results the best-expected objective (such as the minimum system total power losses or generation costs) spanning the planning horizon. Therefore, the co-optimization that needs to be solved in order to get the desired OPF solution can be modeled as the optimization problem (2-3).

$$
\begin{aligned}
min \quad & F(x) \\
s.t. \quad & P_i(V_0,\theta_0,t_0,s_0,b_0) + P_D^i - P_G^i = 0 \\
& Q_i(V_0,\theta_0,t_0,s_0,b_0) + Q_D^i - Q_{G0}^i = 0 \\
& \underline{S_{ij}} \le S_{ij}(V_0,\theta_0,t_0,s_0,b_0) \le \overline{S_{ij}} \\
& \left(\underline{V},\underline{\theta},\underline{t},\underline{s},\underline{b},\underline{Q_G}\right) \le (V_0,\theta_0,t_0,s_0,b_0,Q_{G0}) \le \left(\overline{V},\overline{\theta},\overline{t},\overline{s},\overline{b},\overline{Q_G}\right) \\
& \cdots\cdots\cdots \\
& P_i(V_k,\theta_k,t_k,s_k,b_k) + P_D^i - P_G^i = 0 \\
& Q_i(V_k,\theta_k,t_k,s_k,b_k) + Q_D^i - Q_{Gk}^i = 0 \\
& \underline{S_{ij}} \le S_{ij}(V_k,\theta_k,t_k,s_k,b_k) \le \overline{S_{ij}} \\
& \left(\underline{V},\underline{\theta},\underline{t},\underline{s},\underline{b},\underline{Q_G}\right) \le (V_k,\theta_k,t_k,s_k,b_k,Q_{Gk}) \le \left(\overline{V},\overline{\theta},\overline{t},\overline{s},\overline{b},\overline{Q_G}\right) \\
& \underline{P_G} \le P_G \le \overline{P_G}
\end{aligned}
\tag{2-3}
$$

where

- F(x): the co-optimization objective function;
- $x = (P_G, V_0, \theta_0, t_0, s_0, b_0, Q_{G0}, \cdots, V_k, \theta_k, t_k, s_k, b_k, Q_{Gk})$: the vector of optimization variables;
- V, θ: bus voltage magnitudes and phase angles;
- t, s: transformers tap ratios, phase shifting angles, respectively;
- b: switchable shunt devices;
- P_G: real power generations (same for all scenarios);
- Q_G: reactive power generations;
- $(V_0, \theta_0, t_0, s_0, b_0, Q_{G0})$: base-case variables (excluding P_G);
- $(V_k, \theta_k, t_k, s_k, b_k, Q_{Gk})$: k-th scenario variables (excluding P_G);
- S_{ij}: line flow for the branch connecting i-th and j-th buses;

- $\underline{a}$ and $\overline{a}$: the lower and upper bounds for the variable a.

It can be seen from the problem model (2-3) that the optimization problem that needs to be solved is a very complicated nonlinear optimization problem. The problem size (the number of optimization variables and the number of equality and inequality constraints) will increase linearly as the number of contingent scenarios increases.

It is possible that a solution to the co-optimized OPF problem (2-3) is not achievable, especially for scenarios with

- Severe contingencies, each of which considers dropping of a single or multiple important devices (transmission lines, generators, etc.) of the power network;
- Large variations of renewable energy productions;
- The power network is undergoing a heavy loading condition; and
- Combinations of the above conditions.

To accommodate these situations, extra corrective/preventive controls, which are prepared for the post-contingency system, are required and need to be involved in the problem formulation. One type of such corrective/preventive controls is the up-spinning reserve provided by generators. When these operational generation reserves are considered, the OPF problem to be solved can be updated to the corresponding reserve-constrained format (2-4).

$$
\begin{aligned}
min \quad & F(x) + \sum r_i(R_{Gk}^i) \\
s.t. \quad & P_i(V_0, \theta_0, t_0, s_0, b_0) + P_D^i - P_G^i = 0 \\
& Q_i(V_0, \theta_0, t_0, s_0, b_0) + Q_D^i - Q_{G0}^i = 0 \\
& \underline{S_{ij}} \le S_{ij}(V_0, \theta_0, t_0, s_0, b_0) \le \overline{S_{ij}} \\
& \left(\underline{V}, \underline{\theta}, \underline{t}, \underline{s}, \underline{b}, \underline{Q_G}\right) \le (V_0, \theta_0, t_0, s_0, b_0, Q_{G0}) \le \left(\overline{V}, \overline{\theta}, \overline{t}, \overline{s}, \overline{b}, \overline{Q_G}\right) \\
& \cdots \cdots \cdots \\
& P_i(V_k, \theta_k, t_k, s_k, b_k) + P_D^i - P_G^i - a_{ik} R_{Gk}^i = 0 \\
& Q_i(V_k, \theta_k, t_k, s_k, b_k) + Q_D^i - Q_{Gk}^i = 0 \\
& \underline{S_{ij}} \le S_{ij}(V_k, \theta_k, t_k, s_k, b_k) \le \overline{S_{ij}} \\
& \left(\underline{V}, \underline{\theta}, \underline{t}, \underline{s}, \underline{b}, \underline{Q_G}\right) \le (V_k, \theta_k, t_k, s_k, b_k, Q_{Gk}) \le \left(\overline{V}, \overline{\theta}, \overline{t}, \overline{s}, \overline{b}, \overline{Q_G}\right) \\
& \underline{P_G} \le P_G \le \overline{P_G} \\
& P_G + a_k R_{Gk} \le \overline{P_G} \\
& 0 \le R_{Gk} \le \overline{R_{Gk}}
\end{aligned}
\tag{2-4}
$$

where, compared to the formulation (2-3), the newly introduced variables are

- a_{ik}: the status (0 or 1 binary constant value) for the availability of reserve of i-th generator for k-th contingency;
- R_{Gk}^{i}: the up-spinning reserve provided by i-th generator;
- $r_i(R_{Gk}^{i})$: the auxiliary term in the objective function for the reserve offered by i-th generator.

For online applications, the scheduling horizon might be minutes, instead of hours for off-line planning. During this short scheduling horizon, because of the physical limitations imposed on them, generators usually cannot exercise the full range of their generation capability. Instead, the ramping capability of generators needs to be considered in computation. As a result, additional ramping constraints need to be introduced in the OPF formulation, as described by the formulation (2-5). This formulation is represented as a single-period co-optimization; therefore, inter-period ramping constraints are not covered. It needs to be noted that, however, SuperOPF program is also capable of handling inter-period ramping constraints for multi-time-period co-optimization.

$$
\begin{aligned}
min \quad & F(x) + \sum r_i(R_{Gk}^{i}) \\
s.t. \quad & P_i(V_0, \theta_0, t_0, s_0, b_0) + P_D^i - P_G^i = 0 \\
& Q_i(V_0, \theta_0, t_0, s_0, b_0) + Q_D^i - Q_{G0}^i = 0 \\
& \underline{S_{ij}} \le S_{ij}(V_0, \theta_0, t_0, s_0, b_0) \le \overline{S_{ij}} \\
& \left(\underline{V}, \underline{\theta}, \underline{t}, \underline{s}, \underline{b}, \underline{Q_G}\right) \le (V_0, \theta_0, t_0, s_0, b_0, Q_{G0}) \le \left(\overline{V}, \overline{\theta}, \overline{t}, \overline{s}, \overline{b}, \overline{Q_G}\right) \\
& \cdots \cdots \cdots \\
& P_i(V_k, \theta_k, t_k, s_k, b_k) + P_D^i - P_G^i - a_{ik} R_{Gk}^i = 0 \\
& Q_i(V_k, \theta_k, t_k, s_k, b_k) + Q_D^i - Q_{Gk}^i = 0 \\
& \underline{S_{ij}} \le S_{ij}(V_k, \theta_k, t_k, s_k, b_k) \le \overline{S_{ij}} \\
& \left(\underline{V}, \underline{\theta}, \underline{t}, \underline{s}, \underline{b}, \underline{Q_G}\right) \le (V_k, \theta_k, t_k, s_k, b_k, Q_{Gk}) \le \left(\overline{V}, \overline{\theta}, \overline{t}, \overline{s}, \overline{b}, \overline{Q_G}\right) \\
& \max(\underline{P_G}, P_{G0} - DR) \le P_G \le \min(P_{G0} + UR, \overline{P_G}) \\
& P_G + a_k R_{Gk} \le \min(P_{G0} + UR, \overline{P_G}) \\
& 0 \le R_{Gk} \le \overline{R_{Gk}}
\end{aligned}
\tag{2-5}
$$

where, compared to the formulation (2-4), the newly introduced parameters are

- DR and DU: the ramping-down and ramping-up capabilities of the generators in the system.

3. SuperOPF Solution Engine

3.1 Introduction

The optimal power flow (OPF) is relevant in power system operations, scheduling, and planning. The main objective of the OPF problem is to determine the optimal steady-state operation of an electric power system while satisfying technical and economic constraints. With the structural deregulation of electric power systems, OPF is becoming a basic tool in the power market. Existing solvers and programs for OPF computation are mostly focused on achieving an optimal solution to the study objective for the base case system, without any security considerations. However, it is crucial for the OPF solutions being not only economic and but also secure. A widely accepted system security concept is the so-called "N-1 security", which follows the "N-1" contingency standard established by the North American Electric Reliability Corporation (NERC). Essentially, an electric power system is required to be operated in a way such that it could survive the occurrence of any single credible contingency where any single component in the system goes offline suddenly.

In order for them to be applicable for current fast changing and increasingly stressed power system operations and for the deregulated power markets, practical OPF solvers must meet the following requirements. Firstly, the OPF solvers are required to have a comprehensive modeling capability. Different utilities and venders may use different data models for recording and snapshotting the operating conditions of their systems. Among existing models, the PSS/E model should be the most widely used in the power industry. Aiming for enhanced exchangeability, recently introduced CIM-compliance model is becoming popular. A practical OPF solver should be comprehensive and flexible enough to support these data models. Secondly, the OPF solvers need to be fast. In order for the OPF solvers to be suitable for the fast changing power system operations, it is a natural requirement that the desired optimal power flow solutions can be achieved quickly. Thirdly, the OPF solvers are required to be robust. The OPF problem is a large-scale, constrained, nonlinear optimization problem. The underlying nonlinearity of the OPF problem renders its feasible region, that is, the set of all operating conditions where all constraints are satisfied and the optimal solution is contained, to be very complicated. The robustness requirement suggests that the OPF solver be able to find the optimal solution consistently when an OPF solution exists. Fourthly, the OPF solvers need also to be versatile and flexible, that is, they can be used to handle different practical problems interested in the power industry. Specifically, they can optimize real-power related problems, such as the production cost problem, as well as reactive-power related problems, such as the voltage problem and the transmission loss problem. Fifthly, the OPF solvers can handle contingencies. A power system needs to be operated not only optimally, but also securely to survive the occurrence of potential contingencies. Therefore, it is required that the solvers are able to handle not only the static security constraints, but also the dynamic security constraints under a large set of contingencies.

Finally, the OPF solvers need also to embrace stability constraints. Besides the security constraints mentioned above, the OPF solution obtained must satisfy the voltage stability, transient stability and small-signal stability under a large set of contingencies.

To this end, we have developed a commercial-grade OPF package that meets the first through fifth requirements, and potentially meets the final stability requirement. More specifically, we have developed a four-stage, homotopy-enhanced OPF solution engine to serve as the kernel to our package.

3.2 SuperOPF Solution Engine

Mathematically, OPF is modeled as a nonlinear programming (NLP) problem, which usually minimizes the total generation dispatch cost, transmission loss, or their combination subject to a set of equality and inequality constraints. From a computational viewpoint, the OPF problem is a large-scale non-convex NLP problem, in which both the objective function and constraint functions can be nonlinear.

Referring to the problem formulation (2-2), it is observed that the number of thermal limits is almost twice the number of the branches in the system and that the thermal limits are the only source of nonlinear inequality constraints. Simultaneously handling this large number of nonlinear inequality constraints can cause convergence difficulties in finding an OPF solution.

Many current OPF methods treat all of the thermal limits at the same time. In fact, most of the thermal constraints are *inactive* throughout the computational procedure. Considering inactive thermal constraints unnecessarily enlarges the problem size and makes the computation of an OPF solution hard to converge or even diverge. To overcome these difficulties, two schemes are developed and incorporated into the proposed four-stage method. The first scheme is the homotopy-enhanced OPF method that starts from a simple OPF problem without considering the thermal limits and then gradually solves a sequence of homotopied OPF problems until it solves the original problem that is the hard problem. The second scheme is the active-set technique that treats the active constraints while the inactive thermal constraints are not included into the current computation.

A multi-stage, multi-level OPF method has been developed and implemented in the SuperOPF program. As illustrated in Figure 3-1, this method consists of the following four stages:

- Stage 1: Constraint analysis for improving convergence and avoiding infeasibility.
- Stage 2: Solving the OPF problem without thermal constraints.
- Stage 3: Solving the OPF problem using the proposed homotopy-enhanced solver and the active set technique.

- Stage 4: Determine values for discrete control variables.

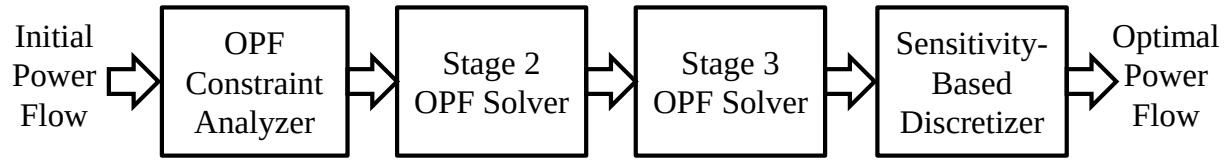

Figure 3-1: The four-stage SuperOPF engine

3.2.1 Stage I: Constraint Analysis

Practical large systems are vulnerable to data or parameter errors, which may result in infeasible OPF problems and cause the OPF solver diverges. On the other hand, using a feasible point as the initial point can usually improve the convergence property of the OPF solver. Therefore, it is desirable to have a dedicated and automatic feasibility analyzer to correct infeasible configurations and provide a feasible initial point for the OPF solver. To this end, the first stage of the SuperOPF solver realizes the procedure of feasibility analysis of the constraints of the OPF problem (3-1).

Two types of data errors are illustrated here, which have been found in the model data of the large-scale power systems involved in our numerical simulation.

1) Improper generation upper bounds

The Issue: The upper generation bound is larger than the thermal limit of Line 1 or Line 2, as shown in the following figure. For this thermal limit constraint, the upper bound of generator 1 is greater than the thermal limit of line 1 so that a continual back-and-forth adjustment of real power generation at generator 1 can occur. Hence, it may slow down the optimization procedure or it can lead to a divergence.

Correction: Lower the upper bound of generator 1.

Effects: 1) Such corrections result in the same OPF problem with tightened generation bounds within an allowable range; 2) Such corrections can improve the convergence of the OPF computation.

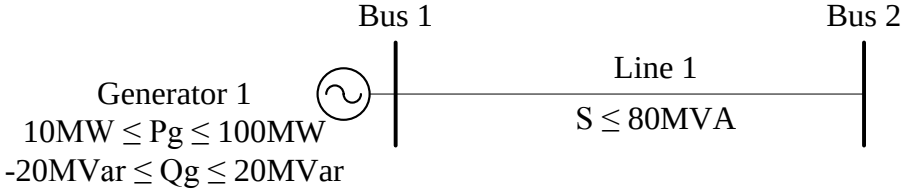

Figure 3-2: Illustration of improper generation bounds

2) Infeasible generation/thermal limits

Issue: Referring to Figure 3-3, the lower generation limit is larger than the thermal limit of Line 1 or Line 2 so that thermal violation *always* occurs at Line 2 for *any* allowable output from the generator.

Correction: Lower the generation lower bound for Generator 1 or increase the thermal limit imposed on Line 2.

Effects: Such correction restores the feasibility of the OPF computation.

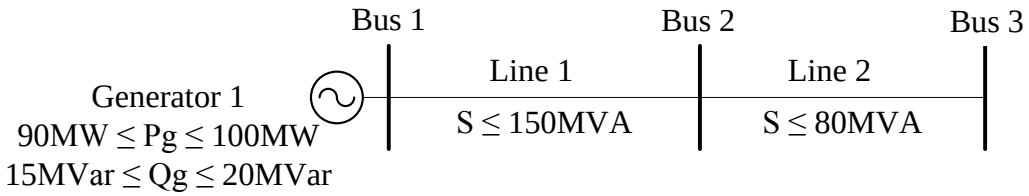

Figure 3-3: Illustration of infeasible generation bounds or thermal limits

The goal of the feasibility analyzer is twofold. For a feasible problem, the feasibility analyzer will find a feasible solution to the problem first, which will be used as the initial point for the full OPF problem. For an infeasible OPF problem, the feasibility analyzer will figure out why the OPF problem is infeasible and what is the minimum effort (constraint relaxation) to restore feasibility of the problem.

In order to figure out whether the OPF problem is feasible or not, an energy-minimizing problem is first solved. Using the following general formulation (3-1),

$$\begin{aligned} min_{x=(x_s,x_c)} \quad & f(x_s, x_c) \\ s.t \quad & h(x) = 0 \\ & g(x) \leq 0 \\ & x^l \leq x \leq x^u \end{aligned} \tag{3-1}$$

the original nonlinear program of OPF can be transformed to the energy minimization problem:

$$\begin{array}{ll} min & f(x) \\ s.t. & h(x)=0 \\ & g(x)\le 0 \\ & \underline{x}\le x\le \overline{x} \end{array} \Rightarrow \min_{x,s} E(x,s)=\left\|\begin{pmatrix} h(x) \\ g(x)-s_g^2 \\ x-\bar{x}+\bar{s}^2 \\ x-\underline{x}-\underline{s}^2 \end{pmatrix}\right\|^2 \tag{3-2}$$

where, $x=\left(V,\theta,t,\phi,b,P_g,Q_g\right)^T$ is the vector of optimization variables, $s=\left(s_g,\ \bar{s},\underline{s}\right)^T$ is the vector of slack variables for equality and inequality constraint, and $E(x,s)$ is the energy function to be minimized. Obviously, if there is a solution to (3-2) of energy being 0, then the OPF problem (3-1) is feasible and a feasible point is found; otherwise, the OPF problem (3-1) is infeasible.

3.2.2 Stage 2: OPF without thermal constraints

Thermal limit constraints are the source of nonlinear inequality constraints in the OPF problem (3-1) and are the most complicated nonlinear constraint in (3-1). To solve the OPF problem (3-1), other OPF methods usually consider all thermal limits at the same time. In fact, most of the thermal constraints are inactive throughout the computation; therefore, these inactive constraints do not contribute to the OPF problem (3-1). Involving inactive thermal limit constraints, it not only unnecessarily enlarges the problem complexity, but also more importantly makes the computation hard to converge or even diverge.

To take advantage of this property of the OPF problem, the SuperOPF process of the present invention first solves an OPF problem without considering thermal limit constraints. The OPF problem without thermal limit constraints is of the form (3-3). Compared to (2-1), the problem size of (3-3) is significantly reduced and the OPF computation can converge fast and more robustly because nonlinear inequality constraints, that is, thermal limit constraints are not involved in the computation.

$$\begin{array}{ll} min & f(V,\theta,t,\phi,b,P^G,Q^G) \\ s.t. & P_i(V,\theta,t,\phi,b)+P_i^L-P_i^G=0, i=1,\cdots,n_B \\ & Q_i(V,\theta,t,\phi,b)+Q_i^L-Q_i^G=0, i=1,\cdots,n_B \\ & \underline{V_i}\le V_i\le \overline{V_i}, i=1,\cdots,n_B \\ & \underline{t_i}\le t_i\le \bar{t}_i, i=1,\cdots,n_T \\ & \underline{\phi_i}\le \phi_i\le \bar{\phi}_i, i=1,\cdots,n_P \\ & \underline{b_i}\le b_i\le \overline{b_i}, i=1,\cdots,n_S \\ & \underline{P_j^G}\le P_j^G\le \bar{P}_j^G, j=1,\cdots,n_G \\ & \underline{Q_j^G}\le Q_j^G\le \bar{Q}_j^G, j=1,\cdots,n_G \end{array} \tag{3-3}$$

In the SuperOPF solver, the feasible point obtained in stage 1 of feasibility analysis is used as the initial point for solving the OPF problem (3-3).

3.2.3 Stage 3: OPF with thermal limits

Usually, only few thermal limits are violated (less than 100 out of 20,000 branches) in the OPF solution without thermal limit constraints that are obtained in stage 2. In stage 3 of the Super-OPF solver, thermal limit constraints are considered in the OPF problem but are handled in a homotopy manner. The OPF problem to be solved in this stage is of the form (3-4).

$$
\begin{aligned}
min \quad & f(V,\theta,t,\phi,b,P^G,Q^G) \\
s.t. \quad & P_i(V,\theta,t,\phi,b)+P_i^L-P_i^G=0, i=1,\cdots,n_B \\
& Q_i(V,\theta,t,\phi,b)+Q_i^L-Q_i^G=0, i=1,\cdots,n_B \\
& S_{ij}(V,\theta,t,\phi,b)\le(1+\lambda)\bar{S}_{ij},(i,j)\in L_\alpha \\
& S_{ji}(V,\theta,t,\phi,b)\le(1+\lambda)\bar{S}_{ij},(i,j)\in L_\alpha \\
& \underline{V_i}\le V_i\le\bar{V_i}, i=1,\cdots,n_B \\
& \underline{t_i}\le t_i\le\bar{t_i}, i=1,\cdots,n_T \\
& \underline{\phi_i}\le\phi_i\le\bar{\phi}_i, i=1,\cdots,n_P \\
& \underline{b_i}\le b_i\le\bar{b_i}, i=1,\cdots,n_S \\
& \underline{P_j^G}\le P_j^G\le\bar{P}_j^G, j=1,\cdots,n_G \\
& \underline{Q_j^G}\le Q_j^G\le\bar{Q}_j^G, j=1,\cdots,n_G
\end{aligned}
\tag{3-4}
$$

In the OPF problem (3-4), only active thermal constraints are involved. Therefore, compared to the OPF problem (3-3) without thermal limit constraint, the problem complexity does not increase much. The homotopy parameter λ is decreased during the homotopy process and if the thermal relaxation factor is decreased to λ=0, the OPF problem (3-4) has been solved. Numerical studies carried out on large power systems, such as the 13183-bus PJM system, showed that only two iterations with λ_1=0.55 and λ_2=0 are usually sufficient for eliminating all thermal violations and reach to an optimal solution to the full OPF problem (2-2).

In the SuperOPF solver, the feasible point obtained in stage 2 of the OPF problem without thermal limit constraints is used as the initial point for the OPF problem (3-4).

3.2.4 Stage 4: determining values for discrete control variables

There are many control devices, such as tap changing and phase shifting transformers and switchable shunt capacitors, in the power system that can only take discrete values selected from a set of allowable values. If the discreteness of these control variables is considered in the OPF formulation, the OPF problem becomes a mixed-integer nonlinear optimization problem (NLP) of the form (3-5).

$$\begin{array}{ll} min_{x,y} & f(x,y) \\ s.t & h(x,y)=0 \\ & g(x,y)\leq 0 \\ & x\in R^n, y\in Z^m \end{array} \tag{3-5}$$

where, $x=(V,\theta,P^G,Q^G)$ is the vector of continuous variables and $y=(t,\phi,b)$ is the vector of discrete variables.

In the SuperOPF solver, an enhanced sensitivity-based method is developed and used for determining values of discrete control variables. A detailed description of this method is presented in the next section.

3.3 Determining Discrete Control Variables

The incorporation of transformer taps and shunt capacitors into OPF problem gives rise to a mixed integer nonlinear programming problem (MINLP), also termed as mixed integer AC-OPF problem (MIOPF). MINOP provides a fairly general and powerful framework to model optimization problems involving both discrete and continuous variables. In this framework, the nonlinear expression better approximates real-world phenomena while its discrete variables offer great flexibility to represent an indivisible quantity or applications involving decision-making. Although MINLP provides great flexibility and accuracy, the task of solving such problems is usually challenging. The computational complexity of MIOPF for obtaining rigorous solution tends to increase exponentially with the number of discrete variables. Hence, MIOPF becomes intractable for large-scale problems [34]. The traditional integer programming methods such as branch-and-bound, cutting-plane are non-polynomial and slow for solving large-scale problems. In fact, it has been shown that a rigorous mixed integer nonlinear programming method would be orders of magnitude slower than the ordinary nonlinear programming methods.

Hence, the task of solving MINOP problems is very challenging. Indeed, the diverse nonlinear behavior in MINOP problems creates great challenging not only in algorithmic developments but also numerical implementations. From a theoretical viewpoint, it is well known that the major difficulty in solving general continuous nonlinear programming problems arises from the non-convexity of objective functions and/or nonlinear constraints. A large variety of algorithms have been proposed for solving MINLP problems. Many of these proposed algorithms basically integrate and extend schemes designed for handling non-convexity arising from nonlinear expressions and the presence of integral variables. Algorithms of this type reported in the literature include Branch and Bound [1, 2], Generalized Benders Decomposition [3], Outer Approxi-

mation [4], Extended Cutting Plane Method [5] and so forth. Details of these proposed algorithms may be found in [6].

Although schemes such as the branching or cutting plane method might alleviate adverse effects due to the presence of discrete variables, these algorithms are still limited by the non-convex nature arising from the inherent nonlinear expression. For instance, the Branch and Bound algorithm creates a sequence of sub-problems from the original MINLP problem and seeks to identify optimal solutions by solving some sub-problems. Its overall efficiency depends heavily on whether good solutions could be identified at an early stage to help its pruning scheme. To identify potential solutions, it will be indispensable to solve some non-convex sub-problems (even without integral variables). Without the aid of other supplemental techniques, the performance of stand-alone, deterministic, local-type algorithms is greatly restricted by such non-convexity. The presence of integral variables further deteriorates the situation since it leads to an explosive increase in the number of solutions. Developing efficient and robust tools for solving MINLP problems continue attracting a lot of attentions of many researchers.

At present, a majority of OPF algorithms treat all control variables as continuous variables during the initial solution process. Once a solution is found, each discrete variable is moved to its nearest discrete setting. This scheme gives acceptable solutions provided the step sizes for the discrete controls are sufficiently small, which is usually the case for transformer taps and phase shifter angles. However, shunt capacitors and reactors with large tank sizes usually have greater impact on the accuracy of this scheme.

Currently, there are two schemes useful after the round-off scheme. One is to execute a conventional power flow solution with all the discrete variables fixed on their steps. The other scheme is to solve the optimization problem again with respect to the remaining continuous variables using the previous continuous solution as the initial point. The former scheme is popular because of its computational efficiency. The latter scheme gives a better solution in the sense of feasibility and optimality at the cost of increased computational efforts. The final solutions obtained by these two schemes are still not guaranteed to be locally optimal because incorrect values for the discrete variables may have been selected.

The purpose of this section is to present an enhanced sensitivity-based method for solving MIOPF problems, that is, to determining values for discrete control variables in OPF problems. The motivation behind this method is that, given the intractability of rigorous methods for MIOPF problems, approximate solution methods that can produce near locally optimal solutions appear to be a reasonable alternative. The use of sensitivity analysis for discrete variables is to take advantage of the continuous approximations of discrete variables for movements away from their discrete steps. One attractive feature of the sensitivity analysis scheme is that it can merge well with existing interior point methods for OPF problems. The enhanced sensitivity based method for determining values of discrete control variables has been implemented in SuperOPF

and has been tested on large-scale power systems. Numerical studies on large power system, such as the PJM 13183-bus system, indicate that the proposed method is promising in dealing with discrete variables for practical large-scale systems.

3.3.1 Problem Formulation

Power system contains discrete variables (transformer tap ratios, phase shifts, switchable shunts). Therefore, an OPF problem can be modeled as a mixed-integer nonlinear programming problem (MINLP) in the form of (3-5). The general formulation (3-5) of an MINLP contains several aspects that are difficult to solve. Features such as nonlinearity in the discrete variables and non-separability of continuous and discrete variables are included. The Generalized Benders Decomposition [3] can be implemented to solve the above mixed-integer nonlinear optimization formulation. In addition, two other algorithms have been proven effective against this problem: the Outer Approximation algorithm [4] and the Equality Relaxation algorithm. These three algorithms make use of projection, outer approximation and relaxation. The basic idea behind all three algorithms is to solve an alternating finite sequence of nonlinear programming (NLP) subproblems, which provide upper bounds for the optimal solution, and mixed-integer linear programming (MILP) master problems, which pro-vide lower bounds for the optimal solution.

A mixed integer OPF problem (MIOPF) has its specific set of discrete variables, namely, transformers and switchable shunt devices. For tap-changing and phase-shifting transformers, the i-th allowable discrete value for a variable y can be represented as

$$y_i = \underline{y} + i \cdot y_s, i = 0, \cdots, n_y,$$

where $\underline{y}$ is the lower bound value, y_s is a uniform step size, and n_y is the maximum allowable adjustment steps with $\overline{y} = \underline{y} + n_y \cdot y_s$ being the upper bound value. For switchable shunts, the allowable discrete values

$$y_j \in \{\hat{y}_1, \cdots, \hat{y}_{n_y}\},$$

where $\{\hat{y}_1, \cdots, \hat{y}_{n_y}\}$ is the set of allowable configurations of the switchable shunt, which represent valid combinations of the switchable shunts attached to the same bus.

3.3.2 Determining Discrete Controls

An enhanced sensitivity based method is developed in SuperOPF for determining values of discrete variables. The method comprises three major steps, namely, problem relaxation, sensitivity analysis, and problem reduction.

Problem relaxation

The proposed method for solving the MINLP problem (3-5) first relaxes the original problem by treating all the discrete variables y_k as continuous variables. The corresponding relaxed problem is then described as below nonlinear program:

$$\begin{array}{ll} min & f(x,y) \\ s.t. & g(x,y)=0 \\ & h(x,y)\le 0 \\ & x\in R^n, y\in R^m \end{array} \tag{3-6}$$

This continuous constraint problem (3-6) is then handled by the corresponding solution method, such as the enhanced homotopy-based interior point method (IPM) solver that has been developed for SuperOPF. A (local) optimal solution to the optimization problem (3-6) can be obtained after applying the solution method. This solution is a potential local optimal solution to the MINOP (3-5), and is denoted as (x∗, y∗).

Sensitivity analysis

At the local optimal solution (x∗, y∗) to the relaxed optimization problem (3-6), sensitivity analysis is per-formed to determine the value of discrete variables. The sensitivity of the change of the objective function to the change of discrete variables can be evaluated as follows [7,36]:

$$\begin{aligned} S_y^f &= \frac{\partial f}{\partial y} - \left(\frac{\partial g}{\partial y}\right)^T \left[\left(\frac{\partial g}{\partial x}\right)^T\right]^{-1} \frac{\partial f}{\partial x} \\ S_y^h &= \frac{\partial h}{y} - \frac{\partial h}{\partial x}\left(\frac{\partial g}{\partial x}\right)^{-1} \frac{\partial g}{\partial y} \end{aligned} \tag{3-7}$$

where, S_y^f and S_y^hrepresent the sensitivity of the objective function and inequality constraints with respect to the discrete variable changes, respectively.

Using the sensitivity computed with (3-7), we can compute a linear estimation of the change in the objective and the inequality constraints when moving the discrete variable y_i from its current value $y_i^{j_i}$ to its nearest upper or lower value by the following formulation:

$$\begin{aligned} \Delta f_i^+ &= S_{y_i}^f \cdot (y_i^{j_i+1} - y_i^{j_i}) \\ \Delta f_i^- &= S_{y_i}^f \cdot (y_i^{j_i-1} - y_i^{j_i}) \\ \Delta h_{k_i}^+ &= S_{y_i}^{h_k} \cdot \left(y_i^{j_i+1} - y_i^{j_i}\right), \qquad \forall k = 1,\cdots,n_h \\ \Delta h_{k_i}^- &= S_{y_i}^{h_k} \cdot \left(y_i^{j_i-1} - y_i^{j_i}\right), \qquad \forall k = 1,\cdots,n_h \end{aligned} \tag{3-8}$$

where, $y_i^{j_i+1}$ and $y_i^{j_i-1}$ represent the nearest upper and lower discrete values of $y_i^{j_i}$, respectively; f_i^+ and f_i^- are the estimated change in the objective, $h_{k_i}^+$ and $h_{k_i}^-$ are the estimated change in the k-th inequality constraint.

To facilitate determining discrete control values, the following merit functions are defined by combining the variation of the objective and the variation of the constraint violation:

$$\begin{aligned} \eta_i^+ &= w_f \Delta f_i^+ + \sum_{k=1}^{n_h} w_h \max[0, h_k(\hat{x}, \hat{y}) + \Delta h_{k_i}^+] \\ \eta_i^- &= w_f \Delta f_i^- + \sum_{k=1}^{n_h} w_h \max[0, h_k(\hat{x}, \hat{y}) + \Delta h_{k_i}^-] \end{aligned} \tag{3-9}$$

where, $w_f > 0$ and $w_h > 0$ are weights on the objective and constraints, respectively. These merit functions are designed to evaluate the influence caused by the movement of yi to its nearest upper and lower discrete values by combining the variation of the objective and the variation of the amount of constraint violations. It can be observed from (3-9) that only violated inequality constraints (after altering the discrete variable) contribute to the merit functions. Obviously, the lower the value of the merit functions, the better the effect of moving a discrete variable.

Based on these merit functions, it can be determined how to move the discrete variable y_i to its nearest discrete value through the following rules:

$$\begin{aligned} y_i^{j_i} &\leftarrow y_i^{j_i+1} \;\; if \;\; \eta_i^+ \le \eta_i^- \; and \; \eta_i^+ \le \eta_{th} \\ y_i^{j_i} &\leftarrow y_i^{j_i-1} \;\; if \;\; \eta_i^- \le \eta_i^+ \; and \; \eta_i^- \le \eta_{th} \end{aligned} \tag{3-10}$$

In order to provide flexibility for explicitly controlling the progress of the discretization procedure, relative merit function values defined as follows are evaluated:

$$\hat{\eta}_i^+ = \frac{|\eta_i^+|}{|\eta_i^+| + |\eta_i^-|} \quad and \quad \hat{\eta}_i^- = \frac{|\eta_i^-|}{|\eta_i^+| + |\eta_i^-|} \tag{3-11}$$

It is obvious that these relative merit functions satisfy $0.0 \le \hat{\eta}_i^-, \hat{\eta}_i^+ \le 1.0$ and $\hat{\eta}_i^- + \hat{\eta}_i^+ = 1.0$. Accordingly, for a threshold value $\hat{\eta}_{th}$ (which is always less than or equal to 0.5), the adjustment rule is updated to the follows:

$$y_i^{j_i} \leftarrow y_i^{j_i+1} \;\; if\; \hat{\eta}_i^+ \le \hat{\eta}_{th}$$
$$y_i^{j_i} \leftarrow y_i^{j_i-1} \;\; if\; \hat{\eta}_i^- \le \hat{\eta}_{th} \qquad (3\text{-}12)$$

It needs to be noticed that for a threshold value $\hat{\eta}_{th} = 0.5$, the method will determine values for all undetermined discrete variables.

Problem reduction

Given a potential local optimal solution (x∗, y∗) with values for discrete variables have been determined by the sensitivity analysis, the corresponding reduced MINOP problem can be represented as follows:

$$\begin{array}{ll} min & f(x, y^*) \\ s.t. & g(x, y^*) = 0 \\ & h(x, y^*) \le 0 \\ & x \in R^n \end{array} \qquad (3\text{-}13)$$

The reduced MINLP problem (3-13) can be solved again by the corresponding solution method, such as the enhanced homotopy-based interior point method (IPM) solver that has been developed for SuperOPF. Using the solution method, we can obtain a (local) optimal solution to the problem (3-13). The computed local optimal solution to the optimization problem (3-13) is a local optimal solution to the original MINLP problem (3-5).

3.3.3 The solution method

We are now in a position to describe the solution method that has been implemented in SuperOPF for determining values of discrete control variables. The proposed sensitivity-based method for determining discrete control variables is presented as follows.

<u>The sensitivity-based method for discretization</u>

Step 0: Solve the relaxed OPF problem with all discrete variables treated as continuous ones.

Step 1: Compute merit function values for all those undetermined discrete variables based on equations (3-7) through (3-11).

Step 2: For those undetermined discrete variables with merit function value $\hat{\eta}_i^+ \le \hat{\eta}_{th}$ or $\hat{\eta}_i^- \le \hat{\eta}_{th}$, adjust them to their best discrete values according to the rules defined in (3-11).

Step 3: Re-optimize the OPF problem where those determined discrete variables are fixed at their discrete values while undetermined discrete variables are treated as continuous ones.

Step 4: If all discrete variables have been set to discrete values, stop; otherwise, go to step 1 for the next adjustment iteration.

By implementing the above discretization method in SuperOPF, the user can easily control the number of iterations (and roughly the closeness to the true optimal MINLP solution) he wants to be carried out to determine all discrete variables. For example, if the user wants to finish the discretization in 5 adjustments, he can specify the threshold values to be, for example, $\hat{\eta}_{th}$ =0.1, 0.2, 0.3, 0.4, 0.5 for the five discretization iterations. The threshold value for the last discretization iteration is always set to 0.5 to ensure all discrete variables are determined in the final solution. In this way, the SuperOPF program provides user enough flexibility to balance between the quality of the discretization and the computational time to be consumed.

3.6 Summary

In summary, SuperOPF solution engine is built on the native nonlinear models for optimal power flow analysis and it implements a four-stage, multi-level homotopy-enhanced interior point OPF solver. In this way, it is able to realize the optimal system operating configurations minimizing operation costs, system vulnerability and environmental impacts. These involved techniques are incorporated in a smart way in SuperOPF to effectively and reliably solve specified optimal power flow problems.

4. Multi-Scenario Co-optimized SuperOPF Program

4.1 Introduction

Power systems, including their planning and operation, have been undergoing radical changes in recent years according to the smart grid vision and will keep on undergoing such changes in the near future. The smart grid initiatives aim to introduce new technologies and services in power systems to make the electrical power networks more reliable, resilient, efficient, secure and environment-friendly [1]. The strategy to achieve this vision hinges upon activities that directly address the technical, business, and institutional challenges to realizing a smarter grid. Study has shown that the U.S. accounts for 4% of the global population while contributing 25% of the world's greenhouse gases [2]. Renewable sources of energy like solar, wind and geothermal must be integrated into the power grid in order to reduce the carbon footprint, thus making the power grid environmentally friendly. Utilities around the world are aiming to reach a baseline goal of a 25 percent renewable energy mix globally by 2025. In particular, legislation has been signed that requires California's utilities to obtain 33 percent of their electricity from renewable energy sources by the end of 2020 [3]. More specifically for solar energy, the U.S. passed 10 GW of installed photovoltaic capacity in mid-2013 and utility scale solar power generated 8.86 million megawatt-hours, or 0.22% of total US electricity in 2013 [4]. Therefore, allowing the seamless integration of as much as possible renewable energy sources, such as wind and solar energy, into the power grid is one of the most important goals of the smart grid.

However, energy generated from renewable resources such as a wind turbine, solar panel, or any other source must be promptly consumed because large amounts of electricity cannot be stored in a cost-effective manner. Therefore, inherent variability of renewable resource can bring deleterious effects to the power grid operations. For instance, if an electric utility powers down a coal or natural gas facility in anticipation of wind- or solar-driven energy, those plants may not be able to power up fast enough should the winds fail to blow or the cloud cover increases. The only option in such a scenario is to buy energy on the spot market, which can be very costly. In other words, the forecasting error can result in significantly increased operating costs. To this regard, economic and reliable operation of power systems requires accurate renewable resource forecasts. Obviously, the importance and value of accurate renewable resource forecasts will increase with the size of the renewable energy generation portfolio. Accurate forecasts can save utilities and their customers millions of dollar each year, and thus can produce a major return on investment for utilities and helps make solar energy more cost competitive, to achieve the goal of solar electricity being as cheap or cheaper than that produced by fossil fuels by the year 2020.

Despite its importance, accurate solar forecasting still remains a challenging task. First, it is because the solar resource availability is complex and exhibits several levels of seasonality. Sec-

ondly, it is because there are many important factors, especially weather-related ones, which must be considered in the forecasts. For instance, the daily movements of the sun and short-term changes in weather conditions both have real, direct impact on a PV system's electric output. Indeed, a lot of research and studies have been carried out at National Renewable Energy Laboratory (NREL) and a large number of data records have been produced. However, the relationship between the data records and the solar resource forecast can be very nonlinear. Therefore, advanced data aggregation techniques and analytical models and systems are required in order to take full advantage of these data resources. In a word, a successful and economically feasible integration of a large portion of solar power into the electrical power grid requires accurate solar resource forecasting, as well as reliable quantification of the state-dependent uncertainty associated with the solar power forecast.

The optimal power flow (OPF) is relevant in power system operations, scheduling, and planning. The main objective of the OPF problem is to determine the optimal steady-state operation of an electric power system while satisfying technical and economic constraints. With the structural deregulation of electric power systems and prevalence of power markets, OPF is becoming a basic tool for planning and operations of the power network.

Existing solvers and programs for OPF computation are mostly focused on achieving an optimal solution to the study objective for a single scenario, namely, the base case system, without considering any uncertainties that might arise during the planning horizon. In fact, with more and more penetrations of renewable energy, whose output is stochastic in nature, in the power networks and requests for regulatory compliance (such as compliance to FERC regulations), these uncertainties cannot be neglected any longer. It is crucial for the OPF solutions to not only be economic for the base-case system, but also maintain economic and secure for the whole planning horizon even if one or more uncertain scenarios (with the largest probabilities) occur.

This motivates the development of the multi-scenario SuperOPF (SuperOPF-MS) solver and program, to address the need of computing OPF solutions involving uncertain scenarios for power networks nowadays that are operated in a more and more dynamic environment. This document details the design and implementation of the SuperOPF-MS program.

4.2 Multi-Scenario Co-optimized OPF

Under the stochastic co-optimization framework of SuperOPF, this stage will develop the single-period, stochastic optimal power flow (OPF) solver and program to deal with uncertainties of the operating conditions which will be expected at the decision-making moment or during the planning horizon. These uncertainties encountered during the planning horizon can be categorized into two types. The first type of uncertainties relates to discrete events such as failure of devices (lines, generators, shunts, etc.), that is, contingencies. The so-call “N-1” criteria, that is,

there is only one device of the power network fails for a single contingency, will be considered in the stochastic problem formulation. The other type of uncertainties stems from limited knowledge about future model parameters, for example, uncertainty in the forecasts of load, climate, wind or river flow, which are stochastic in nature. Such uncertainties become increasingly non-neglectable because of the increasing penetrations of renewable energy in the power networks.

In the spirit of SuperOPF, these types of uncertainties will be described as a set of probability distributions for the uncertain parameters and events and will be materialized as multiple scenarios (sets of system states) with associated probabilities. Combination of contingency and stochastic scenarios will result in a tree-like structure of system states with associated probabilities, where the contingent events provide a set of base scenarios while the stochastic consideration adds a set of stochastic scenarios to each base scenario. The objective of the OPF computation is thus a probability-weighted sum of the objectives of the materialized scenarios. The resulting OPF solver and program will be able to co-optimize these multiple materialized scenarios to realize the desired stochastic OPF computation, such that an optimal operating plan can be reached at which the total expected operating objective is optimized (such as the system production cost is minimized, or the total expected net benefit is maximized, or the system power losses are minimized), while all physical and operational limits imposed on the power system are satisfied (such as, no voltage violations and no thermal violations).

The central task for the SuperOPF-MS solver is to solve the optimal power flow problem that will result the best expected objective (such as the minimum system total power losses or generation costs) spanning the planning horizon. Therefore, the co-optimization that needs to be solved in order to get the desired optimal power flow solution can be modeled as the optimization problem (4-1).

It can be seen from the problem model (4-1) that the optimization problem that needs to be solved is a very complicated nonlinear optimization problem. The problem size (the number of optimization variables and the number of equality and inequality constraints) will increase linearly as the number of internal scenarios increases.

$$\begin{aligned} min \quad & f(x) = f_0(x_0) + \sum_{k=1}^{K} p_k[f_k(x_k) + c_k(x_k - x_0)] \\ s.t. \quad & h_0(x) = 0 \\ & g_0(x) \le 0 \\ & \cdots\ \cdots \\ & h_K(x) = 0 \\ & g_K(x) \le 0 \end{aligned} \tag{4-1}$$

4.3 SuperOPF-MS Problem Representations

An overall structure of the SuperOPF solution framework is presented in Figure 4-1. The solver takes several types of input data, namely, the base case power flow data, the contingency list, and the renewable energy forecasts. Based on the input data, internal scenarios will be formatted in a tree-like structure. For each of these internal scenarios, an internal nonlinear optimization (NLP) model is constructed, along with the master optimization model associated with the co-optimization problem spanning the whole set of scenarios. All these internal optimization models are then fed to the SuperOPF-MS co-optimization solver for computing the optimal power flow solution that achieves the best-expected objective value.

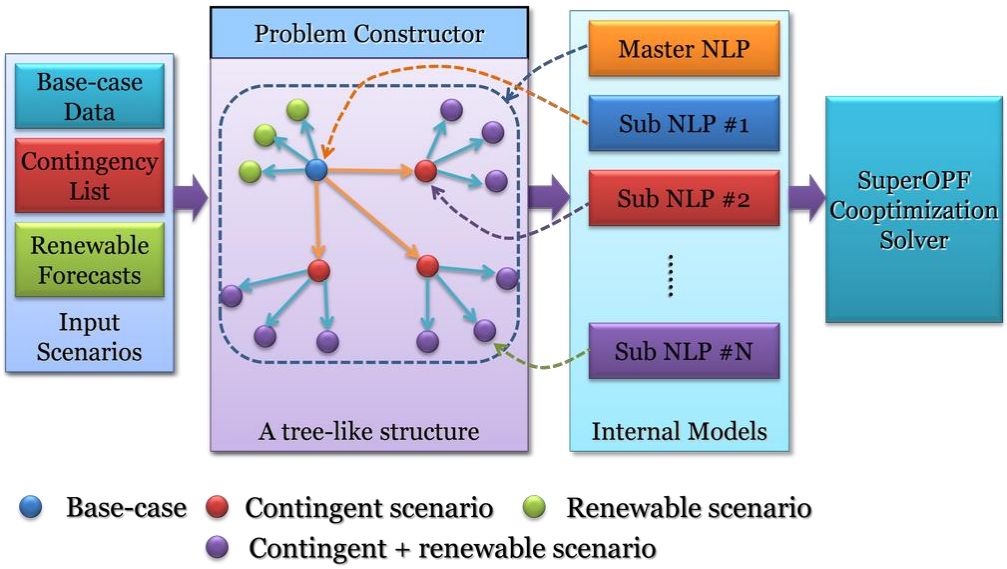

Figure 4-1: Illustration of the SuperOPF-MS procedure

Internal scenarios are categorized into four types, namely, type-1 through type-4 scenarios. Format of these four types of scenarios are summarized as follows:

- Type-1 base case problem where there is no any contingency in the power network and not consider renewable energy outputs.

Type-1 scenario:

$$\begin{aligned} min \quad & f(x) \\ s.t. \quad & P_i(x) + P_{Di} - P_{Gi} = 0 \qquad 1 \le i \le n_B \\ & Q_i(x) + Q_{Di} - Q_{Gi} = 0 \\ & S_k = \sqrt{P_{ij}^2(x) + Q_{ij}^2(x)} \le S_k^{max} \qquad (i,j) \in L \\ & x^{min} \le x \le x^{max} \end{aligned} \tag{4-2}$$

where, n_B is the number of buses and L stands for the set of branches.

- Type-2 scenario problems, where there is a single contingency involved in the power network.

$$\text{Type-2 scenario:}\quad \begin{aligned} min \quad & f(x) \\ s.t. \quad & P_i(x) + P_{Di} - P_{Gi} = 0 \qquad 1 \le i \le n_B \\ & Q_i(x) + Q_{Di} - Q_{Gi} = 0 \\ & S_k = \sqrt{P_{ij}^2(x) + Q_{ij}^2(x)} \le S_k^{max} \qquad (i,j) \in \hat{L} \\ & x^{min} \le x \le x^{max} \end{aligned} \tag{4-3}$$

where, $\hat{L}$ is L excludes contingent branches.

- Type-3 scenario problems, where there includes a single set of forecasts of the renewable energy generations.

$$\text{Type-3 scenario:}\quad \begin{aligned} min \quad & f(x) \\ s.t. \quad & P_i(x) + \hat{P}_{Di} - P_{Gi} = 0 \qquad 1 \le i \le n_B \\ & Q_i(x) + \hat{Q}_{Di} - Q_{Gi} = 0 \\ & S_k = \sqrt{P_{ij}^2(x) + Q_{ij}^2(x)} \le S_k^{max} \qquad (i,j) \in L \\ & x^{min} \le x \le x^{max} \end{aligned} \tag{4-4}$$

where, $\hat{P}_D$ and $\hat{Q}_D$ are equivalent loads with renewable energies.

- Type-4 scenario problems, where the combinatorial occurrence of a contingency and a renewable forecast is considered.

$$\text{Type-4 scenario:}\quad \begin{aligned} min \quad & f(x) \\ s.t. \quad & P_i(x) + \hat{P}_{Di} - P_{Gi} = 0 \qquad 1 \le i \le n_B \\ & Q_i(x) + \hat{Q}_{Di} - Q_{Gi} = 0 \\ & S_k = \sqrt{P_{ij}^2(x) + Q_{ij}^2(x)} \le S_k^{max} \qquad (i,j) \in \hat{L} \\ & x^{min} \le x \le x^{max} \end{aligned} \tag{4-5}$$

Assuming there are M contingencies in the input contingency list and N renewable forecasts, then the total number of internal analysis scenarios will be (M+1)*(N+1). The numbering of the

internal scenario for a session with 3 contingencies and 2 renewable forecasts is illustrated in Table 4-1.

Table 4-1: Numbering of the internal scenarios

Scenario Index	Base case	Contingency 1	Contingency 2	Contingency 2
Base case	1 (type 1)	2 (type 2)	3 (type 2)	4 (type 2)
Forecast 1	5 (type 3)	6 (type 4)	7 (type 4)	8 (type 4)
Forecast 2	9 (type 3)	10 (type 4)	11 (type 4)	12 (type 4)

4.4 Solution Methods

Two solution methods are implemented in the SuperOPF-MS solver, namely, the one-short scheme and the decomposition scheme.

4.4.1 One-shot solution schemes

The one-shot scheme is the most direct way to solve the co-optimization problem. Considering the complexity of the co-optimization problem, a feasible point could be a good initial point. To this end, the one-shot scheme is implemented as the following steps of propagation of initial points, as illustrated in Figure 4-2.

Step 1. Solve the type-1 base case problem where there is no any contingency in the power network and not consider renewable energy outputs.

Step 2. Using the solution to the base case problem obtained in step 1 as the initial point, solve the type-2 and type-3 scenario problems where there considers only single contingency or single renewable forecast.

Step 3. Using the solutions to the type-3 scenario problems as the initial point, solve the type-4 scenario problems, where the combinatorial occurrence of a contingency and a renewable forecast is considered.

Step 4. Using the solutions to all the type-1 throughout type-4 scenario problems to form the initial point to the co-optimization problem (4-1).

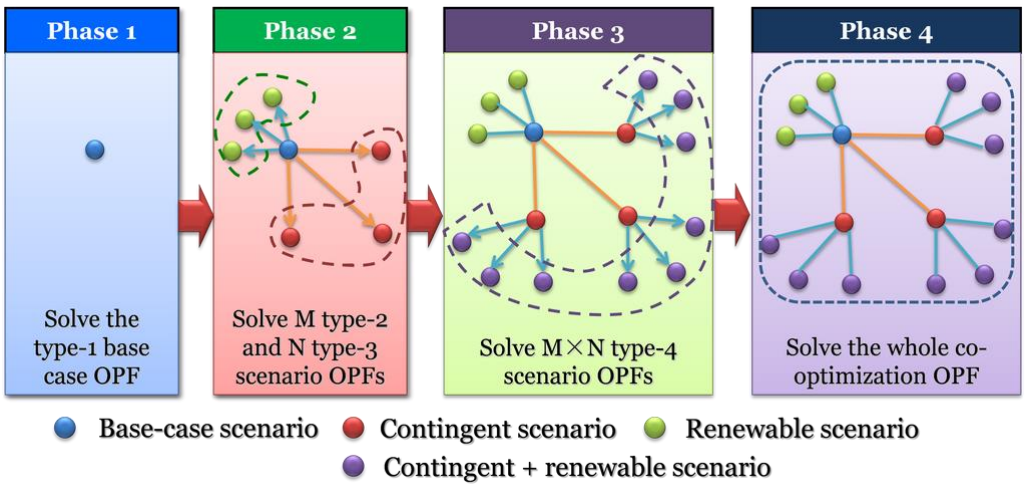

Figure 4-2: Illustration of the solution method

4.4.2 Decomposition based solution scheme

The one-shot scheme can successfully solve multi-scenario co-optimization problems involving a small number of scenarios on medium to large-scale power systems. Indeed, complexity of the co-optimization problem grows very quickly as the number of scenarios increases. Therefore, as the number of involved scenarios increases, the required computational resources will soon exceed the available capability. Therefore, a more resource-efficient way is favorable. The decomposition method is considered in the SuperOPF-MS solver to avoid solving the whole co-optimization problem directly.

The proposed decomposition method takes advantage of the idea of feasible direction method and consists of the following steps.

Step 1. Same as in the one-shot scheme, all the subproblems are solved. By combing the solutions to the subproblems, a feasible solution $\hat{x}$ to the master co-optimization problem is formed.

Step 2. Compute the feasible direction d that can improve the objective function using the decomposition scheme. Can be achieved by solving sub-directions d_k, $k = 1, \cdots, K$. This direction can be computed by solving the following linear program:

$$\begin{aligned} min \quad & \nabla^T f(\hat{x}) d \\ s.t. \quad & \begin{pmatrix} \nabla^T h_0(\hat{x}_0) \\ \dots \dots \\ \nabla^T h_K(\hat{x}_K) \end{pmatrix} d = 0 \\ & \begin{pmatrix} \nabla^T g_0(\hat{x}_0) \\ \dots \dots \\ \nabla^T g_K(\hat{x}_K) \end{pmatrix} d \leq 0 \end{aligned} \tag{4-6}$$

It can be observed that contributions from each scenario in this linear program are independent to each other; in other words, it can be further decomposed into solving following small linear programs.

$$\begin{aligned} min \quad & \delta_0^T d_0 \\ s.t. \quad & \nabla^T h_0(\hat{x}_0) d = 0 \\ & \nabla^T g_0(\hat{x}_0) d \leq 0 \\ \dots \quad & \dots \\ min \quad & \delta_K^T d_K \\ s.t. \quad & \nabla^T h_K(\hat{x}_K) d = 0 \\ & \nabla^T g_K(\hat{x}_K) d \leq 0 \end{aligned} \tag{4-7}$$

Step 3. Compute the step size in the feasible direction that improves the objective function the most, which is implemented as solving the following 1-dimensional optimization or a line search problem.

$$\begin{aligned} min \quad _{\lambda} \quad & f(\hat{x} + \lambda d) \\ s.t. \quad & h_0(\hat{x}_0 + \lambda d) = 0 \\ & g_0(\hat{x}_0 + \lambda d) \leq 0 \\ & \dots \dots \\ & h_K(\hat{x}_K + \lambda d) = 0 \\ & g_K(\hat{x}_K + \lambda d) \leq 0 \end{aligned} \tag{4-8}$$

Step 4. Considering the trial point computed in step 3 can be away from the feasible region, a correction step to restore feasibility is necessary.

The above steps will be carried out repeatedly, until the desired stopping criteria are satisfied. In this way, it can be avoided to solve the huge co-optimization problem in one-shot. This primal decomposition scheme is applicable for single-period co-optimization. For multi-period co-optimization, the dual decomposition scheme should be the option in order to handle the introduced inter-period constraints (e.g. ramping constraints).

4.5 The Program Structure

The SuperOPF-MS program has a modularized structure and is designed to be ready for future extensions. It is flexible and convenient for further development, in order to support more data formats and to enclose other effective linear and nonlinear solvers into the current implementation. A block diagram for the structure of SuperOPF-MS program is shown in Figure 4-3. The program is composed of two major parts, that is, the solver modules and the user interface programs.

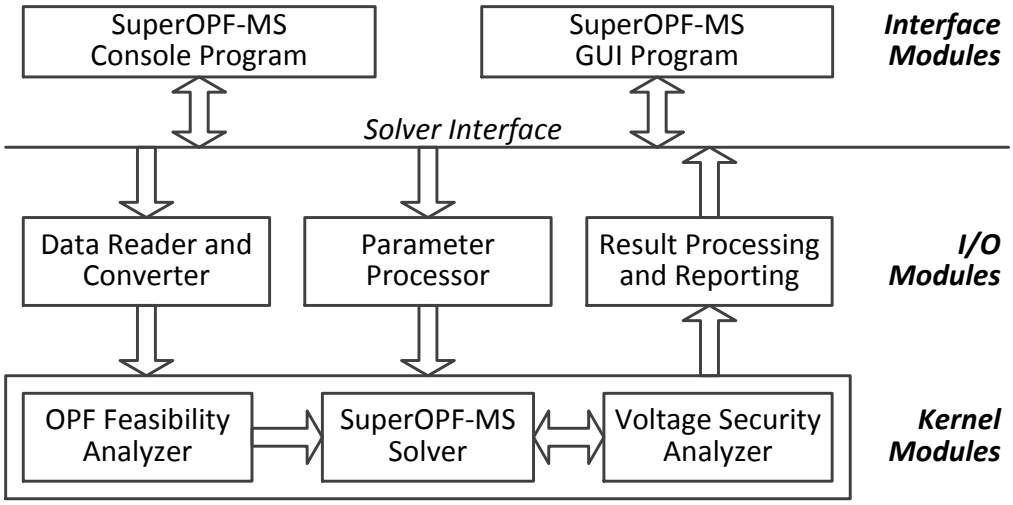

Figure 4-3: SuperOPF-MS program structure

4.5.1 The SuperOPF-MS Solver Modules

The kernel part is designed to take over all the computationally intensive and architecture independent tasks. These tasks mainly include data file reading, parameter settings, result presenting and output file writing, and SuperOPF-MS computations. To this end, the solver modules of the SuperOPF-MS program can be divided into two categories, that is, the data input/output (I/O) and representation modules and the kernel computing modules.

The data representation modules handle the tasks of data file reading and converting required by the SuperOPF-MS program, parameter settings for computation, and result presenting. Therefore, this category consists of components for reading power flow files and other data files. The most important data file to be processed is the power flow file, where the structure of the power network under study, parameters of the involved network components, and the initial state of the power network are specified. There are many data formats used by different ven-

dors and utilities in the power industry, among which PSS/E, PSLF, PSF, and CIM are the most popular ones. In the SuperOPF-MS program, different power flow data I/O modules are implemented, each of which is dedicated to one data format. All these data I/O modules are derived from the power flow I/O base module. External power flow files in different formats are read and processed by the I/O engine and then converted to an internal, unified power network representation. In such a way, efforts for future support of other data formats can be minimized. The data file I/O engine implements the procedure of reading other data files following the same philosophy of flexibility and extensibility. The other data files need to be processed in the SuperOPF-MS program include the generation cost model file for minimizing the system generation cost and the contingency related files for scenarios of OPF with security constraints. Another important data file for SuperOPF-MS program is the scenario specification file, which specifies the list of scenarios to be analyzed by the program. The specification of the scenario file is detailed in Section 5. Besides the data reader and converter module, the data representation category also includes a module for handling parameter settings that interprets the user configured parameters and converts them to internal representations that are understandable by the compute engine. The last module in this category is the module for result data representation, which is designed to interpret and archive the output files produced by the compute engine.

The kernel computing modules handle the actual multi-scenario optimal power flow computation and voltage security analysis. All the data collected and processed by the I/O engine is fed to the compute data module of the compute engine. This data module defines all data structures for hosting data to be used during the actual optimization process. Necessary transformations of the data fed from the I/O engine are carried out in this module. Computation parameters are processed by the parameter setting module. The data and parameters are then fed to the OPF solver module and the actual OPF computation is executed. The first module of the SuperOPF core engine is a feasibility analyzer, which is designed to compute a feasible point if the study model is feasible or to compute a restored feasible point with an optimal constraint relaxation if the study model is infeasible. The second module, SuperOPF-MS solver, and the third module, voltage security analyzer, then use computed feasible point as the initial condition to carry out a combined optimal power flow computation and voltage security analysis, which will produce in a secure optimal power flow solution.

The SuperOPF-MS program is designed to support different effective solvers, such as the interior point method (IPM) solver and the sequential quadratic programming (SQP) solver. To this end, the central part of the computation engine is the OPF solver base module (NLP), where the general nonlinear program modeling and solver calling are implemented. All solver modules for realizing specific optimization methods or optimizers are derived from this base module. Furthermore, the SuperOPF kernel part is implemented in C++ language using only standard, architecture independent libraries. Therefore, the kernel part can easily be ported to other architectures and operation systems with minimum efforts. The SuperOPF-MS interfaces are developed in C++ with Microsoft MFC libraries and C#, which provide natively-supported and con-

venient resources for developing a user-friendly and feature-rich GUI in Microsoft Windows environments for the SuperOPF-MS program.

4.5.2 SuperOPF-MS User Programs

The user interface part also consists of two components. The first component is a graphical user interface (GUI) program. This GUI program provides the user a convenient and feature-enriched interface to interact with the underlying OPF computation.

There are three major functional parts in this GUI program, that is, the data selection and display part, the parameter and model setting part, and the resulting reporting part. The first part, that is, the data selection and display part handles the task of selecting required data file paths for the OPF computation. The usual data files required for an OPF computation include the power flow file and generation cost file (when the OPF objective is to minimize the system generation cost). The selected data files will also be displayed by the GUI program in an organized way and can be easily reviewed or modified by the user. The second part of the GUI program is for parameter and model settings. Responsive interfaces are designed for the user to set up a desired OPF computation scenario by specifying the problem model (the optimization objective, the cost model, etc.) and editing computation parameters (the optimization strategy, the optimizer to use, the detailed optimization parameters, etc.). Therefore, the user has a full control over the computation to be carried out. The third part handles the result reporting. Taking advantage of existing reporting engines, namely Microsoft Reports, feature-enriched and meaningful representations of the OPF computation results can be automatically produced and reported to the user.

Besides the GUI program, a SuperOPF-MS console program is also considered in the implementation. This console program eliminates all graphical interactions and can only be run in a command line environment. However, the user still has full control over the computation scenarios through specifying the parameters to the SuperOPF console command. This results in a stand-alone, lightweight SuperOPF program suitable for low-end hardware environments. Moreover, such command-line based execution of the SuperOPF program provides the user a convenient way to effectively cooperate with other computation and management programs. For example, the user can include the call of the SuperOPF console program in a script to automate his/her analysis tasks of sequential execution of multiple programs or the task of analyzing a batch of scenarios.

4.6 Summary

In summary, SuperOPF is a powerful and easy-to-use electric power network analysis tool. It goes beyond traditional power flow analysis to provide you with the ability to fully optimize

and refine your transmission system. Cooperating with other power system analysis tools, SuperOPF helps realize comprehensive and reliable optimization of your power system under rapidly changing operating conditions. The major features of SuperOPF can be summarized as follows:

- Comprehensive and flexible nonlinear modeling capability.
- Reliable and effective large scale power networks (>10,000 buses) optimization.
- Genuine locational marginal price (LMP) computation.
- Contingency oriented optimization for system security maintenance.
- Exceptional nonlinear convergence with the patented Trust-Tech methodology.
- Constraint feasibility analysis and diagnosis of infeasible scenarios.
- Multiple optimal solutions computation for enhanced flexibility.
- Comprehensive analysis result reporting and database bridging.
- Support of major power system data formats.
- Easy to use program and informative interfaces for smooth user interactions.

5. Voltage Stability Based Contingency Analysis

5.1 Introduction

Power system operations need to be planned to accommodate various possible contingencies, such that the power system can still operate securely and economically should any considered contingency occur within the planning horizon. Contingency analysis involving contingencies produced following the "N-1" and/or "N-2" rules has become a routine. However, the number of credible contingencies can be large. For instance, the number of all possible "N-1" contingencies equals to the number of in-service devices in the system, and that of "N-2" contingencies is almost the square of this number. Such a large number of contingencies make it prohibitive to carry out the desired analysis if all contingencies need to be considered simultaneously, such as security-constrained optimal power flow analysis that needs to co-optimize the involved contingencies. Therefore, a preprocessing procedure becomes a necessity for reducing the number of contingencies to be involved in the actual computation for analysis while still being able to capture representative patterns of the whole set of contingencies.

One natural option for reducing the number of contingencies is to consider only worst contingencies in terms of security indices in co-optimized OPF computation. To this end, a dedicated contingency analysis tool is desired for determining the set of "worst contingencies". In this study, BSI Voltage Stability Analysis (VSA) program is used to accomplish this task. More specifically, worst contingencies with smallest load margins (critical contingencies) or even zero load margins (instable contingencies) are determined by BSI VSA and considered in contingency-constrained co-optimized OPF computation. In this chapter, BSI VSA program for determining the worst contingencies in terms of voltage stability indices is introduced.

5.2 Theoretical Part

A power system subject to load disturbances can be modeled as a set of parameter-dependent nonlinear differential and algebraic equations with parameter variation. Power systems are normally operated near a stable equilibrium point. When the system load parameters are away from their bifurcation values and their variations are continuously but slowly, it is very likely that

- the stable equilibrium point of the underlying power system changes position but remains a stable equilibrium point, and
- the old stable equilibrium point lies inside the stability region of the new stable equilibrium point.

Consequently, the power system dynamics starting from the old stable equilibrium point will converge to the new stable equilibrium point and will make the system state track its new stable equilibrium point, whose position is changed continuously but slowly, and yet the system remain stable under this load disturbance.

The only typical ways in which a study power system may lose stability, under the influence of load variations are through the following:

- a stable equilibrium point and another equilibrium point coalesce and disappear in a saddle-node bifurcation as parameter varies, or
- a stable equilibrium point and another equilibrium point coalesce and disappear in a limit-induced bifurcation as parameter varies, or
- the stable equilibrium point and an unstable limit cycle coalesce and disappear and an unstable equilibrium point emerges in a subcritical Hopf bifurcation as parameter varies,
- the stable equilibrium point bifurcates into an unstable equilibrium point surrounded by a stable limit cycle in a supercritical Hopf bifurcation as parameter varies.

It can be shown that for general power system models, the saddle-node bifurcation is inevitable if the load of the system increases in the form of constant powers and is avoidable in the form of constant impedance. The P-V curve and Q-V curve widely used by voltage stability analysis are examples of saddle-node bifurcations. On the other hand, the Hopf bifurcation may not occur if the system damping is sufficient. If it occurs, it must occur before the saddle-node bifurcation.

The Continuation Power Flow component of BSI VSA is capable to generate the P-V, Q-V, or P-Q-V curve and detect the above typical bifurcations along the solution curve. The voltage security assessment of BSI VSA was developed on the basis of the following bifurcation-based model for explaining voltage collapse in power systems due to load variations. Recall that ``slow load variations" means the dynamics of load variations are relatively slower than the dynamics occurring in the state vector.

5.2.1 Bifurcation-based voltage collapse model

We next present a model, called the saddle-node voltage collapse model (hereafter called the SAD voltage collapse model) to address power system behaviors due to slow load variations in three stages. We note that this model is applicable to analyze the static aspects of power system behaviors after a contingency (branch outages).

SAD Voltage Collapse Model

Stage 1: the system is in quasi-steady state and is tracking a stable equilibrium point.

Stage 2: the system reaches its ``steady-state" stability limit when the stable equilibrium point undergoes a saddle-node bifurcation or a limit-induced bifurcation.

Stage 3: depending on the type of bifurcation encountered in Stage 2, the system dynamics after bifurcation are captured either by the center manifold trajectory of the saddle-node bifurcation point or by the unstable manifold of the limit-induced bifurcation point.

We note that Stage 1 is related to the feasibility of "load flow" solutions (i.e., the existence of a system operating point in a feasible region). Stage 2 determines the steady-state stability limit based on the bifurcation point. Stage 3 describes the system dynamical behavior after bifurcation to assess whether the system, after bifurcation, remains stable or becomes unstable; and determines the types of system instability (voltage collapse and/or angle instability). Hence, the voltage collapse model describes both the static aspect (stages 1 and 2) and the dynamic aspect (stage 3) of the problem. Furthermore, it can be shown that stages 1 and 2 of the SAD voltage collapse model encompass many existing voltage collapse models such as the multiple load-flow solutions model, the load flow feasibility model, the static bifurcation model, the singular Jacobian model and the system sensitivity model. Stage 3 of the model goes beyond the static aspect of the problem to describe the dynamic aspect of the problem.

5.2.2 Performance indices for assessing voltage collapse

While continuation power flow methods can generate P-V and Q-V curves in a reliable manner, they may be too slow for on-line applications. To overcome this difficulty, a number of performance indices intended to measure the severity of the voltage collapse problem have been proposed in the literature. They can be divided into two classes: state-space-based approach and the parameter-space-based approach. The former approach includes the minimum singular value, the eigenvalue, the condition number of the system Jacobian that all attempting to provide some measure of how far the system is away from the point at which the system Jacobian becomes singular. These performance indices can be viewed as providing some measure of the "distance" between the current operating point and the bifurcation point in the state space of power system models and hence, they cannot directly answer questions such as: "Can the system withstand a 100 MVar increase on bus 11?" or: "Can the system withstand a simultaneous increase of 70 MW on bus 2 and 50 MVar on bus 6?"

One basic requirement for useful performance indices is their ability to reflect the degree of direct mechanism leading the underlying system toward an undesired state.

In the context of voltage collapse in power systems, a useful performance index must have the ability to

1. Measure the amount of load increase that the system can tolerate before collapse (when the underlying mechanism of collapse is due to load variations), or
2. Assess whether the system can sustain a contingency without collapse (when the underlying mechanism of collapse is caused by a contingency) and measure the severity of the contingency.

The state-space-based performance indices, however, generally do not exhibit any obvious relation between their value and the amount of the underlying mechanism that the system can tolerate before collapse.

In order to provide a direct relationship between its value and the amount of load increases that the system can withstand before collapse, the performance index for assessing the load margins before collapse must be developed in the parameter space (i.e., the load/generation space). Development of performance indices in the parameter space is a relatively new concept that has been spurred by the local bifurcation theory.

The performance index, implemented in BSI VSA, provides a direct relationship between its value and the amount of load demand that the system can withstand before a saddle-node voltage collapse was developed. This index makes use of the information contained in the power flow solutions of the particular branch of interest. One feature that distinguishes the performance index is its development in the load-demand space and its ability to answer questions such as: "Can the system withstand a simultaneous increase of 70 MW on bus 2 and 50 MVar on bus 6?" Moreover, the computation involved in the performance index is relatively inexpensive in comparison with those required in the existing ones.

We acknowledge that he parameter-space-based performance index implemented in BSI VSA cannot take into account the physical limitations of typical control devices such as generator VAR limits and ULTC tap ratio limits; making their computed load/generation margins may bear some `distance' with the exact margins. Hence, its function is mainly for ranking the severity of a list of credible contingencies or for ranking the effectiveness of different locations in the network to install certain control devices. Exact load/generation margins that accounts for all control devices and their physical limitations can be calculated by the continuation power flow approach.

5.2.3 On-line voltage monitoring systems

In modern power system control centers, energy management systems are designed, among other functions, to periodically perform the task of on-line power system (static) security monitoring, assessment and control attempting to ensure the ability of the power system to withstand credible contingencies (disturbances). Software packages for security monitoring, assessment and control have been implemented in modern energy control centers. These packages provide comprehensive on-line security analysis and control based almost exclusively on steady-state analysis, making them only applicable to static security analysis and control.

The strategy of using an effective scheme to screen out a large number of "unharmed" contingencies and to apply detailed simulation programs only to potentially dangerous disturbances

is well recognized. This strategy has been successfully implemented in on-line SSA. The ability of screening several hundred contingencies to filter out tens of the critical contingencies has made the on-line SSA feasible.

This strategy has been applied to BSI VSA. Given a set of credible contingencies, the strategy would break the task of on-line VSA into three stages of assessments:

Stage 1: perform the task of contingency screening (for voltage collapse) to screen out contingencies that are definitely "safe" from a set of credible contingencies using a sensitivity-based approach

Stage 2: perform detailed assessment of dynamic performance for each contingency remained in Stage 1 to identify the potential dangerous contingencies using the performance index approach

Stage 3: Perform detailed analysis for each contingency identified in Stage 2 using the continuation power flow approach.

5.2.4 Persistence of local bifurcations under un-modeled dynamics

Many physical systems contain slow and fast dynamics. These slow and fast dynamics are not easy to model in practice. Even if these dynamics can be modeled properly, the resulting system model (the original model) is often ill-conditioned. This difficulty has motivated developments of several model reduction or simplification approaches to derive reduced models from the original model. One popular model reduction approach (to derive a reduced model) is to neglect both the fast and slow dynamics in an appropriate way. On the other hand, traditional practice in system modeling has been to use the simplest acceptable model that captures the essence of the phenomenon under study. A common logic used in this practice is that the effect of a system component or control device can be neglected when the time scale of its response is very small or very large compared to the time period of interest.

Electric power systems comprise a large number of components interacting with each other in nonlinear manners. The dynamical response of these components extends over a wide range of time scales. The difference between the time constants of excitation systems (fast control devices) and that of governors (slow control devices) is a couple orders of magnitudes. The dynamic behavior after a disturbance occurring on a power system involves all the system components to varying degrees. The degree of involvement from each component determines the appropriate system model necessary for simulating the dynamic behaviors after the disturbance. For instance, an extended power system dynamical model contain both fast variables, such as the damping flux in the direct and quadrature axis of generators, and slow variables, such as the field flux and the mechanical torque of generators. For simulating the dynamic behaviors of a power system after an event disturbance, the effect of these fast and slow variables can be neglected in the system modeling because the time scale of these variables is very small or very

large compared to the time period of the disturbance of interest. A reduced system model is thus obtained from the original system model.

It can be shown that, under fairly general conditions, a power system (with both fast and slow dynamics) will encounter a saddle-node bifurcation relative to a varying parameter if the associated reduced system, derived by neglecting both fast and slow dynamics, encounters a saddle-node bifurcation relative to the varying parameter. An error bound between the bifurcation point of the reduced system and that of the original system can be derived. Furthermore, it can be shown that the system behaviors after the saddle-node bifurcation of the reduced system and that of the original system are close to each other in state space. These general analytical results can be applied, among others, to justify the usage of simple power system models for analyzing voltage collapse in electric power systems.

5.3 Computational Part

5.3.1 Computing exact bifurcation points

We consider a comprehensive (static) power system model expressed in the following form $f(x,\lambda)=0$, where λ is a varying parameter. Let (x^*,λ^*) be a saddle-node bifurcation point, then the necessary conditions for an SNBP can be stated as follows:

$$\begin{bmatrix} f(x^*,\lambda^*) \\ f_x(x^*,\lambda^*)v \\ v^T v-1 \end{bmatrix}=0 \tag{5-1}$$

where

- $f(x^*,\lambda^*)$ implies that the point (x^*,λ^*) must satisfy the power flow equations.
- $f_x(x^*,\lambda^*)v$ states that the Jacobian evaluated at (x^*,λ^*) must have a single zero eigenvalue
- v is the normalized right eigenvector associated with the zero eigenvalue.

These conditions are only necessary and not sufficient, since they do not guarantee that the solution curve is quadratic in a neighborhood of the SNBP. However, if a point satisfies the above necessary conditions, then by examining the graph of an appropriate state variable versus parameter, one can still identify whether or not the candidate point is a SNBP. A numerical method can be applied to directly solve the extended (2n+1)-dimensional nonlinear equations for the saddle-node bifurcation point. The success of the method depends greatly on a good initial guess of the desired saddle-node bifurcation point. Without a proper initial guess, the method may diverge or converge to an undesired saddle-node bifurcation point.

To overcome the above numerical problem, we use an indirect method to solve for the exact bifurcation point. Beside the saddle-node bifurcation point, there is another kind of bifurcation phenomena called limit-induced bifurcation which is induced by that the status of one constraint in power system changed from inactive into active, especially the generator reactive power limit constraints.

In CPFLOW, a direction indicator describes the sign of the quantity $d\lambda/ds$ [85]. When $d\lambda/ds$ changes sign, it indicates that the continuation process has passed through a BP. If a change of sign is detected, then we can approximate the zero by the secant iteration scheme.

$$s^{k+1} = s^k - \frac{s^k - s^{k-1}}{q(s^k) - q(s^{k-1})} q(s^k) \tag{5-2}$$

where $q(s) = d\lambda/ds$ and k represents the iteration index.

CPFLOW employs a Newton search in the neighborhood of where the $d\lambda/ds$ sign change to calculate the exact BP (within the specified user tolerance). Once the solution trace passes through this point, we have information from either side of the BP as follows:

Before BP	After BP
λ_1 $d\lambda_1/ds$	λ_2 $d\lambda_2/ds$

where $d\lambda_1/ds$ represents the derivative of λ with respect to the arc-length s evaluated at the first solutionλ_1. Since the graph of λ versus s is quadratic in a neighborhood of the SNBP, the Newton search will converge quickly to the exact SNBP. The $d\lambda/ds$ values must be computed by the tangent predictor, so if the secant predictor was being used to trace the curve, then CPFLOW will temporarily use different types of predictors. Based on the sign and magnitude of $d\lambda/ds$, CPFLOW determines the proper step length to compute the SNBP. If a computed point is close to the exact bifurcation point (x_{BP}, λ_{BP}) of (x, λ) and its $d\lambda/ds$ is smaller than a tolerance, then we can identify this point as (x_{BP}, λ_{BP}), the saddle-node bifurcation point.

If $d\lambda/ds$ is not close to zero but close to two nonzero values respectively, then the computed point can be a limit-induced Bifurcation Point. At the computed point, one can check the following index to make sure that the point is indeed a limit-induced bifurcation point: calculating the total number; say K_1 and K_2 of buses of PV-type of the entire system which it is loaded at point λ_1 and point λ_2 respectively. If $K_1 - K_2 = 1$, then record the bus ID whose type has been changed between λ_1 and λ_2. The capability of the generator reactive power at this bus is likely the key constraint that induces the voltage collapse.

Next, we will show that when $d\lambda/ds = 0$, the SNBP necessary condition (1) is satisfied. The linear system with the inflated Jacobian shown below is the tangent predictor computed at step j.

$$\begin{bmatrix} f_x(x_{j-1},\lambda_{j-1}) & f_\lambda(x_{j-1},\lambda_{j-1}) \\ dx_{j-1}^T & d\lambda_{j-1} \end{bmatrix} \begin{bmatrix} dx_j \\ d\lambda_j \end{bmatrix} = \begin{bmatrix} 0 \\ 1 \end{bmatrix} \tag{5-3}$$

First, notice that the tangent predictor at continuation step j, $(dx_j, d\lambda_j)$ is right null vector of the inflated Jacobian. Second, when $d\lambda/ds = 0$ the last element of the right null vector is equal to zero. Third, the vector dx_j is the right null vector of the original Jacobian and it's nonzero. Therefore, our indirect method calculates the point that satisfies the three conditions of the exact SNBP.

5.3.2 Sensitivity formula

Once the exact saddle-nose bifurcation point or limit-induced bifurcation point is obtained, the sensitivity of the margin to voltage collapse with respect to almost every power system parameter can be obtained for very little additional computational cost. This chapter explains and derives the formula for the sensitivity of a margin with respect to an arbitrary parameter vector.

It is necessary to show that the sensitivity theory is not only for margin to voltage collapse, but also arbitrary events such as the first low voltage limit or line thermal limit. The formula derivations for both are basically same. In BSI-VSA, there are two main sensitivity-based functions to

1. fast quantify the effect of varying power system controls or parameters on the proximity to voltage collapse; and
2. fast rank the severity of contingencies with respect to voltage collapse.

5.3.3 Sensitivity of margin to an arbitrary event

We consider the following static power flow equations:

$$f(z,\lambda,u) = 0 \tag{5-4}$$

where $z \in R^n$ is system state vector which represents the system state such as bus voltage magnitudes and voltage angles and $\lambda \in R^m$ is a (controlling) parameter vector which represents the change in a certain load direction. u is the real control vector. Assume that (z_0, λ_0, u_0) is a stable operating point. Let the point (z_*, λ_*, u_*) be a bifurcation point corresponding the variation of the λ parameter in the direction k. Let $\hat{k}$ be a unit vector in the norm used to measure the margin.

$$\hat{k} = (\lambda_* - \lambda_0)/|\lambda_* - \lambda_0| \tag{5-5}$$

The security margin M to the event is $M = |\lambda_* - \lambda_0|$. Here the event can be the system voltage collapse or one bus voltage reaches its limit. The equilibrium equations are valid at (z_*, λ_*, u_*). For many limits, including voltage, flow, and power limitations, defining the event equation E is simple.

Suppose that it is of interest how changing a selected parameter $p(\in u)$ changes the state and remaining parameters at which the event described by the event equation E occurs. At the event point characterized by $\begin{pmatrix} F(z_*, \lambda_*, p) \\ E(z_*, \lambda_*, p) \end{pmatrix} = 0$, we define the map H as

$$H(z, \lambda, p) = \begin{pmatrix} F(z, \lambda, p) \\ E(z, \lambda, p) \end{pmatrix} \tag{5-6}$$

The curve (if it exist) that the continuation method estimates is a subset of the set of equilibria that satisfy the event conditions in state and parameter space around the nominal boundary point. This set of equilibria, the pre-image of the zero set of H, is denoted $H^{-1}(0)$. Using calculus on $H^{-1}(0)$ is defensible only when $H^{-1}(0)$ is a differentiable manifold. It turns out that for very general conditions this will indeed be true and we are justified in the assumption that there are curves on $H^{-1}(0)$ that describe the sets of interest to us. The conditions are

1. $H_z|_{(z_*, \lambda_*)}$ has rank n.
2. $\left(H_z \; H_\lambda \hat{k}\right)|_{(z_*, \lambda_*)}$ has rank $n + 1$.

Condition 2 is a transversality condition stating that a vector through (z_*, λ_*) in the $\hat{k}$ direction intersects $H^{-1}(0)$ transversally. Condition 1 can be interpreted as a condition of uniqueness. Simply stated, Condition 1 specifies that only one event occurs at a time. Assume that $H^{-1}(0)$ is a smooth manifold and a smooth curve on that manifold parameterized by p is $(Z(p), \Lambda(p))$ so that $\left(Z(p_0), \Lambda(p_0)\right) = (z_*, \lambda_*)$ and

$$\begin{pmatrix} F(Z(p), \Lambda(p), p) \\ E(Z(p), \Lambda(p), p) \end{pmatrix} = 0 \tag{5-7}$$

Since the system is assumed stable at the nominal operational point, $\tilde{F}_z$ is nonsingular as p is varied in a neighborhood about p_0. Then as p is adjusted each new equilibrium $\left(\tilde{Z}(p), \lambda_0, p\right)$, satisfying $F\left(\tilde{Z}(p), \lambda_0, p\right) = 0$, can be associated with one corresponding point $(Z(p), \Lambda(p), p)$ satisfying $H(Z(p), \Lambda(p), p)$=0 that is the closest point on $H^{-1}(0)$ in the direction $\hat{k}$. The difference in parameter space between the operating point $\left(\tilde{Z}(p), \lambda_0, p\right)$ and the corresponding boundary point $(Z(p), \Lambda(p), p)$ is

$$\Lambda(p) - \lambda_0 = L(p)\hat{k} \tag{5-8}$$

where $L(P)$ is a scalar step in the $\hat{k}$ direction as a function of p. The margin as a function of p is

$$\mathrm{M}(p) - \lambda_0 = \left|L(p)\hat{k} + \lambda_0 - \lambda_0\right| = \left|L(p)\hat{k}\right| \tag{5-9}$$

Since $\hat{k}$ is a unit vector in the norm used for the margin, the margin as a function of p is $M(p) = L(p)$. Write $\Lambda(p)$ in terms of the margin $L(p)$

$$\Lambda(p) = \lambda_0 + L(p)\hat{k} \tag{5-10}$$

Equation (5-7) can then be written

$$\begin{pmatrix} F\big(Z(p), \lambda_0 + L(p)\hat{k}, p\big) \\ E\big(Z(p), \lambda_0 + L(p)\hat{k}, p\big) \end{pmatrix} = 0 \tag{5-11}$$

Differentiating (5-11) at (z_*, λ_*) with respect to p and applying the chain rule for derivatives yields a linear system

$$\begin{pmatrix} F_z & F_\lambda \hat{k} \\ E_z & E_\lambda \hat{k} \end{pmatrix}\Bigg|_* \begin{pmatrix} Z_p \\ L_p \end{pmatrix} = -\begin{pmatrix} F_p \\ E_p \end{pmatrix}\Bigg|_* \tag{5-12}$$

The matrix $\begin{pmatrix} F_z & F_\lambda \hat{k} \\ E_z & E_\lambda \hat{k} \end{pmatrix}\Big|_*$ is nonsingular by condition 2. Solution of equation (5-12) then yields L_p, the sensitivity of the security margin with respect to p. The first order estimate of the change in margin corresponding to the change in p of Δp is

$$\Delta L = L_p \Delta p \tag{5-13}$$

Solution of (5-12) additionally yields Z_p, the tangent vector at (z_*, λ_*, p_0) to the curve in state space that describes how the state variables change to satisfy the equilibrium and event conditions as p varies. Thus, $Z_p \Delta p$ is the first order Taylor series estimate of how the state changes on $H^{-1}(0)$ for a parameter change of Δp.

Since the matrix $\begin{pmatrix} F_z & F_\lambda \hat{k} \\ E_z & E_\lambda \hat{k} \end{pmatrix}\Big|_*$ is the same for any parameter p, once the matrix is factored and the sensitivities obtained for one parameter, computing the sensitivities for any additional parameters only requires obtaining the derivatives $\begin{pmatrix} F_p \\ E_p \end{pmatrix}\Big|_*$ and one forward and backward substitution.

If obtaining L_p for many parameters is of primary interest, and there is no desire to obtain Z_p, then full solution of the linear system (5-12) is not necessary. Since any set of $n+1$ vectors in R^n are linearly dependent there is a non-zero vector w such that

$$w \begin{pmatrix} F_z \\ E_z \end{pmatrix}\Bigg|_* = 0 \tag{5-14}$$

w is a vector orthogonal to the range of $\begin{pmatrix} F_z \\ E_z \end{pmatrix}\Big|_*$ and w is unique up to a scalar multiplication when $\begin{pmatrix} F_z \\ E_z \end{pmatrix}\Big|_*$ is full rank, which is guaranteed by condition 1. Pre-multiplying (5-12) by w yields

$$w \begin{pmatrix} F_\lambda \hat{k} \\ E_\lambda \hat{k} \end{pmatrix}\Bigg|_* L_p = -w \begin{pmatrix} F_p \\ E_p \end{pmatrix}\Bigg|_* \tag{5-15}$$

$w\begin{pmatrix} F_\lambda \hat{k} \\ E_\lambda \hat{k} \end{pmatrix}\Big|_*$ is not zero since $\begin{pmatrix} F_z & F_\lambda \hat{k} \\ E_z & E_\lambda \hat{k} \end{pmatrix}\Big|_*$ is nonsingular, so (5-15) can be solved to obtain the sensitivity with respect to p of the margin to the event.

$$L_p = -\frac{w\begin{pmatrix} F_p \\ E_p \end{pmatrix}\Big|_*}{w\begin{pmatrix} F_\lambda \hat{k} \\ E_\lambda \hat{k} \end{pmatrix}\Big|_*} \tag{5-16}$$

Note that regardless of the number of parameter under consideration, w needs to be computed only once.

The sensitivity of the security margin to changes in many parameters is effectively just an indexing operation once the scaled normal vector is obtained. The normal vector to the event boundary in parameter space defines to first order the proportions by which all the parameters must vary to keep the equilibrium at the security boundary. The normal vector is useful in determining the relative effectiveness of different parameters on the security margin. Note that if a point on the security boundary is obtained using a direct method that uses the E equations as corrector equations, obtaining the normal vector requires only one additional forward and backward substitution using the previously factored Jacobian matrix.

5.3.4 Sensitivity of margin to a Saddle-node bifurcation point

Suppose that we are concerned with locating the points at which the system equations F become singular, at points just like voltage collapse phenomena.

Suppose that the equilibria of the power system satisfy the equations

$$f(x, \lambda, p) = 0 \tag{5-17}$$

At a saddle node bifurcation, the Jacobian matrix f_x is singular. For each (x, λ, p) corresponding to a bifurcation, there is a left eigenvector $w(x, \lambda, p)$ (a row vector) corresponding to the zero eigenvalue of f_x such that

$$w(x, \lambda, p) f_x(x, \lambda, p) = 0 \tag{5-18}$$

The points (x, λ, p) satisfying (4-17) and (4-18) correspond to bifurcation and a curve of such points can be obtained by varying p about its nominal value p_*. Linearization of this curve about the bifurcation (x_*, λ_*, p_*) yields

$$f_x|_* \Delta x + f_\lambda|_* \Delta\lambda + f_p\big|_* \Delta p = 0 \tag{5-19}$$

where f_λ is the derivative of f with respect to the load powers λ and f_p is the derivative of f with respect to the parameter p. "$|_*$" means "evaluated at (x_*, λ_*, p_*)". Pre-multiplication by $w = w(x_*, \lambda_*, p_*)$ yields

$$wf_\lambda|_* \Delta\lambda + wf_p\big|_* \Delta p = 0 \tag{5-20}$$

since (5-18) implies that $wf_\lambda|_* = 0$. Equation (5-20) can be interpreted as stating that $(wf_\lambda|_*, wf_p|_*)$ is the normal vector at (λ_*, p_*) to the bifurcation set in a load-power parameter space.

Using the parameterization of λ by L from (4-5) yields $\Delta\lambda = \hat{k}\Delta L$ and it follows

$$wf_\lambda \hat{k} \Delta L + wf_p \Delta p = 0 \tag{5-21}$$

The sensitivity of load margin to the change in parameter is

$$L_p\big|_* = \frac{-wf_p\big|_*}{-wf_\lambda|_* \hat{\mathrm{k}}} = 0 \tag{5-22}$$

For the linear estimate we use (4-22) and

$$\Delta L = L_p\big|_* \Delta p \tag{5-23}$$

The linear estimate holds for multiple parameters p, in which case $wf_p|_*$ is a vector.

5.3.5 Sensitivity-based branch outage contingency analysis

Contingencies such as unexpected line outages can lead to voltage collapse blackouts. These contingencies generally reduce or even eliminate the load margin to collapse. It is hence desirable to estimate the effect of contingencies on voltage stability margin. The line outage can be modeled by changing the admittance of the underlying line. The loading margin can then be recomputed. However, re-computing the loading margin can be avoided: if the loading margin can be viewed as a smooth function of the line admittance, then the sensitivity of the loading margin with respect to changes in the admittance can be calculated and used to estimate the change in the loading margin due to the line outage.

For each single non-radial line outage the parameter p is a vector with only three components – one each for conductance, susceptance, and shunt capacitance of the outage line. The first step in the computation is to obtain the projected direction of load increase from the short-term load forecast. For λ_0, the current vector of load parameters and λ_1, the forecasted short term load, the vector $\hat{k} = \frac{\lambda_1 - \lambda_0}{|\lambda_1 - \lambda_0|}$ defines a unit vector in the direction of load increase.

The second step is to compute the corresponding SNBP or LIBP by CPFLOW. During the continuation, the system equations will change due to the occurrence of limits such as reactive power limits. The third step is to compute the various quantities at the bifurcation point and then, for each contingency, evaluate the sensitivity formulas.

Let Δp be the negative of the admittance vector for the outage branches. The linear estimate for the resulting change in margin is:

$$\Delta L = L_p \Delta p = -\frac{w F_p \Delta p}{w F_\lambda \hat{k}} \tag{5-24}$$

The denominator of (4-24) is a scaling factor that is the same for all contingencies. The numerator of (4-24) contains the vector $F_p \Delta p$ which, since p appears linearly in F, is just the terms in F that contain p. For F representing real and reactive power balance, $F_p \Delta p$ is the vector of the pre-contingency real and reactive power injections on the outage branch. The linear formula is simply the power injections from the outage lines scaled by the normalized left eigenvector $\tilde{w} =$ tor $\tilde{w} = -w/w F_\lambda \hat{k}$:

$$\Delta L = \tilde{w}^{P_i} P_i + \tilde{w}^{Q_i} Q_i + \tilde{w}^{P_j} P_j + \tilde{w}^{Q_j} Q_j \tag{5-25}$$

where P and Q are the pre-contingency real and reactive power injections to the outaged line, i and j indicate the buses connected by the outage line, and $\tilde{w}^{P_i}$ represents the scaled left eigenvector component corresponding to real power balance at bus i. Formula (5-25) implies that lines with small flows are guaranteed to have small linear estimates.

Radial line outages that isolate a portion of the network are a special case in which the power balance equations of the isolated bus should be deleted from F. Thus, for a radial line outage F_P has only 2 nonzero rows corresponding to power balance at the connected bus.

5.3.6 The enhanced look-ahead contingency ranking technique

To improve the speed and accuracy of estimating load margins, we develop a sensitivity-based scheme to determine the 'location' on the power flow solution curve for computing the second power flow solution. We also develop a reselection scheme to select two power flow solutions for curve fitting of the power flow solution curve passing through the nose point. These two schemes are described in the following.

Sensitivity-based scheme

Whereas the sensitivity-based method is very fast, the load margin estimation results obtained by this method are usually inaccurate. In addition, the method cannot identify insecure contingencies that lead to voltage collapse. We propose to use the load margin estimated by this fast method as a guideline to compute the second power flow solution. We next briefly describe the sensitivity-based method.

For a single branch-outage contingency i, the change of load margin relative to the base-case load margin can be linearly approximated as follows:

$$dM_i = \frac{\partial M}{\partial g_i} g_i + \frac{\partial M}{\partial b_i} b_i + \frac{\partial M}{\partial c_i} c_i \tag{5-26}$$

where, g_i, b_i and c_i are the conductance, susceptance and shunt capacitance of branch respectively. $\partial M/\partial g_i$, $\partial M/\partial b_i$ and $\partial M/\partial c_i$ are the sensitivities of load margin with respect to conductance, susceptance, and shunt capacitance of branch i at the nose point of base-case. Hence,

$$M_i = M - dM_i \tag{5-27}$$

where M is the load margin of the base-case and M_i is the estimated load margin for single branch contingency i. A multiple-branch-outage can be similarly treated and super-imposed.

For a generator outage j, the change of load margin can be approximated as:

$$dM_j = \frac{\partial M}{\partial P_{g,j}} P_{g,j} + \frac{\partial M}{\partial Q_{g,j}} Q_{g,j} \tag{5-28}$$

where $P_{g,j}$ and $Q_{g,j}$ are the real power and reactive power of generator respectively. $\partial M/\partial P_{g,j}$ and $\partial M/\partial Q_{g,j}$ are the sensitivities of load margin with respect to generator real power and reactive power respectively. Hence, the estimated load margin can be linearly approximated as follows:

$$M_j = M - dM_j \tag{5-29}$$

A multiple-generator-outage can be similarly treated and super-imposed. Since the load margin calculation is a nonlinear problem, the above sensitivity-based method cannot yield accurate results. However, due to its fast speed, we propose to apply the sensitivity-based method to obtain a suitable step-size described below for computing the second solution

$$\lambda_{step,k} = \lambda_{M_k} \tag{5-30}$$

where λ_{M_k} is the parameter value corresponding to the load margin M_k obtained by the sensitivity-based method. We then apply the CPFLOW to compute the second power flow solution with the step-size described in (5-30).

To compensate the possible inaccuracy in the step-size selection scheme (4-30), we develop an automatic step-size shrinking scheme incorporated into continuation power flow for new step length selection. When CPFLOW fails to compute the second power flow solution, the following scheme applies: run CPFLOW with a new step-size, which equals 80 percent of the current step-size; repeat this step-size selection, if necessary, for a few iterations.

Reselection scheme

The estimated load margin by the look-ahead method is likely to be inaccurate if the computed power flow solution is still far away from the corresponding saddle-node bifurcation point. It then calls for computing another power flow solution closer to the saddle-node bifurcation

point. We use the following criterion to check whether the computed power flow solution can be used to estimate the load margin.

$$\frac{\lambda_b - \lambda_2}{\lambda_2} < k \tag{5-31}$$

where, λ_b is the load margin estimated by the look-ahead function method, λ_2 is the parameter value associated with the second power flow solution, k is a pre-defined value; say 0.15. When this criterion is satisfied, it implies that the second power flow solution is close to the bifurcation point and the estimated load margin is accurate and yet conservative. The conservative property, a desired property, is a by-product during the procedure of power flow computation.

If the criterion (5-31) is not satisfied (i.e. the computed power flow solution is far away from the bifurcation point), then another power flow solution closer to the bifurcation point than the current one is needed. Under this situation, we set this second solution as the first solution point and use the following step size to compute next power flow solution:

$$\lambda_{step} = \alpha(\lambda_b - \lambda_2) \tag{5-32}$$

where, α is step size factor. It is set to 0.5 in this paper. This step size definitely is smaller than $\lambda_b - \lambda_2$.

When this scheme is used, it needs to compute three or more power flow solutions. However, it is worthy to spend a little more time to obtain more accurate results. Fortunately, our numerical experiences indicate that only a few contingencies in a contingency list need this scheme.

Step by step description of the method

A step-by-step description of the enhanced method is given below:

Step 1: For a load/generation variation direction, apply CPFLOW to compute the exact bifurcation point of base case.

Step 2: For a credible contingency set, apply the sensitivity-based scheme to compute a suitable step length for each contingency.

Step 3: For each contingency, say, contingency i, compute the estimated $\lambda_{b,i}$ via the following seven steps.

Step 3.1: Compute the power flow solution of post-contingency system. If a power flow solution is found, set this solution x_1 the first point and go to step 3.2; if the power flow diverges, this contingency is insecure and set $\lambda_{b,i} = 0$.

Step 3.2: Compute the second power flow solution x_2 by CPFLOW using the step length obtained at step 2.

Step 3.3: If the power flow solution cannot be found, then compute the second point by using the automatic step length shrinking technique until a solution is obtained.

Step 3.4: Use the curve fitting technique to estimate the load margin $\lambda_{b,i}$ for this contingency.

Step 3.5: Check whether the estimated load margin $\lambda_{b,i}$ is satisfied with criterion (5-31). If the criterion is satisfied; then go to Step 3.1; otherwise, check whether the second power flow solution obtained is via the step-size shrinking technique (not via the sensitivity-based scheme). If it is, then a limit-induced bifurcation point is detected and this point is far away from the nose point and go to Step 3.6; otherwise, go to Step 3.7.

Step 3.6: Reset the estimated load margin by using the load margin to the second power flow solution as the estimated load margin $\lambda_{b,i}$ for this contingency and go to Step 3.1.

Step 3.7: Set this second point as the first point and compute a new second point by using the step-length obtained by (5-32) and go to step 3.3.

Step 4: Rank the contingency list based on the estimated load margin $\lambda_{b,i}$.

Remarks

For a contingency with an associated limit-induced bifurcation point, the above enhanced method estimates the load margin in the following way: if the limit-induced bifurcation point is close to the nose point (i.e. criterion (5-31) is satisfied), then the estimated load margin is set to be the estimated load margin to the nose point; otherwise, we use Step 3.5 and Step 3.6 to estimate its load margin.

5.4 Indices for On-line VSA

A number of performance indices intended to measure the severity of the (static) voltage stability problem have been proposed in literature. These indices intend to provide some measure of how far the system is away from the point at which the system Jacobian becomes singular. Among them, the following indices receive considerable attention of different degree:

- Minimum singular value
- Voltage drops
- Real and/or reactive power losses
- Condition number of the system Jacobian
- Angular distance between the current stable equilibrium point and the closest unstable equilibrium point in a Euclidean sense.
- Energy distance between the current stable equilibrium point and the closest unstable equilibrium point using an energy function.

These performance indices can be viewed as providing some measure relative to the distance between the current operating point and the bifurcation point. These performance indices, however, are defined in the state space of power system models instead of in the parameter space. Thus, these performance indices cannot directly answer questions such as: "Can the system withstand a 100 MVAR increase on bus 11?" or: "Can the system withstand a simultaneous increase of 70 MW on bus 2 and 50 MVARs on bus 6?"

In order to provide a direct relationship between its value and the amount of load increases that the system can withstand before instability, the performance index must be developed in the parameter space (i.e. the space of load demands) rather than the state space where the existing performance indices were developed. A look-ahead performance index intended for on-line application was proposed and evaluated in [86,87]. Given (i) the current operating condition (obtained from the state estimator and the topological analyzer), (ii) the near-term load demand at each bus (obtained from predictive data, and short-term load forecaster), (iii) the real power dispatch (say, based on economic dispatch), this index provides a load margin measure (MW and/or MVAR) to assess the system's ability to withstand both forecasted load demands and real power variations. However, like all the existing performance indices developed so far, the look-ahead performance index also does not take into account considerations of physical constraints on OLTC and generator VAR limits. The look-ahead performance index is used for contingency ranking.

5.5 Contingency Analysis on Voltage Stability

On-line voltage stability analysis includes contingency screening, ranking and detailed analysis and provides a list of the insecure contingencies, critical contingencies and secure contingencies in terms of voltage stability margins, from a full, comprehensive contingency list. The load margin calculation determines the voltage stability margin in megawatts (MW) and megavar (MVAR), between the voltage collapse point (or the thermal limit violation point) and the current power system operation point. The VSA&E package also provides the operators as well as reliability engineers look-ahead analysis, enhancement control (for critical contingencies) and preventive control (against insecure contingencies) along with the load margin and sensitivity information with respect to voltage collapse, voltage violation and thermal limit violation.

For practical applications, a contingency is composed of a single or multiple items. Line, transformer, shunt, load and generator outages are considered in the contingency. A contingency can be a combination of line outages, generator outages, shunt capacitor outage, or load outages.

An *insecure contingency* is a contingency whose corresponding load margin to voltage collapse is negative or zero. The base-case power system will suffer from a voltage collapse should an inse-

cure contingency occur. A *critical contingency* is a contingency whose corresponding load margin to voltage collapse is positive but small. The base-case power system will be close to the verge of a voltage collapse should a critical contingency occur. Given a list of credible contingencies, it is imperative to identify the insecure contingencies and the critical contingencies.

Given a set of credible contingencies, the contingency screening strategy would break the task of on-line VSA into three stages of assessments:

1. Screening stage: perform the task of contingency screening to screen out contingencies which are definitely voltage stable from a set of credible contingencies
2. Ranking stage: perform the task of contingency ranking in terms of load margin for each contingency remaining in Stage 1.
3. Detailed Analysis stage: perform detailed analysis via computation of P-V, Q-V and P-Q-V curves for the top-ranked contingencies

There are three major components in the architecture of the online VSA: a contingency screening program, a contingency ranking program and a fast and reliable continuation power flow simulation program. A new cycle of VSA is initiated based on the present state, network topology and the predictive data of the power system. When a new cycle of VSA is warranted, a list of credible contingencies, along with information from the state estimator and topological analysis, are applied to the contingency screening program whose basic function is to screen out contingencies that are definitely stable. Contingencies that are classified to be definitely stable are eliminated from further analysis.

It is the ability to perform contingency screening on a large number of contingencies and filter out a smaller number of contingencies requiring further analysis that would make on-line VSA feasible. Contingencies which are either undecided or identified as unstable are then sent to the ranking function program whose basic function is to select from the undecided contingencies those critical contingencies for detailed analysis using the continuation power flow method.

It is important to accurately identify the top most severe contingencies that include insecure contingencies from a list of credible contingencies. To this end, we propose the following three-stage approach [89]

1. Perform contingency screening to the contingency list using a linear, sensitivity based method.
2. Perform contingency ranking to the contingencies screened out at Stage 1 using an enhanced look ahead load margin quadratic approximation method.
3. Perform detailed analysis to the top-ranked contingencies at Stage 2 using the Continuation Power Flow Method.

It is interesting to note that a linear method is used in stage 1 for speedy analysis, a quadratic estimation method is used in stage 2 for more accurate estimation of load margin with a modest speed while a comprehensive nonlinear method is used in stage 3 for accurate and detailed analysis of top-ranked contingencies.

5.6 Characterization of Nose Points

It is well known that the nose point can be a saddle-node bifurcation point [76,77,83-85]. It is less known that the nose point can be a peculiar bifurcation point, structure-induced bifurcation point [80-82]. Structure-induced bifurcation (also termed Q-induced bifurcation) manifests itself as a sudden disappearance of stable equilibrium point as one or more parameters are varied and the underlying vector field is altered. Indeed, traditional local bifurcations are usually caused by the (independent) parameter variations of a vector field while Q-induced bifurcations are caused by the parameter variations of a parameter-dependent vector field; resulting in the changes of the vector field. The structure-induced bifurcation has been studied and illustrated on a 3-bus power system in [80]. Further insights of structure-induced bifurcation in power systems on both small and large systems such as a 5200-dimensional system can be found in [82].

Q-induced bifurcation is different from traditional bifurcations such as saddle-node bifurcations and Hopf bifurcations. One common feature of these traditional bifurcations is that one of the system eigenvalues crosses the imaginary axis as parameters vary. On the other hand, Q-induced bifurcation in power systems occurs while the real parts of all of its corresponding eigenvalues remain negative. Physically speaking, a structure-induced bifurcation in power system occurs due to load increases (parameter variation); causing one or more generators reach their reactive power (also termed Q) limits which in turns changes the underlying power flow equations (i.e. the vector field is altered).

The mathematical mechanism behind the transition is the switching of the system model from one set of power flow equations into another set of power flow equations and is characterized by the following:

- the stable equilibrium point suddenly disappears.
- a new unstable equilibrium point emerges when the parameter decreases.
- a new unstable equilibrium point emerges when the parameter increases.
- there is no other stable equilibrium point (of the corresponding new system) beyond the structure-induced bifurcation value.

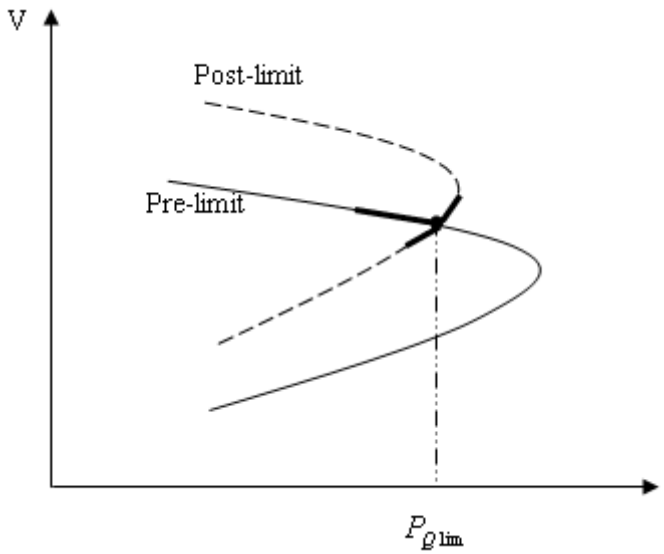

Figure 5-1: The case that system loses its stability when reactive power of generator reaches its limit (the bus type is changed from PV to PQ), structure-induced bifurcation causes voltage collapse immediately

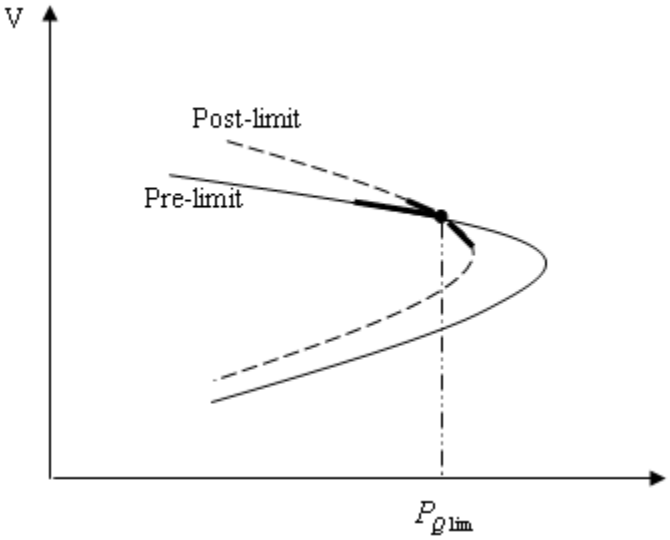

Figure 5-2: The case that system remain its stability when reactive power limit of generator is encountered (the bus type is changed from PV to PQ), load can be increased until saddle node bifurcation (SNB) causes voltage collapse

The corresponding bifurcation diagram is shown in Figure 5-1 in which the stable equilibrium point disappears beyond the structure-induced bifurcation value and a new unstable equilibrium point emerges. Furthermore, the new unstable equilibrium point is of type-one. Hence,

there is no near-by stable equilibrium point after the bifurcation. The consequence of structure-induced bifurcation is an immediate instability induced by generator reactive power limits. The dynamic consequence of Q-induced bifurcation is dangerous since, beyond the structure-induced bifurcation value, there is no stable equilibrium point nearby. This dynamic consequence is quite similar to the dynamic consequence of saddle-node bifurcation point.

A structure-induced exchange process occurs in which the stable equilibrium point suddenly jumps into another stable equilibrium point when the structure-induced exchange value is crossed. The dimension of new SEP is different from that of the old SEP. The corresponding 'bifurcation' diagram is shown in Figure 5-2. We note that the structure-induced exchange process is not a bifurcation.

Another fundamental difference between the structure-induced bifurcations and the traditional bifurcation is that the number of system equations before the structure-induced bifurcation and that after the bifurcation is different by one while the dimension before and the dimension after the traditional local bifurcation are the same. In this regard, SIB is similar to the new type of bifurcation of non-smooth dynamical systems; the so-called border collision bifurcation has been discovered in recent years. Border collision bifurcation involves some kind of switching action that makes the system toggle between two or more different types of dynamic behavior. In general, a border collision bifurcation occurs when a fixed point collides with the borderline between two smooth regions in the discrete state space, resulting in an abrupt change in the system behavior. The system usually jumps into another stable operating orbit after border collision.

Physically speaking, SNB is related to transmission limitation while SIB is related to reactive power deficiencies. Hence, the following two different types of bifurcation points and their corresponding load margins and sensitivities are computed.

- Saddle node bifurcation point (SNB nose point)
- Structure-induced bifurcation point (SIB nose point).

The exact computation of SNB is based on the simplified set of characteristic equations derived in [78,79] while the exact computation of SIB is based on the set of characteristic equations derived in [82]. In addition, the voltage violation points and the thermal limit violation points and sensitivity calculations at these points (violation points, bifurcation point or limit point) are needed as they provide a variety of valuable information to operators.

6. A Renewable-Energy-Integrated Analysis Platform

6.1 Introduction

The drive for cleaner sources of energy has led to the proliferation of renewable energy sources, such as wind and solar energy, in today's power systems. However, most of these renewable energy sources are inherently stochastic and as a result introduce more uncertainty into the power system. Forecasters, which are constructed based on different disciplines, are used by power utilities to predict most probable renewable energy outputs in the planning horizon. These forecasters are never perfect due to the inherent variability of the renewable energy. On the other hand, power system operations need to be planned to accommodate various possible scenarios, such that the power system can still operate securely and economically should any considered scenario occur within the planning horizon. Therefore, power system computation and analysis, such as voltage stability analysis (VSA), dynamic stability analysis (DSA) and optimal power flow (OPF) computation, involving probabilistic scenarios become more and more common because of the increasing penetration of renewable energies into the power grid.

However, the number of renewable energy scenarios credible for computation and analysis can be large. These renewable scenarios follow some proper probabilistic distribution function of the energy output of the renewable source under study; therefore, there could be a countless number of possible renewable scenarios in theory. In practice, renewable scenarios are generated through probabilistic distribution sampling techniques, but the number of scenarios can still be large. Such a large number of scenarios make it prohibitive to carry out the desired computation and analysis for the power system if all scenarios need to be processed concurrently. Therefore, a preprocessing procedure for reducing the number of scenarios to be involved in the actual computation for analysis becomes a necessity.

We have developed a renewable-energy-integrated computation and analysis platform for power utilities to effectively deal with increasing penetrations of renewable energy. A high-level structure of our solution is illustrated in Figure 6-1. The system consists of two major parts, that is, BSI renewable scenario program and our power system computation and analysis tools. The renewable scenario program is composed of three modules, which are

- Module I – Error distribution function: this module models the error distribution of the renewable energy forecasts, based on historical records of the forecasted and real outputs of the renewable energy.
- Module II – Scenario generation: this module generates a large list of renewable scenarios through sampling the associated distribution function.
- Module III – Scenario reduction: this module reduces the list of renewable scenarios to a reasonable size, while still capturing representative patterns of the whole set of scenarios.

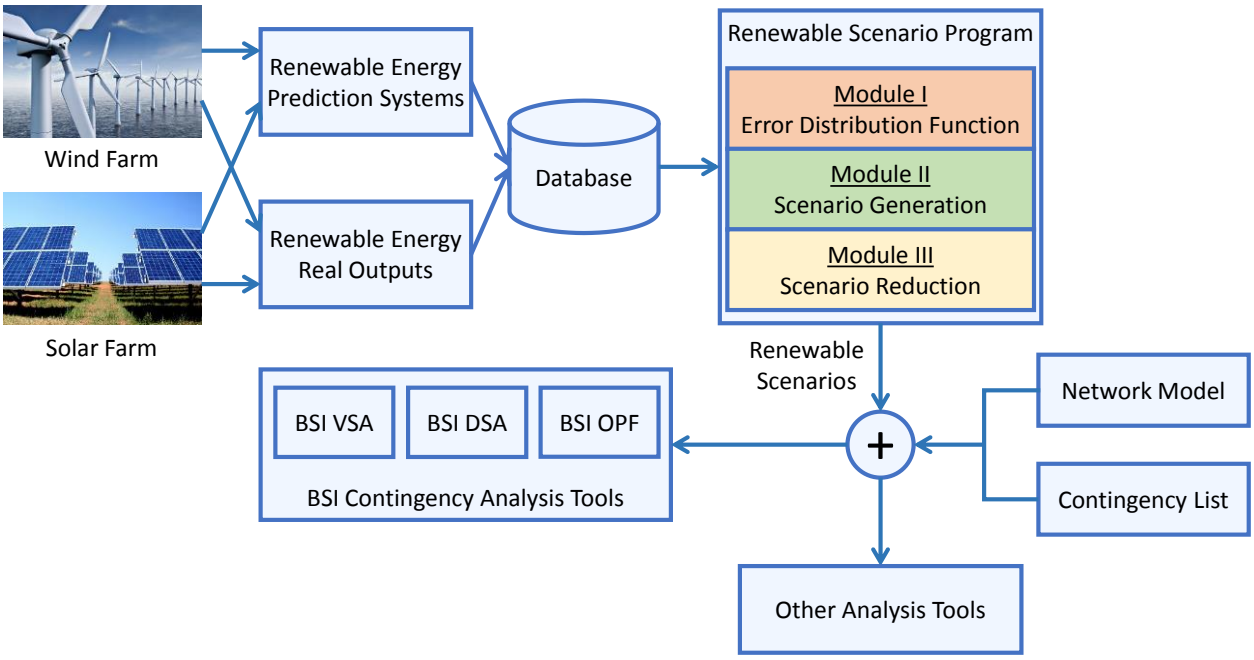

Figure 6-1: The renewable-energy-integrated analysis platform

Along with the system network model and a contingency list, the resulting concise set of renewable scenarios are ready to be used for routine power system computation and contingency analysis. Since the inception 20 years ago, we have developed a portfolio of advanced power system computation and contingency analysis tools. Part of the portfolio includes:

- VSA&E: the program to evaluate voltage security of the system based on real-time system operating conditions.
- TEPCO-BCU: the program to perform on-line exact transient stability assessment and available transfer capability evaluation.
- SuperOPF: the program to perform AC OPF analysis with comprehensive modeling capability and reliable and high-quality solutions.

Empowered by our proprietary methodology of ***screening***, ***ranking*** and ***detailed analysis***, our solution provides a portfolio of viable tools for comprehensive analysis and assessment of power systems with high penetration of renewable energy. The three modules of the proposed renewable scenario program are detailed in the following sections of this document.

6.2 Module I: Error Distribution Function

There are two major sources of uncertainty in renewable energy, of which one is introduced by the forecast error and the other is introduced by the unplanned outages of the renewable power units. The first source of uncertainty is related to the impossibility of producing a perfect renewable energy forecast. Different methods to estimate the uncertainty of deterministic (i.e. point) forecasts have been developed. The uncertainty of the deterministic forecast can be represented by different approaches. For wind power, the most common one is a nonparametric probabilistic forecast represented by quantities, intervals or probability density functions; the other two representations are the risk indices of the forecasts, and scenarios incorporating temporal or spatial interdependence structures of prediction errors. For solar energy, the uncertainty introduced by the irradiation forecast error could also be represented by different approaches including probability density functions, standard deviation models or auto-regression models.

In the proposed renewable energy platform, the probability density function approach is implemented. To this end, we have developed a dedicated module for modeling the distribution functions of renewable forecast errors. The structure of this module is illustrated in Figure 6-2.

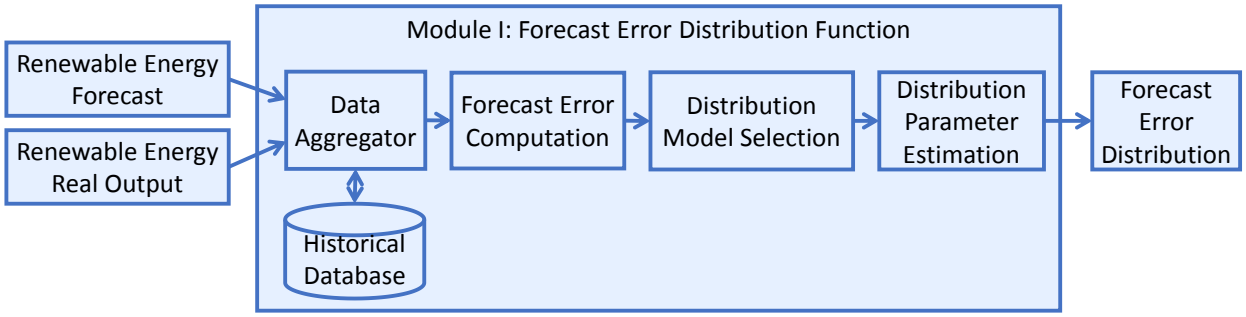

Figure 6-2: The renewable forecast error distribution function module

This module aggregates both real and forecasted outputs for the renewable source and stores them in a historical database. The forecast error, that is, the difference between the synchronized forecasted outputs and the real outputs, is computed throughout the historical horizon. Based on the aggregated renewable forecast error data, a proper distribution model will be selected and parameters of the model will be computed, which combined specify the resulting forecast error distribution.

Each renewable node (a substation) in the power grid will be assigned a unique error different distribution function, according to following facts:

- The type of renewable source.
- The forecaster employed for predicting renewable energy.

- The geographical location of the node.

It needs to be noted that the distribution of error or forecast output is a conditional probability function with respect to the forecast value. Therefore, for different ranges of forecast values, different set of model parameters will also be determined.

We have implemented a set of popular distribution function models in this module. These functions, including their probability distribution function (PDF), cumulative distribution function (CDF), and model parameters, are summarized in Table 6-1.

Table 6-1: Supported probability distribution functions

Distribution	PDF	CDF	Parameters
Normal	$f(x) = \frac{1}{\sigma\sqrt{2\pi}} e^{-\frac{(x-\mu)^2}{2\sigma^2}}$	$F(x) = \frac{1}{2}\left(1 + \text{erf}\left(\frac{x-\mu}{\sigma\sqrt{2}}\right)\right)$	μ, σ
Beta	$f(x) = \frac{\Gamma(\alpha+\beta)}{\Gamma(\alpha)\Gamma(\beta)} x^{\alpha-1}(1-x)^{\beta-1}$	$F(x) = \frac{\Gamma(\alpha+\beta)}{\Gamma(\alpha)\Gamma(\beta)} \int_0^x t^{\alpha-1}(1-t)^{\beta-1} dt$	α, β
Cauchy	$f(x) = \frac{1}{\pi\gamma}\left(1 + \left(\frac{x-x_0}{\gamma}\right)^2\right)^{-1}$	$F(x) = \frac{1}{\pi}\arctan\left(\frac{x-x_0}{\gamma}\right) + \frac{1}{2}$	$x_0, \gamma > 0$
Weibull	$f(x) = \begin{cases} \frac{k}{\lambda}\left(\frac{x}{\lambda}\right)^{k-1} e^{-\left(\frac{x}{\lambda}\right)^k} & x \geq 0 \\ 0 & x < 0 \end{cases}$	$F(x) = \begin{cases} 1 - e^{-\left(\frac{x}{\lambda}\right)^k} & x \geq 0 \\ 0 & x < 0 \end{cases}$	$\lambda > 0,$ $k > 0$
Versatile	$f(x) = \frac{\alpha\beta e^{-\alpha(x-\gamma)}}{(1+e^{-\alpha(x-\gamma)})^{\beta+1}}$	$F(x) = \left(1 + e^{-\alpha(x-\gamma)}\right)^{-\beta}$	α, β, γ

6.3 Module II: Scenario Generation

The computed error distribution function in module I is used for scenario generation. The structure of the module for scenario generation is provided in Figure 6-3. For each renewable energy unit, its error distribution functions and the expected or forecasted power injection (i.e., the renewable generation) into the power network are provided. Based on the error distribution functions and the expected or forecasted value of renewable generation, the probability distribution function of the renewable power injection into the power network at the node can be computed. More specifically, the nodal renewable power injection distribution function is

$$g(x) = f(x - p_0), \tag{6-1}$$

where, p_0 is the expected or forecasted value of the power injection. It needs to be reiterated that though the model of the distribution function is fixed for the node, parameters of the distribution function are dependent on the value of p_o.

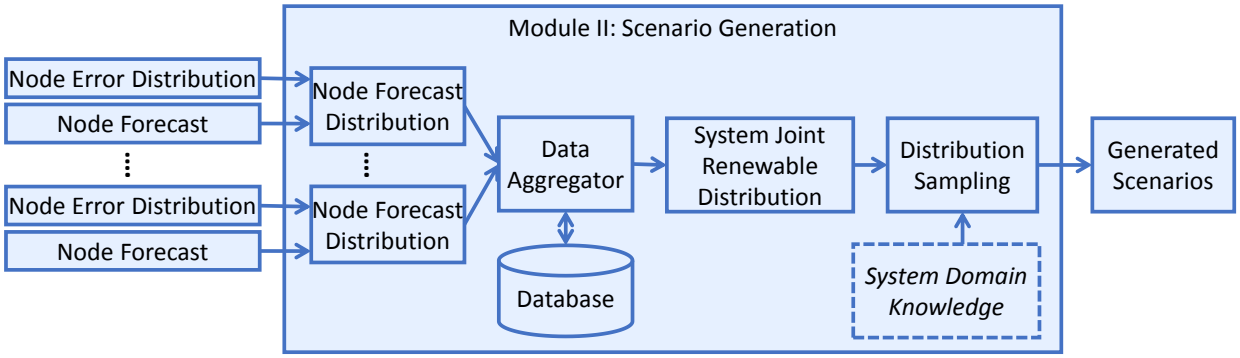

Figure 6-3: The scenario generation module

Power injection distribution functions for all renewable energy nodes in the network are aggregated and stored in the database. Based on the aggregated data, a joint probability distribution function is determined for the system renewable power injections. Since the distribution function is a continuous real-valued function, it is not plausible to use the distribution function directly in the follow-up computation and analysis. Therefore, a sampling process is necessary, such that discrete scenarios obeying the distribution can be produced.

Sampling the distribution function to generate renewable scenarios can be realized through different methods. The basic method naively utilizes conventional distribution sampling techniques, such as

- Monte Carlo (MC) sampling: MC generates scenarios randomly from the renewable distribution function over the domain (the multi-dimensional allowable range of renewable generation outputs, where the dimension equals to the number of renewable generation units).
- Latin hypercube sampling (LHS): LHS is a statistical method for generating a sample of plausible collections of parameter values from a multidimensional distribution, where each sample is the only one in each axis-aligned hyperplane containing it. LHS ensures that the ensemble of random numbers is representative of the real variability.

Besides the basic version, we have also developed an advanced version of the scenario generation module. The advanced module takes advantage of domain knowledge into the procedure of distribution sampling. Instead of naively following the probability distribution function, the sampling is also biased by the importance of each renewable generation unit. More specifically, more scenarios will be generated associated with renewable generation units that are important to the application target; while fewer scenarios will be generated associated with renewable generation units with less influence to the application target.

6.4 Module III: Scenario Reduction

The number of forecast scenarios generated through distribution sampling can still be large. Such a large number of scenarios make it prohibitive to carry out the desired analysis if all scenarios need to be considered simultaneously, such as security-constrained optimal power flow analysis that needs to co-optimize the involved contingencies. Therefore, a preprocessing procedure becomes a necessity for reducing the number of scenarios involved in the actual computation for analysis while still being able to capture representative patterns of the whole set of scenarios.

Studies have found that different scenarios (contingencies, renewable energy forecasts, etc.) may possess varying degrees of similarity, in terms of their influences to the system operating states. More specifically, different scenarios can have a group property; in other words, scenarios within the same group are close to each other in terms of some similarity metrics. In addition, influence of the scenarios in a same group upon the system can be well described by a few representative scenarios belonging to the group. This consideration provides a way to reduce the number of scenarios to be involved in actual computation.

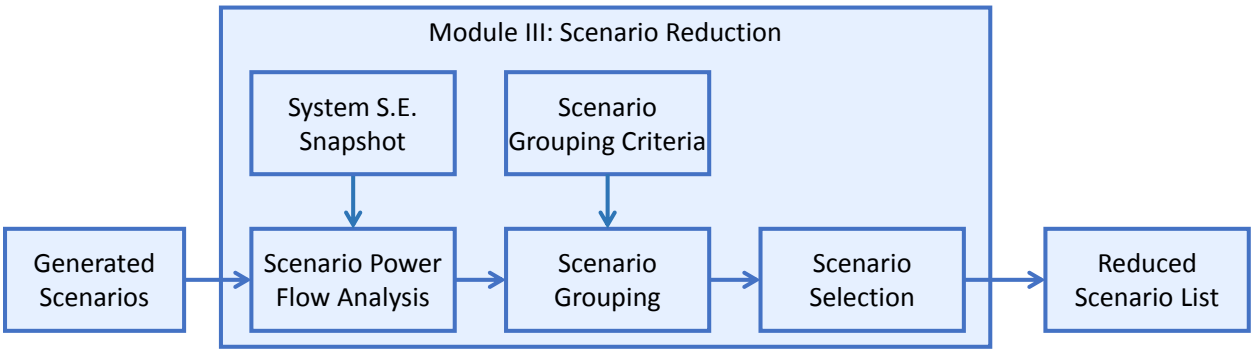

Figure 6-4: The scenario reduction module

We have developed a dedicated module for scenario reduction, whose structure is illustrated in Figure 6-4. This module implements the following procedure for scenario reduction:

- Step 1: Obtain the preliminary list of scenarios to be reduced.
- Step 2: Perform scenario power flow analysis. Potential influence of each scenario on the system is evaluated by performing a power flow analysis on the system with the scenario enforced.
- Step 3: Carry out scenario grouping. Similar scenarios should have similar influences on the system. Therefore, the scenarios under study can be grouped based on the system values obtained after the power flow analysis. For example, scenarios can be grouped

based on their similarity of system voltage profiles, using some clustering techniques. In practice, the criteria used for grouping scenarios are application-oriented.

- Step 4: Select representative scenarios. Once the groups of the generated scenarios have been found, representative scenarios in each group are to be determined. For example, the center and a few points in each group can be selected as representative scenarios. This pool of selected scenarios will be the actual list of scenarios to be involved in computation.

To perform scenario reduction, the following data is required by the program as input:

- The system network data: it provides the network topology and base case operating states of the power system under study, which can be a state estimation (SE) snapshot of the system. The data should be organized in industrial standard file formats, such as PSS/E, PSLF, and CIM formats that are supported by the program.
- The preliminary list of scenarios: it provides a list of scenarios (contingencies, renewable energy forecasts, etc.). This list can contain a large number of scenarios, based on which the scenario grouping will be carried out.
- The scenario grouping and selection settings: Several preferences might also be specified as input to the program. The user might provide preferences on the grouping criteria, such as 1) based on which values (the voltage profile, system violations, etc.) the scenarios will be grouped and 2) the approximate number of final scenarios to be output by the program.

After applying the procedure of scenario reduction, a significantly reduced list of scenarios will be determined by the module. This selected list of scenarios will be the ones that are actually involved in the follow-up computation and analysis.

7. Basic OPF Functionality Evaluations

In this chapter, the basic functional aspects of SuperOPF is evaluated and compared with that of PSSE OPF. PSSE OPF implements an interior point method (IPM) as the solution method [58]. In PSSE OPF, discrete controls (transformers and switched shunts) are treated as continuous and then rounded off to the nearest discrete value.

7.1 Solution Quality and Speed

The OPF solution are computed by PSSE OPF and SuperOPF and their objective values (system generation costs) are compared. For the 118-bus system, both programs can compute the OPF solution under the three loading conditions, as shown in Table 7-1. It can be observed that, the cost of solution by SuperOPF is consistently lower (better) than that by PSSE OPF, although the different (about 0.3%) is not that significant.

Table 7-1: OPF solution objective of 118-bus system

CASE 118	System Load	PSSE OPF	SuperOPF	
			Continuous	Improvement
Load1	4242.00MW	130098.01	129615.03	0.37%
Load2	6777.88MW	234316.95	233612.61	0.30%
Load3	7313.51MW	257394.50	256527.03	0.34%

For the 3120-bus system, PSSE OPF cannot complete the computation (blown up after a few iterations); that is, this case is unsolvable for PSSE OPF. Therefore, only the solution by SuperOPF is included in Table 7-2.

Table 7-2: OPF solution objective of 3120-bus system

CASE 3120	Load	PSSE OPF	SuperOPF
Base case	21174.71MW	Unsolvable	3164727.15

On the 118-bus system, the CPU times required by the two solvers are summarized. It can be observed that, in terms of computational speed, PSSE OFP is better in that it can achieve the OPF solution in fewer iterations and thus using less CPU time. However, the time difference is not that significant and the two solvers are at the same level, as shown in Table 7-3.

Table 7-3: Solution time

CASE 118	Load	PSSE OPF	SuperOPF
Load1	4242.00MW	14 iter, 0.039 sec	16 iter, 0.054 sec
Load2	6777.88MW	14 iter, 0.027 sec	16 iter, 0.053 sec
Load3	7313.51MW	14 iter, 0.020 sec	16 iter, 0.053 sec

CPU time used by SuperOPF for the two testing system is summarized in Table 7-4. It needs to be noted that, for the 3120-bus system, the two-staged method (that is, SuperOPF-IPM followed by SuperOPF-TJU) is used to speed up the computation.

Table 7-4: CPU time vs problem size

CASE	118-bus	3120-bus		
CPU Time	16 iter, 0.054 sec	Total Time	SuperOPF-TJU Stage	SuperOPF-IPM Stage
		5.12 sec	62 iter, 2.62 sec	27 iter, 2.17 sec

7.2 Discrete Variables

Power system contains discrete variables (transformer tap ratios, phase shifts, switchable shunts). SuperOPF is able to enforce discrete values for these variables by solving a corresponding mixed-integer nonlinear program. The method for BSI SuperOPF to handle discrete variables is detailed in Appendix A. By implementing the mentioned discretization method in SuperOPF, the user can easily control the number of iterations (and roughly the closeness to the true optimal MINLP solution) he/she wants to be carried out to determine all discrete variables. For example, if the user wants to finish the discretization in 5 adjustments, he/she can specify the threshold values to be, for example, $\hat{\eta}_{th}$ =0.1, 0.2, 0.3, 0.4, 0.5 for the five discretization iterations. The threshold value for the last discretization iteration is always set to 0.5 to ensure all discrete variables are determined in the final solution. In this way, SuperOPF program provides

user enough flexibility to balance between the quality of the discretization and the computational time to be consumed.

SuperOPF supports full discrete control adjustment with a sensitivity-based method (Appendix A), while PSSE has only a very limited capability to enforce discrete controls by simple rounding off. The discretization results on the 118-bus system are shown in Table 7-5. It can be observed that, the solution objective after SuperOPF discretization is very close to the relaxed continuous solution.

Table 7-5: Discretization on 118-bus system

CASE 118	Load	PSSE OPF	SuperOPF		
			Continuous	Discrete	Change
Load1	4242.00MW	130098.01	129615.03	129615.49	0.000355%
Load2	6777.88MW	234316.95	233612.61	233613.99	0.000591%
Load3	7313.51MW	257394.50	256527.03	256528.38	0.000526%

In the test on the 3120-bus system, the number of discretization steps is 5 and the discretizing threshold values are 0.1, 0.2, 0.3, 0.4, 0.5 for the five steps. The evolution of the primal-dual gap and objective value is shown in Figure 7-1.

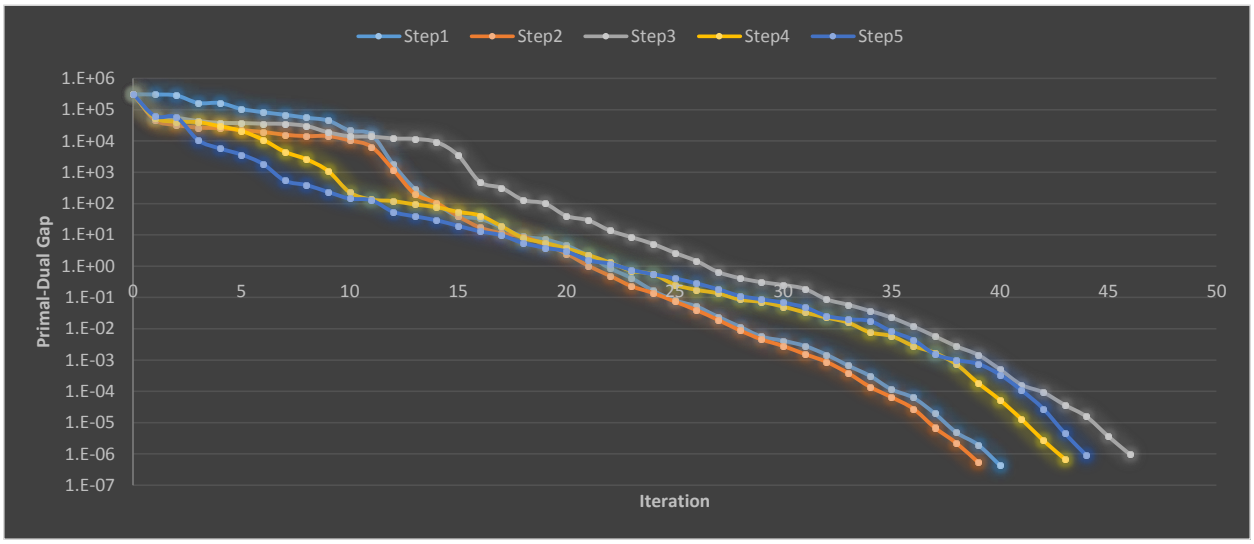

(a) Primal-dual gap

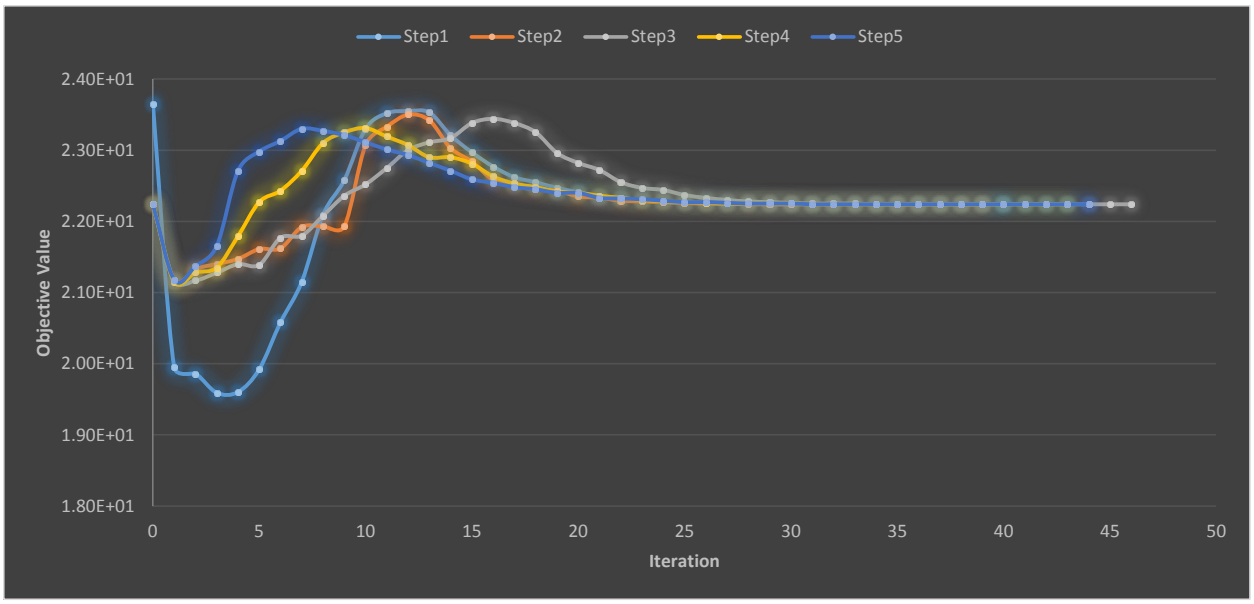

(b) Objective value

Figure 7-1: Change of primal-dual gap and objective values during re-optimizations for determining discrete control variables

7.3 Robustness and Optimality

In this test, several popular optimal power flow (OPF) solvers are tested with comparison of their robustness to different initial conditions on the two benchmarking systems. The solvers involved in the test include different solvers available in the newest MATPOWER V5.0, the OPF solver provided in the PSSE package, and SuperOPF package. It needs to note that MATPOWER supports only the following categories of optimization variables for OPF computation:

- *Vm*: Bus voltage magnitudes,
- *Va*: Bus voltage phase angles,
- *Pg*: Generator real power output, and
- *Qg*: Generator reactive power outputs.

Besides these four categories of variables, SuperOPF also supports the following categories of optimization variables:

- *Tap*: tap ratio for transformer,
- *Phs*: transformer phase shifter, and
- *Sht*: switchable shunt capacitors.

In order to make the test comprehensive, the following eight solvers are involved in the test:

1. *MIPS*: MATPOWER native MATLAB interior point solver.
2. *FMINCON*: MATLAB native constrained function minimizer.

3. *KNITRO*: the OPF solver using the commercial KNITRO package.
4. *IPOPT*: the OPF solver using the open source IPOPT package.
5. *TRALM*: OPF solver using the trust region based augmented Lagrangian method.
6. *PSSE*: OPF solver provided in the PSSE V33 package.
7. *SuperOPF 1*: BSI SuperOPF solver, with optimization variables same to the above MATPOWER solvers, that is, including only *Vm*, *Va*, *Pg*, and *Qg*.
8. *SuperOPF 2*: BSI SuperOPF solver, with extended optimization variables other than the MATPOWER solvers, that is, including all the seven categories, *Vm*, *Va*, *Pg*, *Qg*, *Tap*, *Phs*, and *Sht*.

In carrying out the test, there are 101 test cases for the first six solvers. These 101 test cases include the original base case system and 100 cases which are produced with random values of bus voltage magnitudes, following the uniform random distribution within their lower and upper bounds. For SuperOPF solver, there are 1001 test cases, including the original base case system and 1000 cases with random bus voltage magnitudes.

7.3.1 Evaluation of Robustness

The test results on the 118-bus system are summarized in Table 7-6. It can be observed that, on this small test system, all involved solvers perform very well, in that all solvers can successfully compute the OPF solution for all the involved test cases. Performance of the solvers cannot be well differentiated on this small system.

Table 7-6: Test results on the 118-bus system

Solver	***MIPS***	***FMINCON***	***KNITRO***	***IPOPT***	***TRALM***
Success Rate	69/101	101/101	101/101	101/101	101/101
Solver	***PSSE***	***SuperOPF 1***	***SuperOPF 2***		
Success Rate	101/101	1001/1001	1001/1001		

The test results on the 3120-bus system are summarized in Table 7-7. Compared to the results on the 118-bus system, performance of the solvers is well differentiated on this larger 3120-bus system. It can be observed that, for MATPOWER OPF solvers, all solvers can successfully compute the OPF solution for the original base case system. However, all MATPOWER solvers, ex-

cept the one using the KNITRO package, fail to solve any case with randomly initialized bus voltage magnitudes. Even for the OPF solver based on the KNITRO package, only 35 out of 100 random initialized cases can be solved. The PSSE OPF solver fails to solve all the 101 test cases.

Table 7-7: Test results on the 3120-bus system

Solver	*MIPS*	*FMINCON*	*KNITRO*	*IPOPT*	*TRALM*
Success Rate	1/101	1/101	36/101	1/101	1/101
Solver	***PSSE***	***SuperOPF 1***	***SuperOPF 2***		
Success Rate	0/101	1001/1001	575/1001		

SuperOPF package, on the other hand, shows clearly its robustness in on this 3120-bus test system. When the same optimization variables are considered as other solvers, that is, only *Vm*, *Va*, *Pg* and *Qg* are adjusted for OPF computation, SuperOPF can successfully compute the OPF solution for all 1001 cases. If the other types of variables, that is, *Tap*, *Phs* and *Sht*, are also considered in optimization, SuperOPF can still successfully computes the OPF solution for 575 cases out of the 1001 test cases, though the complexity and nonlinearity of the OPF problem has been significantly increased because of the extra optimization variables. Considering extra optimization variables in computing the OPF solution results improved objective, as shown in Table 7-8.

Table 7-8: Effect of more optimization variables

Solver	*Variables*	*Objective*	*Difference*
SuperOPF 1	*Vm*, *Va*, *Pg*, *Qg*	2229066.93	-
SuperOPF 2	*Vm*, *Va*, *Pg*, *Qg*, *Tap*, *Phs*, *Sht*	2224126.98	-4939.95 (-0.22%)

SuperOPF implements our proprietary two-staged OPF solution method. In the first stage, a nonlinear dynamical system is constructed for the OPF problem, where the stable equilibrium points (SEP) of the dynamical system have a one-to-one correspondence with the local optimal solutions to the OPF problem. Trajectories of the nonlinear dynamical system are investigated and a new point is obtained, which is closer to the OPF solution than the original initial point. Figure 7-2 shows the evolution of the following values during the OPF computation:

- the Lagrange gradient norm (upper graph, blue line),
- the maximum inequality constraint violation (upper graph, orange line),
- the maximum equality constraint violation (upper graph, white line), and
- the objective function (lower graph).

It can be observed that the Lagrange gradient and constraint violations have been successfully reduced in the first stage, which indicates that the obtained point is indeed closer to the feasible region and the OPF solution than the original initial point.

Two typical cases are also shown in Figure 7-3 for situations where SuperOPF failed to compute the OPF solution (when all seven categories of variables are considered for optimization). For the first situation, as shown in Figure 7-3(a), the second stage solver encounters some plateau area in the search space and the Lagrange gradient and constraint violations become steady, therefore, no sufficient step can be found to escape from the plateau area. For the second situation, as illustrated in Figure 7-3(b), the Lagrange gradient blows up in the second stage solver, after traveling in the search space in a few iterations.

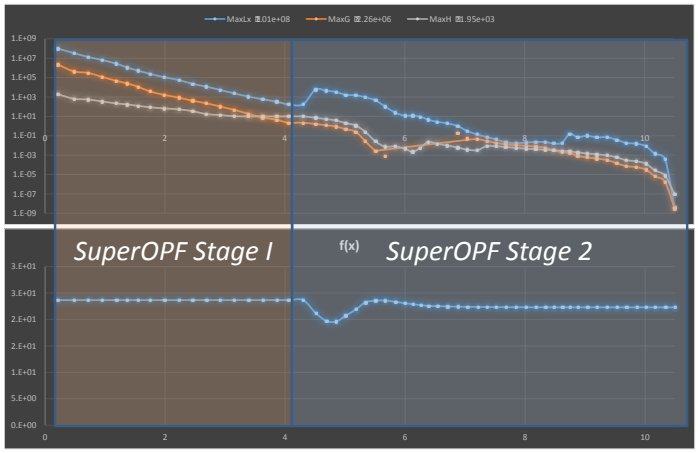

Figure 7-2: SuperOPF converged case

(a) Type 1

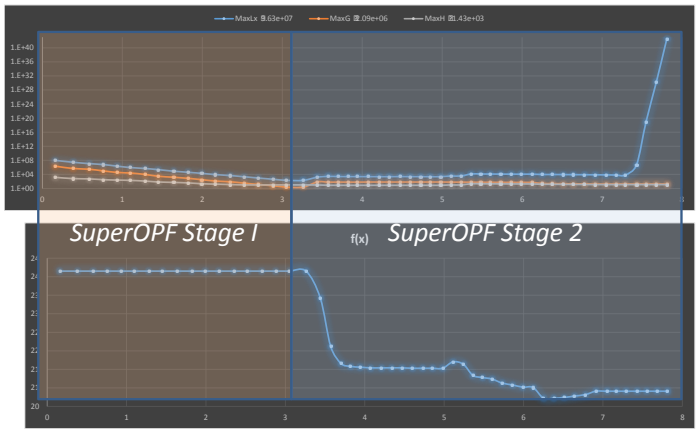

(b) Type 2

Figure 7-3: SuperOPF non-converged cases

7.3.2 Evaluation of Optimality

OPF problem is known to be a complicated nonlinear and nonconvex optimization problem. Therefore, there could have multiple local optimal solutions. However, solution methods like interior point method (IPM) and sequential quadratic programming (SQP) are all local ones, in the sense that starting from a given initial point, they can only attain a local optimal solution and cannot reach other local optimal solutions without extra perturbations (which is still not guaranteed to lead to other local optimal solutions if there indeed exist multiple local optimal solutions).

Recent research by J. Lavaei, et al [57], proposed to convexify the nonlinear AC OPF problem and use a semi-definite programming (SDP) optimization to solve it. The benefit of this procedure is that, under some mild assumptions, the global optimal solution to the original AC OPF problem can be achieved when the primal-dual gap of the SDP reaches zero. The disadvantage of this method is that the dimension of the SDP produced by convexification grows exponential-

ly as the dimension of the original AC OPF problem increases; therefore, SDP-based methods are still only applicable for small systems with reasonable computational resource.

Table 7-9: SuperOPF optimality for 118-bus system

λ	SDP	SuperOPF	Upper bound	Sigma (rank==1)	Optimality degree
1.0	129654.6175	129660.6864	129660.6927	2.4000	99.9953
1. 2	163711.8151	163717.2952	163717.3005	2.4000	99.9966
1.4	198501.5867	198505.4117	198505.4180	2.4000	99.9981
1.6	234070.5966	234070.6542	234070.6541	0.6000	100.0000
1.8	270659.8427	270659.8443	270659.8427	0.0000	100.0000
2.0	309043.8109	309043.8140	309043.8109	0.0000	100.0000

In this simulation, the SDP solutions for the 118-bus system are calculated under different loading conditions and compared to solutions by SuperOPF. The solutions obtained by the two methods are summarized in Table 7-9. It can be observed that, compared with the global optimal solution by the SDP convexification (when the duality gap is zero), the solutions by SuperOPF are numerically the same (optimality degree >99.99%). Therefore, the solution quality of SuperOPF is very appealing, in that its solutions are numerically same to the global optimal solutions obtained by SDP convexification.

7.4 Summary

In this chapter, the two OPF programs, namely the commercial PSSE OPF and SuperOPF are evaluated and compared in terms of the basic OPF functionality. The evaluation shows that SuperOPF outperforms PSSE in the following aspects:

- Objective value: the objective values achieved by SuperOPF are consistently slightly better than that by PSSE OPF.
- Discrete control adjustment: PSSE OPF has only a very limited capability to handle discrete control variables by simple rounding-off to closest discrete values. In contrast, SuperOPF possesses a more complex but also flexible capability for handling discrete control variables.

- Robustness to bad initial conditions: The evaluation also has shown that SuperOPF is very robust to bad initial conditions.

In terms of computational speed, PSSE OPF outperforms SuperOPF, which may be potentially due to that PSSE OPF engine is developed in FORTRAN, while SuperOPF is developed in C++. However, the difference in computational speed is not very significant (at same level in terms of CPU time). The comparison result is also briefly summarized in Table 7-10.

Table 7-10: Overall comparison of the two OPF programs

	PSSE OPF	BSI SuperOPF
Objective Value		√
Discrete Control		√
Robustness		√
Speed	√	
Language	FORTRAN	C++

Our multi-scenario SuperOPF (SuperOPF-MS) solver and program is developed to address the need of computing OPF solutions involving uncertain scenarios (e.g. contingencies, renewable energy forecasts, etc.) for power networks nowadays that are operated in a more and more dynamic environment. The central task for SuperOPF-MS solver is to solve the OPF problem that will result the best expected objective (such as the minimum system total power losses or generation costs) spanning the planning horizon. Therefore, the co-optimization that needs to be solved in order to get the desired optimal power flow solution can be modeled as the optimization problem Eq. (2-3). SuperOPF utilizes an enhanced nonlinear optimizer to solve the complicated nonlinear optimization problem Eq. (2-3) in its genuine nonlinear format. More details about SuperOPF can be found in other parts of this report. Therefore, we can summarize the differences between PSSE PSCOPF and SuperOPF in Table 7-11. As can be seen from the table, SuperOPF provides a more flexible tool to accomplish more comprehensive security-constrained optimal power flow analysis.

Table 7-11: Comparison between SuperOPF and PSCOPF

Solver	SuperOPF	PSSE PSCOPF

Contingency Filtering	Yes. Representative contingencies are identified via a grouping process and retained for computation. The grouping process can be realized based on different criteria preferred by the user, such as • Violation level • Voltage profile • Combination of above two of the post-contingency power flow solution.	Yes. Dominant contingencies are identified and retained for computation. Dominance or non-dominance of a contingency is determined based on the violation level of the post-contingency power flow solution.
Objective Function	A pool of objective functions to be optimized that is more flexible for user to choose, such as • System generation costs. • System power losses. • Deviation of the control between the base case and post-contingency conditions.	To minimize the adjustments of control to avoid violations in both the base case and all post-contingency conditions.
Solution Method	Use our enhanced proprietary solver to optimize the objective function subject to both the base case and all contingency constraints. The co-optimization problem is solved in its genuine nonlinear format.	Use Bender's decomposition technique and successive linear programming method. Controls are determined and applied to the base case system in an iterative process to avoid violations for each contingency.

8. Results on Contingency-Constrained Co-optimization

8.1 Simulation Targets and Settings

The simulation in this report is targeted for the following tasks:

- SuperOPF version which can co-optimize the objective function and the updated worst scenario for voltage stability (requested by CAISO)
- Demonstrate Deliverable 1 on CAISO system data
- SuperOPF version that can co-optimize the objective function, operational reserve and the renewable energies. In addition, the ramp rate of renewable energy should be included.
- Demonstrate Deliverable 3 on CAISO system data

8.1.1 The test system

The test system is a CAISO 6534-bus EMS state estimation case, of the following dimensions:

- Number of buses: 6534
- Number of loads: 2901
- Number of generators: 1903
- Number of branches: 8295
    - Number of transformers: 294
- Number of switched shunts: 520
- System load: 96907.09MW + j 10126.65MVar

The objective function of the simulation is to minimize the base case system real power losses. Two types of scenarios are considered in the simulation, including

- Worst N-1 transmission line contingencies, and
- Wind power generation forecast scenarios.

In this simulation, for co-optimization with reserves, the generator(s) at the slack bus(es) is treated as the reserve source. In other words, the remained generation capability of the slack generator(s) will be considered as available up-spinning reserve for contingency and renewable energy forecast scenarios.

8.1.2 Hardware and software

All the simulations in this report have been carried out on a personal computer of the following configurations:

- CPU: Intel Core i7-3820QM Quad 2.70GHz (Turbo Boost up to 3.7 GHz) with 8MB shared L3 cache
- Memory: 16GB 1600MHz DDR3L SDRAM

- Storage: 512GB Flash Storage Drive
- OS: Ubuntu Linux 14.10 AMD64, Linux Kernel 3.16.0, GCC4.9.1
- Software: BSI SuperOPF v3.80

8.1.3 Optimization variables

In the simulations, the following categories of optimization variables are adjusted by SuperOPF in the OPF computations:

- *Vm*: Bus voltage magnitudes.
- *Va*: Bus voltage phase angles.
- *Pg*: Generator real power outputs.
- *Qg*: Generator reactive power outputs.
- *t:* ULTC transformer tap ratios.
- *s*: phase shifters.
- *b*: switchable shunts.

8.1.4 Stopping criteria

For the involved simulations, the stopping criteria for the OPF computation by BSI SuperOPF are specified as follows:

- The maximum allowable iterations: 500.
- The convergence tolerance for P-mismatches is 0.01MW.
- The convergence tolerance for Q-mismatches is 0.1MVar.
- The convergence tolerance for thermal limits is 0.01MVA.
- The convergence tolerance for voltage magnitude bounds is 1e-4 p.u.
- The convergence tolerance for shunt device bounds is 0.01MVar.
- The convergence tolerance for transformer tap ratio bounds is 1e-4.
- The convergence tolerance for phase shifter phase angle bounds is 1e-4 rad.

8.1.5 Worst Contingencies for Co-optimization

This simulation is to use SuperOPF to co-optimize the objective function and the worst scenarios for voltage stability. In this simulation, all N-1 transmission line contingencies in area #9 are generated and BSI voltage stability analysis (VSA) program is used to calculate load margins for the post-contingency systems. Contingencies are ranked in terms of their margins and worst contingencies are identified as those ones with least load margins.

Table 8-1: Identified worst contingencies

Ctg ID	Contingency Details

8	DISCONNECT BRANCH FROM BUS 99982 TO BUS 10025 CKT 1 /* SNJUAN-B-A 345.0 KV Line
21	DISCONNECT BRANCH FROM BUS 99982 TO BUS 10292 CKT 1 /* SNJUAN-SNJUAN 345.0 KV Line
24	DISCONNECT BRANCH FROM BUS 10369 TO BUS 99986 CKT 1 /* WMESA-FCORNR 345.0 KV Line
28	DISCONNECT BRANCH FROM BUS 11111 TO BUS 11017 CKT 1 /* NEWMN-ARROYO 345.0 KV Line
34	DISCONNECT BRANCH FROM BUS 11093 TO BUS 11213 CKT 1 /* LUNA-LUNA 345.0 KV Line
35	DISCONNECT BRANCH FROM BUS 11217 TO BUS 11093 CKT 1 /* AFTON-LUNA 345.0 KV Line
36	DISCONNECT BRANCH FROM BUS 16104 TO BUS 11093 CKT 1 /* SPRNGR-LUNA 345.0 KV Line

There are seven N-1 transmission line contingencies identified by BSI VSA that have zero load margins; in other words, these contingencies are insecure in that the system cannot support the system load demands should any of these contingences happen. The details of these worst contingencies are summarized in Table 8-1.

8.2 Base-case + Individual Contingency Co-optimization

In this test, SuperOPF is used to co-optimize the base case system and individual worst contingency scenarios. Results of the SuperOPF multi-scenario co-optimization carried over these contingency cases are summarized in Table 8-2 and Table 8-3. More specifically, the co-optimization results without considering operational reserves are summarized in Table 8-2, while the results with operational reserves are summarized in Table 8-3.

Table 8-2: SuperOPF co-optimization results, without reserve

Scenario	Real Losses (MW)	% of System Load	Iterations	CPU Time (sec)
Base case before OPF	2793.42	2.883%	-	-

Base case only OPF	1624.55	1.676%	43	4.88
Base case + Ctg.8	1693.85	1.748%	50	13.10
Base case + Ctg.21	1687.92	1.742%	56	26.58
Base case + Ctg.24	1692.73	1.747%	80	27.42
Base case + Ctg.28	1642.20	1.695%	70	18.33
Base case + Ctg.34	1745.98	1.802%	57	15.28
Base case + Ctg.35	1639.96	1.692%	62	19.71
Base case + Ctg.36	Unsolvable, OPF solution not achievable			

Table 8-3: SuperOPF co-optimization results, with reserve

Scenario	Real Losses (MW)	% of System Load	Iterations	CPU Time (sec)
Base case before OPF	2793.42	2.883%	-	-
Base case only OPF	1624.55	1.676%	43	4.88
Base case + Ctg.8	1624.32	1.676%	68	17.66
Base case + Ctg.21	1624.55	1.676%	54	17.08
Base case + Ctg.24	1624.56	1.676%	69	22.67
Base case + Ctg.28	1623.57	1.675%	131	36.19
Base case + Ctg.34	1633.94	1.686%	70	18.47
Base case + Ctg.35	1624.36	1.676%	65	17.14
Base case + Ctg.36	Unsolvable, OPF solution not achievable			

It can be observed that, SuperOPF contingency-constrained co-optimization can achieve the OPF solution for six out of seven worst contingencies. It can also be observed that the objective values, i.e., (base case) system real power losses can be reduced if operational reserves are available as corrective/preventive controls for the post-contingency operation.

Another observation is that the objective of base case + single contingency (Ctg. 28 and Ctg. 35) can even be better than that of base case only OPF solution. This is because that the involvement of the contingency actually brings the side-effect of reduced OPF cost function. In fact, the enforcement of the contingency, that is, opening the corresponding transmission line, can be regarded as a line switching. Indeed, a separate study carried out on this topic has showed interesting results that proper line switching schemes can be an effective way for improving quality indices of power system operations. These indices can include, but not limited to:

- The objective values (production costs, system losses, system violations, etc.) for optimal power flow analysis.
- System load margins for system voltage stability analysis and enhancement.
- System transient stability analysis and enhancement.

Treating the on-off status of transmission lines in a power system, tine switching can be modeled as a complicated mixed-integer nonlinear programing (MINLP) problem. However, the detailed discussion of line-switching is beyond the scope of this report.

8.3 Base-case + All Contingency Co-optimization

In this simulation, BSI SuperOPF is used to co-optimize the base case system with all the identified worst contingencies (excluding the unsolvable contingencies). The co-optimization results are summarized in Table 8-4, including both co-optimization without considering generation reserves and that with generation servers. A condensed summary of the results of both co-optimizations with individual and all worst contingencies is provided in Figure 8-1.

Table 8-4: All-contingency-constrained co-optimization results

Scenario	Real Losses (MW)	% of System Load	Iterations	CPU Time (sec)
Base case before OPF	2793.42	2.883%	-	-
Base case only OPF	1624.55	1.676%	43	4.88
Base case + All Ctgs (No reserve)	1746.80	1.803%	173	430.25

Base case + All Ctgs (With reserve)	1633.69	1.686%	134	314.83

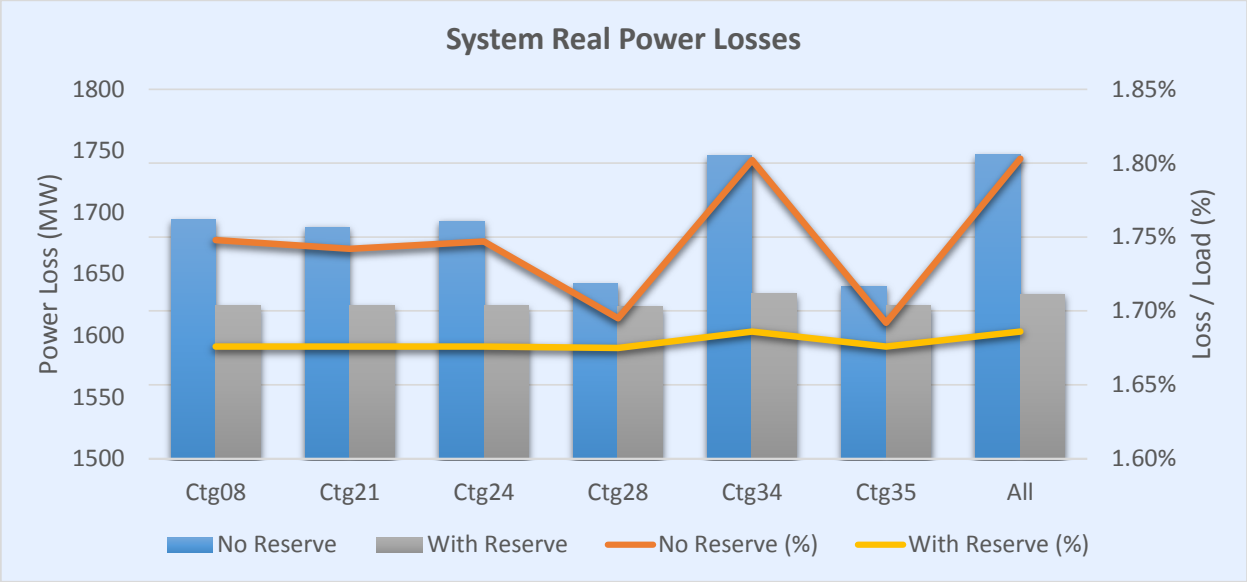

Figure 8-1: Contingency-constrained co-optimization

9. Results on Renewable-Constrained Co-optimization

9.1 Simulation Target

In this simulation, renewable energy-constrained OPF computation is carried out using BSI SuperOPF. To simulate the effects of renewable energy penetration to the system, 20% system generators are randomly selected as wind generators. Therefore, 232 wind power generators are attached to the system.

Seven forecast scenarios of the wind power generations are produced for the simulation. Forecasts of real and reactive power generations for the wind generators are specified in the scenario file, where each forecast scenario is associated with a set of varied wind power outputs. Each forecast consists of random outputs of the generators varying uniformly in the range of $\pm 25\%$ of the initial outputs. For real-life applications, a scenario reduction procedure is indispensable in order to get a reduced list of credible renewable forecasts.

All other simulation settings, namely, the test system, the hardware and software environment, the optimization variables, and the stopping criteria, are the same as that in Chapter 8.

9.2 Base-case + Single Forecast Co-optimization

In this test, BSI SuperOPF is used to co-optimize the base case system and individual renewable energy forecast scenarios. Results of the BSI SuperOPF multi-scenario co-optimization carried over these renewable energy forecast cases are summarized in Table 9-1 and Table 9-2. More specifically, the co-optimization results without considering operational reserves are summarized in Table 9-1, while the results with operational reserves are summarized in Table 9-2.

Table 9-1: Single-forecast-constrained co-optimization results, without reserve

Scenario	Real Losses (MW)	% of System Load	Iterations	CPU Time (sec)
Base case before OPF	2793.42	2.883%	-	-
Base case only OPF	1624.55	1.676%	43	4.88
Base case + Scn.1	1703.15	1.758%	61	18.67
Base case + Scn.2	1623.60	1.675%	148	47.97

Base case + Scn.3	1794.48	1.852%	129	37.59
Base case + Scn.4	1624.43	1.676%	74	23.05
Base case + Scn.5	1681.97	1.736%	79	26.05
Base case + Scn.6	1662.83	1.716%	115	33.03
Base case + Scn.7	1623.90	1.676%	156	74.12

It can be observed that, results similar to that SuperOPF contingency-constrained co-optimization are obtained. It can also be observed that the objective values, i.e., (base case) system real power losses can be reduced if operational reserves are available as corrective/preventive controls for the post-forecast operation.

Table 9-2: Single-forecast-constrained co-optimization results, with reserve

Scenario	Real Losses (MW)	% of System Load	Iterations	CPU Time (sec)
Base case before OPF	2793.42	2.883%	-	-
Base case only OPF	1624.55	1.676%	43	4.88
Base case + Scn.1	1624.31	1.676%	68	24.46
Base case + Scn.2	1624.43	1.676%	91	35.92
Base case + Scn.3	1624.31	1.676%	62	20.07
Base case + Scn.4	1624.18	1.676%	76	29.07
Base case + Scn.5	1624.34	1.676%	101	29.00
Base case + Scn.6	1622.54	1.674%	78	23.49
Base case + Scn.7	1622.65	1.674%	65	20.09

Another observation is that the objective of base case + single renewable scenario co-optimization can even be better than that of base case only OPF solution. This is a consequence of the way of treating the renewable production in the simulation. Considering that all the renewable energy produced needs to be absorbed by the power network, the renewable produc-

tions (for a renewable scenario) are treated as equivalent (negative) loads connected to the system. Therefore, the involvement of renewable production may actually reduce the system total load, which in turn results in reduced system losses in the OPF solution.

9.3 Base-case + All Forecasts Co-optimization

In this simulation, BSI SuperOPF is used to co-optimize the base case system with all the renewable energy forecasts. The co-optimization results are summarized in Table 7, including both co-optimization without considering generation reserves and that with generation servers. A condensed summary of the results of both co-optimizations with individual and all renewable energy forecasts is provided in Figure 3.

Table 9-3: All-forecast-constrained co-optimization results

Scenario	Real Losses (MW)	% of System Load	Iterations	CPU Time (sec)
Base case before OPF	2793.42	2.883%	-	-
Base case only OPF	1624.55	1.676%	43	4.88
Base case + All Ctgs (No reserve)	1796.17	1.853%	330	1212.42
Base case + All Ctgs (With reserve)	1622.66	1.674%	380	1646.38

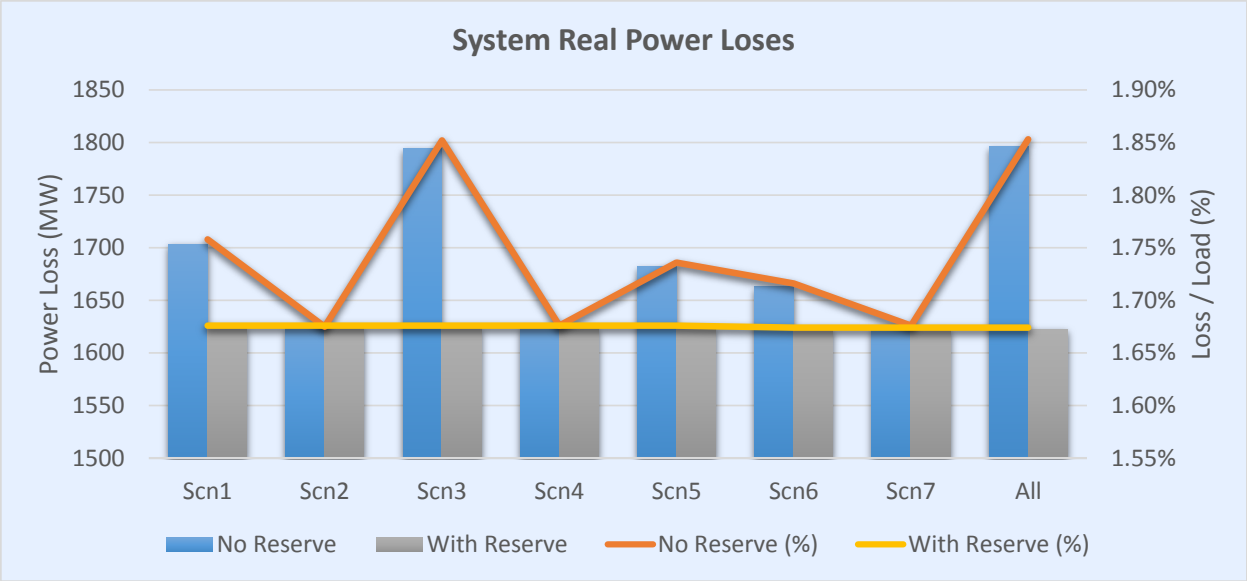

Figure 9-1: Renewable-energy-constrained co-optimization

10. Results on Ramping-Constrained Co-optimization

10.1 Simulation Targets and Settings

The simulation in this report is targeted for the following tasks:

- Co-optimization SuperOPF software equipped with the ramping constraints of generations (requested by CAISO).
- Demonstrate the SuperOPF with ramping constraints on CAISO system data.

The objective function of the simulation is to minimize the base case system real power losses. Two types of scenarios are considered in the simulation, including

- Worst N-1 transmission line contingencies, and
- Wind power generation forecast scenarios.

In the simulations, for co-optimization with reserves, the generator(s) at the slack bus(es) is treated as the reserve source. In other words, the remained generation capability of the slack generator(s) will be considered as available up-spinning reserve for contingency and renewable energy forecast scenarios.

In the simulations, the ramping rates for generators are assigned values uniformly distributed within the range of 5MW through 8MW per minute. The generation ramping rates for practical usage can be specified in the control file for SuperOPF co-optimization, which follows the specification of PSSE OPF raw data file format. Availability of ramping is considered for different time periods in the simulations. More specifically, ramping constraints for 5-minute, 10-minute and 15-minute are considered. The ramping capability for a generation is computed as the product of its ramping rate and the length of the time period. Both ramping-up and ramping-down capabilities for each generator are considered the same in the simulations of this report. SuperOPF program supports specifying different ramping-up and ramping-down rates for a generator.

All other simulation settings, namely, the test system, the hardware and software environment, the optimization variables, and the stopping criteria, are the same as that in Chapter 8.

In this chapter, simulations of SuperOPF co-optimization with ramping constraints are carried out for two themes, namely, co-optimizing worst contingencies and co-optimizing renewable forecasting scenarios.

10.2 Contingency Co-optimization with Ramping Constraints

The first simulation is to use SuperOPF to co-optimize the objective function and the worst scenarios for voltage stability, considering ramping constraints. In this simulation, all N-1 transmission line contingencies in area #9 are generated and BSI voltage stability analysis (VSA) program is used to calculate load margins for the post-contingency systems. Contingencies are ranked in terms of their margins and worst contingencies are identified as those ones with least load margins.

Table 10-1: Identified worst contingencies

Ctg ID	Contingency Details
8	DISCONNECT BRANCH FROM BUS 99982 TO BUS 10025 CKT 1 /* SNJUAN-B-A 345.0 KV Line
21	DISCONNECT BRANCH FROM BUS 99982 TO BUS 10292 CKT 1 /* SNJUAN-SNJUAN 345.0 KV Line
24	DISCONNECT BRANCH FROM BUS 10369 TO BUS 99986 CKT 1 /* WMESA-FCORNR 345.0 KV Line
28	DISCONNECT BRANCH FROM BUS 11111 TO BUS 11017 CKT 1 /* NEWMN-ARROYO 345.0 KV Line
35	DISCONNECT BRANCH FROM BUS 11217 TO BUS 11093 CKT 1 /* AFTON-LUNA 345.0 KV Line
36	DISCONNECT BRANCH FROM BUS 16104 TO BUS 11093 CKT 1 /* SPRNGR-LUNA 345.0 KV Line

There are six N-1 transmission line contingencies identified by BSI VSA that have zero load margins; in other words, these contingencies are insecure in that the system cannot support the system load demands should any of these contingences happen. The details of these worst contingencies are summarized in Table 1.

10.2.1 Base-case + Individual Contingency Co-optimization

In this test, SuperOPF is used to co-optimize the base case system and individual worst contingency scenarios. Results of the SuperOPF multi-scenario co-optimization carried over these contingency cases are summarized in Table 2.

Table 10-2: SuperOPF co-optimization results

Scenario		Real Losses (MW)	% of System Load	Iterations	CPU Time (sec)
Base case before OPF		2793.42	2.883%	-	-
No Ramping Constraints	Base case	1624.55	1.676%	43	4.88
	Base case + Ctg.8	1624.32	1.676%	68	17.66
	Base case + Ctg.21	1624.55	1.676%	54	17.08
	Base case + Ctg.24	1624.56	1.676%	69	22.67
	Base case + Ctg.28	1623.57	1.675%	131	36.19
	Base case + Ctg.35	1624.36	1.676%	65	17.14
	Base case + Ctg.36	1624.24	1.676%	61	14.03
5-Minute Ramping	Base case	1854.04	1.913%	43	4.53
	Base case + Ctg.8	1854.10	1.913%	50	11.84
	Base case + Ctg.21	1854.09	1.913%	49	11.54
	Base case + Ctg.24	1854.09	1.913%	51	12.15
	Base case + Ctg.28	1854.06	1.913%	48	11.26
	Base case + Ctg.35	1878.13	1.938%	48	11.16
	Base case + Ctg.36	1854.09	1.913%	52	12.27
10-Minute Ramping	Base case	1729.78	1.785%	47	4.96
	Base case + Ctg.8	1728.76	1.784%	86	20.36
	Base case + Ctg.21	1729.03	1.784%	52	12.25
	Base case + Ctg.24	1729.02	1.784%	52	12.51
	Base case + Ctg.28	1728.70	1.784%	63	14.72

	Base case + Ctg.35	1751.43	1.807%	62	14.40
	Base case + Ctg.36	1728.70	1.784%	58	13.56
15-Minute Ramping	Base case	1682.87	1.737%	49	5.24
	Base case + Ctg.8	1682.42	1.737%	66	15.48
	Base case + Ctg.21	1681.89	1.736%	72	17.26
	Base case + Ctg.24	1682.64	1.737%	67	16.24
	Base case + Ctg.28	1681.60	1.735%	70	16.22
	Base case + Ctg.35	1702.83	1.757%	78	18.31
	Base case + Ctg.36	1682.19	1.736%	70	16.71

It can be observed that, SuperOPF contingency-constrained co-optimization can achieve the OPF solution for these worst contingencies. It can also be observed that the objective values, i.e., (base case) system real power losses can be reduced if operational reserves are available as corrective/preventive controls for the post-contingency operation. In addition, the ramping constraints newly introduced

10.2.2 Base-case + All Contingency Co-optimization

In this simulation, SuperOPF is used to co-optimize the base case system with all the identified worst contingencies. The co-optimization results are summarized in Table 3. A condensed summary of the results of both co-optimizations with individual and all worst contingencies is provided in Figure 3.

Table 10-3: All-contingency-constrained co-optimization results

Scenario		Real Losses (MW)	% of System Load	Iterations	CPU Time (sec)
Base case before OPF		2793.42	2.883%	-	-
Base case only OPF		1624.55	1.676%	43	4.88
Base case + All	No Ramping	1633.69	1.686%	134	314.83

Contingencies	5-min Ramping	1877.02	1.937%	195	365.86
	10-min Ramping	1750.14	1.806%	137	253.86
	15-min Ramping	1701.81	1.756%	114	212.81

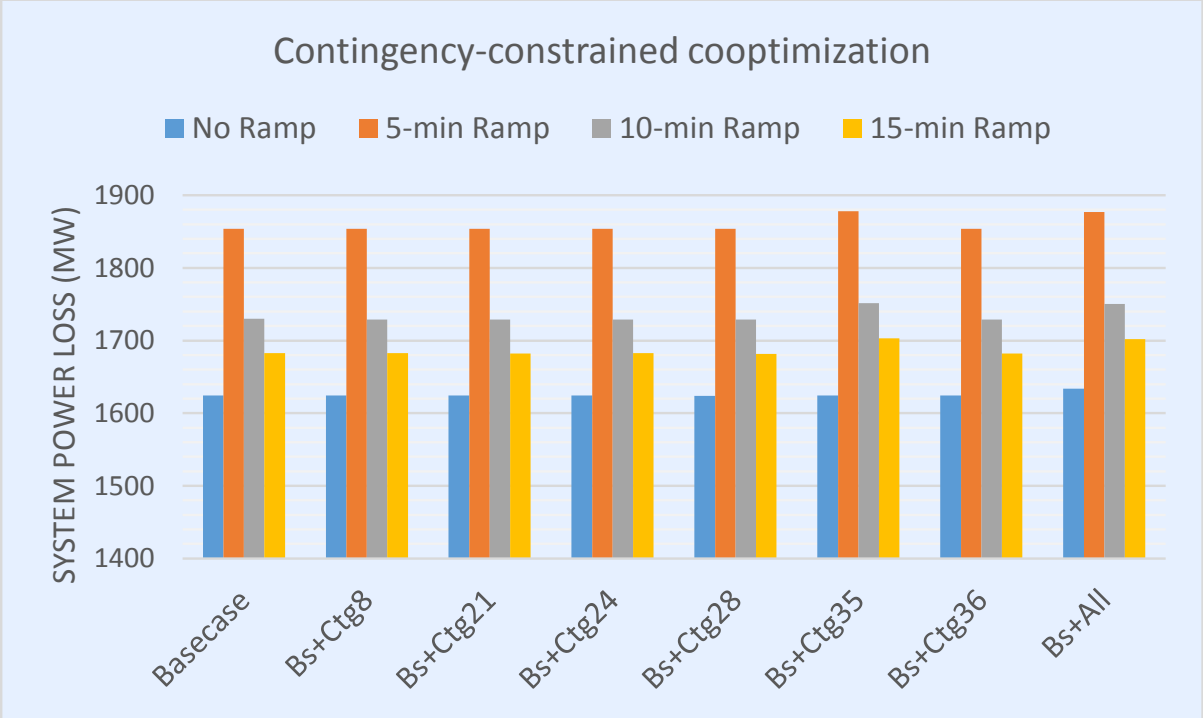

Figure 10-1: Contingency-constrained co-optimization

10.3 Renewable Co-optimization with Ramping Constraints

In the second simulation, renewable energy-constrained OPF computation is carried out using SuperOPF, considering ramping constraints. To simulate the effects of renewable energy penetration to the system, 20% system generators are randomly selected as wind generators. As a result, it is assumed that there are 232 wind-power generators attached to the system.

Seven forecast scenarios of the wind power generations are produced for the simulation. Forecasts of real and reactive power generations for the wind generators are specified in the scenario file, where each forecast scenario is associated with a set of varied wind power outputs. Each forecast consists of random outputs of the generators varying uniformly in the range of $\pm 25\%$ of the initial outputs. For real-life applications, a scenario reduction procedure is indispensable in order to get a reduced list of credible renewable forecasts.

For practical usage of SuperOPF, the assignment of renewable generators and forecasts of their outputs are specified in the input control file.

10.3.1 Base-case + Single Forecast Co-optimization

In this test, SuperOPF is used to co-optimize the base case system and individual renewable energy forecast scenarios. Results of the SuperOPF multi-scenario co-optimization carried over these renewable energy forecast cases are summarized in Table 4.

Table 10-4: Single-forecast-constrained co-optimization results

Scenario		Real Losses (MW)	% of System Load	Iterations	CPU Time (sec)
Base case before OPF		2793.42	2.883%	-	-
No Ramping Constraints	Base case	1624.55	1.676%	43	4.88
	Base case + Scn.1	1624.31	1.676%	68	24.46
	Base case + Scn.2	1624.43	1.676%	91	35.92
	Base case + Scn.3	1624.31	1.676%	62	20.07
	Base case + Scn.4	1624.18	1.676%	76	29.07
	Base case + Scn.5	1624.34	1.676%	101	29.00
	Base case + Scn.6	1622.54	1.674%	78	23.49
	Base case + Scn.7	1622.65	1.674%	65	20.09
5-Minute Ramping	Base case	1854.04	1.913%	43	4.53
	Base case + Scn.1	1854.04	1.913%	53	12.40
	Base case + Scn.2	1854.95	1.914%	55	12.97
	Base case + Scn.3	1853.23	1.912%	63	15.70
	Base case + Scn.4	1854.21	1.913%	62	14.81

	Base case + Scn.5	1854.09	1.913%	50	11.79
	Base case + Scn.6	1853.25	1.912%	61	14.38
	Base case + Scn.7	1854.53	1.914%	73	17.16
10-Minute Ramping	Base case	1729.78	1.785%	47	4.96
	Base case + Scn.1	1728.97	1.784%	73	17.53
	Base case + Scn.2	1729.06	1.784%	72	17.15
	Base case + Scn.3	1729.60	1.785%	58	13.58
	Base case + Scn.4	1729.63	1.785%	55	13.35
	Base case + Scn.5	1729.12	1.784%	65	15.60
	Base case + Scn.6	1729.60	1.785%	60	14.53
	Base case + Scn.7	1729.07	1.784%	61	14.46
15-Minute Ramping	Base case	1682.87	1.737%	49	5.24
	Base case + Scn.1	1681.83	1.736%	71	19.01
	Base case + Scn.2	1682.48	1.736%	67	16.11
	Base case + Scn.3	1682.89	1.737%	58	13.64
	Base case + Scn.4	1682.94	1.737%	55	12.95
	Base case + Scn.5	1682.39	1.736%	57	13.40
	Base case + Scn.6	1682.17	1.736%	63	15.46
	Base case + Scn.7	1682.91	1.737%	55	13.12

It can be observed that, results similar to that SuperOPF contingency-constrained co-optimization are obtained. It can also be observed that the objective values, i.e., (base case) system real power losses can be reduced if operational reserves are available as corrective/preventive controls for the post-forecast operation.

10.3.2 Base-case + All Forecasts Co-optimization

In this simulation, SuperOPF is used to co-optimize, with ramping constraints, the base case system with all the renewable energy forecasts. The co-optimization results are summarized in Table 5. A condensed summary is provide in Figure 4 for the results of both co-optimizations with individual and all renewable energy forecast scenarios.

Table 10-5: All-forecast-constrained co-optimization results

Scenario		Real Losses (MW)	% of System Load	Iterations	CPU Time (sec)
Base case before OPF		2793.42	2.883%	-	-
Base case only OPF		1624.55	1.676%	43	4.88
Base case + All Scenari-os	No Ramping	1622.66	1.674%	380	1646.38
	5-min Ramping	1854.57	1.914%	260	737.60
	10-min Ramping	1728.77	1.784%	274	745.83
	15-min Ramping	1681.81	1.735%	192	513.76

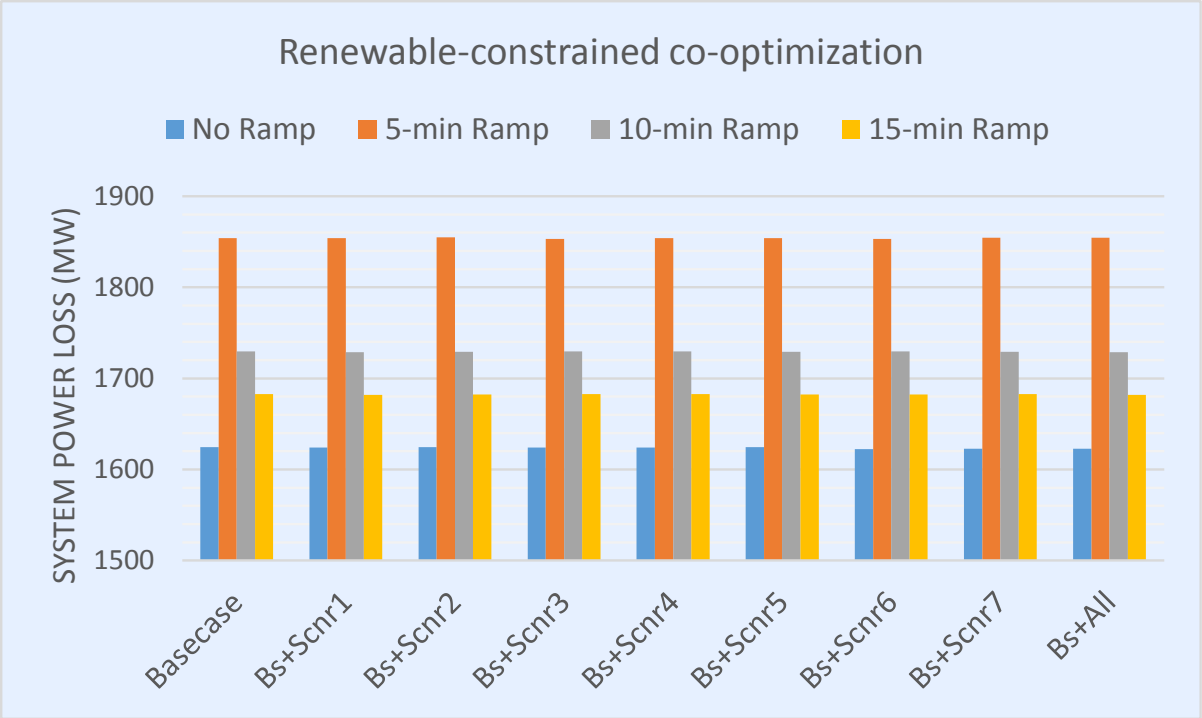

Figure 10-2: Renewable-energy-constrained co-optimization

11. Power Market Related Calculations and Outputs

11.1 CAISO Energy Pricing

Locational marginal pricing (LMP) is the pricing method that a utility uses to price energy purchases and sales in the power market. LMP is "the marginal cost of supplying, at least cost, the next increment of electric demand at a specific location (node) on the electric power network, taking into account both supply (generation/import) bids and demand (load/export) offers and the physical aspects of the transmission system including transmission and other operational constraints [90]".

In CAISO's power market practice, the LMPs for energy are calculated respecting network losses and eventual transmission congestion [91]. Load and generating unit contributions to the system power balance differ with respect to network energy losses and eventual transmission congestion. Energy market clearing prices are differentiated according to specific conditions of actual power injections and withdrawals at market participant locations. In general, energy prices are different at each network node, i.e. they present the LMPs. In CAISO, the components of LMPs are calculated as:

$$\begin{aligned} LMP_{node} &= MCP_{req} && \text{- System marginal energy cost} \\ &+ MCP_{req} \cdot (1 - pf_{node})/pf_{node} && \text{- Loss component} \\ &+ \sum_{line \in N} SF_{line}^{node} \cdot TSC_{line} && \text{- Congestion component} \end{aligned} \tag{11-1}$$

where:

- LMP_{node} is the LMP for energy at network node.
- MCP_{req} is the market clearing price for energy requirement.
- pf_{node} is the loss penalty factor for network node.
- SF_{line} is the shift factor for transmission line and network node.
- TSC_{line} is the transmission shadow cost for *line* constraint.

All these components of LMP are calculated for each pricing node and each time interval.

The co-optimization AC OPF solver calculates shadow prices as a by-product of the optimization process. These shadow prices indicate the effect on the objective function of the various constraints. Shadow prices related to the system power balance represent the marginal energy costs. Therefore, the system marginal energy cost is

$$MCP = \lambda \tag{11-2}$$

where, λ is the vector of Lagrange multipliers associated with the nonlinear equality constraints (i.e., power flow balance equations) of the AC OPF problem.

For aggregated pricing locations presenting *default load zones*, *custom load zones* and *trading hubs*, the aggregated market prices (AMP) are calculated. The AMPs are calculated in post optimiza-

tion processing as a weighted sum of energy LMPs at pricing locations belonging to an aggregated pricing location, that is,

$$AMP_{APnode} = \sum_{Pnode \in APnode} w_{Pnode} \cdot LMP_{Pnode} \quad (11\text{-}3)$$

The weighting factors present contribution of individual energy schedules at pricing locations relative to the total energy schedule at an aggregated pricing location, that is:

$$w_{APnode} = \frac{E_{Pnode}}{\sum_{Pnode \in APnode} E_{Pnode}} \quad (11\text{-}4)$$

When nomogram constraints are considered, the above standard definition of LMP can be extended to reflect impact of nomogram constraints. The nomogram price component is calculated as:

$$LMP_{node}^{nom} = \sum_{line \in NOM} SF_{line}^{node} \cdot ISC_{line} \quad (11\text{-}5)$$

where, ISC_{line} is the interface shadow cost for the line (corridor).

11.2 SuperOPF Calculations and Outputs Related to Power Market

Thanks to the full AC OPF formulation implemented in SuperOPF and its comprehensive modeling capability to handle a comprehensive set of objective function, constraints and optimization variables, there is a ready correspondence between SuperOPF outputs and components needed for LMP calculation.

Table 11.1 LMP calculation and SuperOPF outputs

LMP Component	SuperOPF Output
MCP	The vector of Lagrange multipliers associated with the nonlinear equality constraints (i.e., power flow balance equations) of the SuperOPF solution.
TSC_{line}	The vector of Lagrange multipliers associated with the thermal/flow limit imposed on the line. TSC_{line} takes a nonzero value only if congestion happens (i.e., the thermal limit constraint is binding for the line).
ISC_{line}	The vector of Lagrange multipliers associated with the flow limit imposed on the interface (line group). ISC_{line} takes a nonzero value only if congestion happens (i.e., the flow limit constraint is binding for the interface).

12. CAISO Feedback on SuperOPF

12.1 Introduction

In previous discussion with CAISO, they articulated the need for non-linear OPF for the CAISO power market. Development under this project has provided and demonstrated most of the functionality that was seen as necessary to produce a SuperOPF tool with the necessary functions for application in the power market.

This functionality includes the following.

Operations & Power Market Applications:

- SuperOPF with handling voltage stability as a constraint is of value to the power market
- Ramp Constraints in model
- Co-optimization of worst scenarios especially with renewables
- Inclusion of AGC response into SuperOPF to deal with renewable integration
- Require good real-time performance

General Application:

- Reserve requirements with renewables

Planning & Operations Applications:

- Static & Dynamic stability constraints with contingency

12.2 Feedback from CAISO Director

Bigwood Systems, Inc. (BSI) has demonstrated promising simulation results for the study of co-optimization of stochastic multi-contingency scenarios SuperOPF using BSI's production-grade SuperOPF. The solution method robustly computes the OPF solutions for all the involved scenarios and under all feasible loading conditions, even though the post-contingency state may be insecure. Numerical results based on practical study cases are presented in both the Final Report and the Supplementary Report.

Beside the typical capabilities of traditional OPF programs such as handling industry standard power systems network models data formats, data management for SuperOPF constructs, handling of control variables for real and reactive power and support for objective functions of cost, losses and minimum violations of target voltage profiles, the BSI SuperOPF also possesses the capability of handling static and dynamic stability requirements, handling contingent and varying load and generation scenarios, and handling uncertainties associated with high levels of renewable energy penetrations. The SuperOPF program has a modularized structure and is designed to be ready for future extensions. It is flexible and convenient for further development to support more data formats and to enclose other effective linear and nonlinear solvers into the current im-

plementation. The BSI SuperOPF supported simulation results makes it a very promising and viable analysis tool for power industry.

12.3 Additional SuperOPF Applications identified by CAISO

CASIO - Outage Scheduling

One key ISO's responsibility: scheduling and coordination of transmission equipment outages (periods when equipment is out of service). Outages can last from 15 minutes to several weeks or months, and can be continuous or intermittent.

- Planned outage
- Unplanned outage

CASIO - Advanced Voltage Control

Real-time Power Market

- 5-minute Ahead Power Market
- Project Idea: to apply advanced voltage control before 5-minute ahead power market to relieve congestion

CAISO – Long-term Project

SuperOPF for power market application

- LMP calculation based on ACOPF model (instead of linearized OPF model) with comprehensive and accurate representation of static as well as dynamic constraints.

13. Summary

In this report, the impact of co-optimization in improving key challenges in the CAISO system has been studied. In this report, simulations have been carried out to evaluate contingency-constrained and renewable-energy-constrained co-optimized OPF computation using SuperOPF to perform on CAISO system EMS data. The results suggest that SuperOPF is an effective tool for multi-scenario (either contingencies or renewable energy scenarios or their combinations), co-optimized OPF analysis, which is applicable to handle a diversity of scenarios for large-scale power systems.

In this study, simulations have been carried out using SuperOPF to perform contingency-constrained and renewable-energy-constrained co-optimized OPF computation considering generation ramping constraints on CAISO system EMS data. The results suggest that SuperOPF is an effective tool for multi-scenario cooptimized OPF analysis, which is applicable to handle a diversity of scenarios and a comprehensive set of constraints for large-scale power systems.

In summary, SuperOPF is a powerful and easy-to-use electric power network analysis tool. It goes beyond traditional power flow analysis to provide the utility the ability to fully optimize and refine the power transmission system. Cooperating with other power system analysis tools, SuperOPF helps realize a comprehensive and reliable optimization of power system under rapidly changing operating conditions.

SuperOPF improves the efficiency and throughput of the power system performance studies by adding intelligence to the power flow solution process. Whereas the conventional power flow relies on the engineer to systematically investigate a variety of solutions before arriving at a satisfactory good solution, SuperOPF automatically adjusts controls to determine the best solution. From virtually any reasonable starting point, you are assured that one or multiple optimal solutions are attained, solutions that all simultaneously satisfy system constraints given a predetermined objective. These applications place two primary requirements on an optimal power flow program. First, the modeling must reflect the actual behavior of the system components. Second, the solutions must be obtained in a robust and efficient manner. SuperOPF meets these two requirements. The latest advances in sparse techniques and nonlinear optimization have been incorporated in the solution algorithm. Robust and fast solution algorithms are developed and integrated into SuperOPF.

SuperOPF is capable of dealing with a variety of objective functions needed in power system operation and planning, including:

- Minimizing fuel cost
- Minimizing active power losses
- Minimizing reactive power losses

- Minimizing active power slack generation
- Minimizing reactive power slack generation
- Minimizing adjustable branch reactance
- Minimizing adjustable bus shunts
- Minimizing or maximizing interface flows
- Minimizing or maximizing active power transfers
- Minimizing or maximizing reactive power transfers
- Minimizing or maximizing reactive generation reserve
- Minimizing load adjustments

SuperOPF also allows the user to define optimal power flow problem by combining the objective function with any number of constraints and controls, selectable from the following:

- Bus voltage magnitude limits
- Branch flow limits (MW, MVar, MVA, Ampere)
- Interface flow limits (MW, MVar)
- Generator active power limits
- Generator reactive power limits
- Generation period reserve limits
- Transformer tap ratio limits
- Transformer phase-shift limits
- Adjustable bus shunt limits
- Adjustable branch reactance limits
- Adjustable load limits
- Voltage stability criteria
- Transient stability criteria
- Renewable energy penetrations

Appendix: Simulations on Piece-wise Linear Cost Functions

A1. Data Preparation

This supplementary report creates a new CAISO system dataset and presents SuperOPF simulation results on the dataset. The dataset is grabbed from a recent BSI VSA study case for CAISO. The data header for the PSSE raw data file is shown in Table A1-1.

Table A0-1: The PSSE data header

```
 0  100.0          / PSS/E-30.0     BY BSI VSA
 S=DB62_Version_VSA_H_STATIC_011613.xml   D=CIM_periodic_070213_033022.xml
 Create on 03/10/15 11:20:03
```

The same loading pattern used in BSI VSA study is used to generate CPFLOW solutions under different loading conditions. These CPFLOW solutions will be used as initial conditions for SuperOPF computations. It is known that there is no bus voltage limits specified in PSSE raw data files. In creating the dataset, bus voltage limits are retrieved from the monitor list file of VSA study. A portion of the monitor list file is shown in Table 1-2, which also illustrates the structure of the file. The monitor voltage range for a bus specified in the file is used as the valid range of voltage magnitude for the bus in SuperOPF computations; for other buses not covered in the monitor list file, a generic range of [0.9, 1.1] is used as the bus voltage range for SuperOPF computation. As shown in Table A1-2, it is also specified in the monitor list file the monitor branches. For branches included in the monitor list file, thermal limit constraints will be imposed for SuperOPF computation; no thermal limit constraints will be considered for other branches. The RateA value for branches specified in the PSSE raw data file will be used as the thermal limits in SuperOPF computation.

Table A0-2: The monitor list file

```
MONITOR BRANCHES
 35901     14  1 /* MRGHLJ-GRNVLY_115_BR_2_1
… … …
END
MONITOR VOLTAGE RANGE BUS  18972       0.9500       1.0500     /* COPMT2  1-BUS-230
MONITOR VOLTAGE DEVIATION BUS  18972       0.0500       0.0500 /* COPMT2  1-BUS-230
MONITOR VOLTAGE RANGE BUS  18974       0.9522       1.0507     /* COPMT2  1-BUS-34.5
MONITOR VOLTAGE DEVIATION BUS  18974       0.0500       0.0500 /* COPMT2  1-BUS-34.5
… … …
END
```

Table A0-3: The levelized cost of electricity (LCOE) for different generation resources [1]

	Range for Total System LCOE (2012 $/MWh)			Range for Total LCOE with Subsidies[1] (2012 $/MWh)		
Plant Type	**Minimum**	**Average**	**Maximum**	**Minimum**	**Average**	**Maximum**
Dispatchable Technologies						
Conventional Coal	87.0	95.6	114.4			
IGCC	106.4	115.9	131.5			
IGCC with CCS	137.3	147.4	163.3			
Natural Gas-fired						
Conventional Combined Cycle	61.1	66.3	75.8			
Advanced Combined Cycle	59.6	64.4	73.6			
Advanced CC with CCS	85.5	91.3	105.0			
Conventional Combustion Turbine	106.0	128.4	149.4			
Advanced Combustion Turbine	96.9	103.8	119.8			
Advanced Nuclear	92.6	96.1	102.0	82.6	86.1	92.0
Geothermal	46.2	47.9	50.3	43.1	44.5	46.4
Biomass	92.3	102.6	122.9			
Non-Dispatchable Technologies						
Wind	71.3	80.3	90.3			
Wind – Offshore	168.7	204.1	271.0			
Solar PV[2]	101.4	130.0	200.9	92.6	118.6	182.6
Solar Thermal	176.8	243.1	388.0	162.6	223.6	356.7
Hydroelectric[3]	61.6	84.5	137.7			

The generation cost data is created based on several data sources. The levelized cost of electricity (LCOE) for different generation resources, as shown in Table A1-3, is used as the reference for generating the generation costs. The generation types are retrieved from QFER CEC-1304 Power Plant Owner Reporting Database published by California Energy Commission [2]. Generator names are matched to the generator bus names recorded in the PSSE raw data file. Two types of costs are assigned to the generations, namely, linear and piece-wise linear costs. The cost values are drawn randomly following uniform distribution from the range of the LCOE shown in Table 1-3. Figure 1-1 illustrates the piece-wise linear cost model. Piece-wise linear costs are assigned to 10% of the total number of generators, each has 2 to 5 cost segments in the range of the minimal and maximal generations; other generators are assigned with linear costs.

[1] Levelized Cost and Levelized Avoided Cost of New Generation Resources in the Annual Energy Outlook 2014, U.S. Energy Information Administration.

[2] http://www.energyalmanac.ca.gov/electricity/web_qfer/source_files/q_WebWorks_QFERPlant_Table.txt.

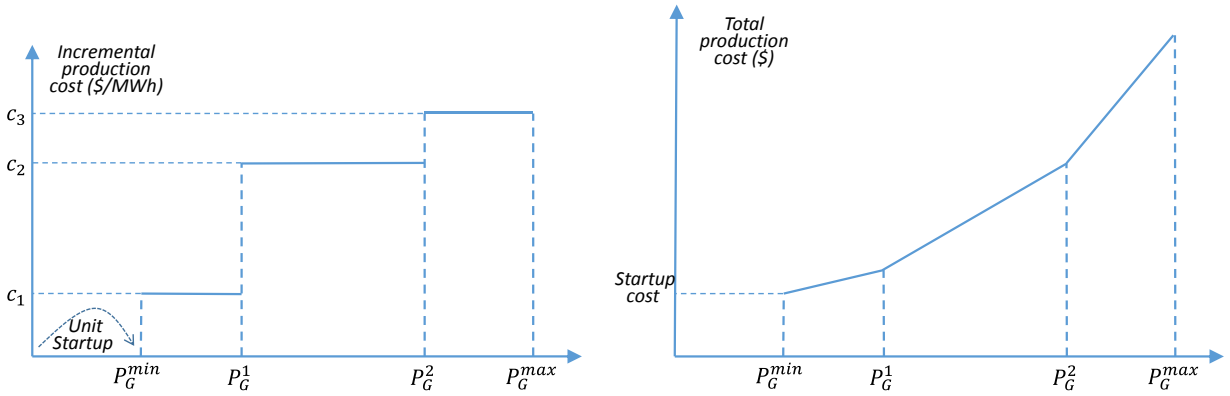

(a) The incremental production costs (b) The corresponding total production cost

Figure A0-1: Illustration of piece-wise cost model

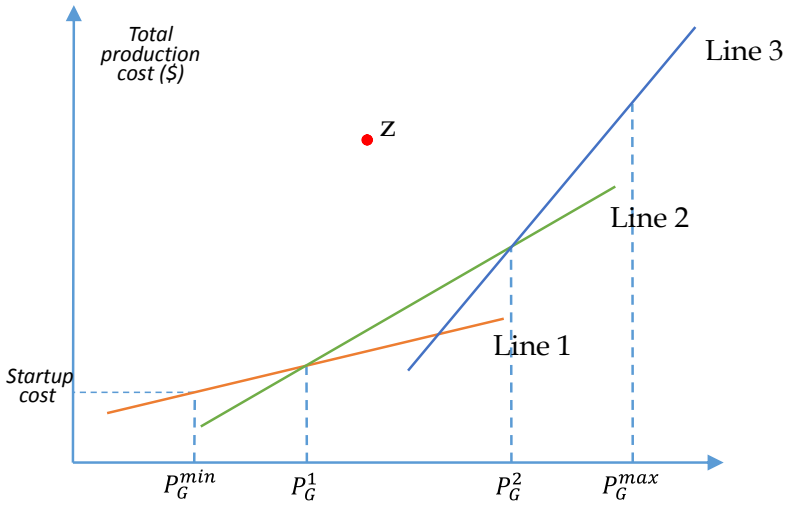

Figure A0-2: Illustration of the proxy variable for piece-wise costs

Figure A1-2 illustrates the technique for handling piece-wise linear costs. Basically, a proxy cost variable, noted as z_i for i-th generator with piece-wise linear cost, is added to the OPF problem formulation, along with the following new set of proxy constraints

$$\begin{aligned} z_i &\geq a_{1i}P_i + b_{1i} \\ z_i &\geq a_{2i}P_i + b_{2i} \\ &\cdots\cdots \\ z_i &\geq a_{Ki}P_i + b_{Ki} \end{aligned},$$

where, K is the number of cost segments, $a_{1i}, \cdots, a_{Ki}$ and $b_{1i}, \ldots, b_{Ki}$ are the cost parameters for the lines of the cost segments.

A2. Simulation Settings

A2.1 The test system

The test system is a CAISO 7199-bus VSA study case, of the following dimensions:

- Number of buses: 7199
- Number of loads: 3004
- Number of generators: 2097
- Number of non-transformer branches: 6551
- Number of transformers: 2533
- Number of switched shunts: 579
- Basecase System load: 76323.36MW+ j 9872.40MVar

A2.2 Simulation Targets

Two types of objective functions are considered in the simulation, including

- To minimize the system real power losses, and
- To minimize the system production costs.

Co-optimization is carried out for worst "N-1" contingencies. All computations will be carried out under different loading conditions.

In this simulation, for co-optimization with reserves, the generator(s) at the slack bus(es) is treated as the reserve source. In other words, the remained generation capability of the slack generator(s) will be considered as available up-spinning reserve for contingency scenarios. Therefore, in the resulted OPF solutions, all non-slack generators will have same outputs across all involved contingencies.

A2.3 Hardware and software

All the simulations in this report have been carried out on a personal computer of the following configurations:

- CPU: Intel Core i7-3820QM Quad 2.70GHz (Turbo Boost up to 3.7 GHz) with 8MB shared L3 cache
- Memory: 16GB 1600MHz DDR3L SDRAM
- Storage: 512GB Flash Storage Drive
- OS: Ubuntu Linux 15.04 AMD64, Linux Kernel 3.19.0, GCC5.1.1
- Software: BSI SuperOPF v3.90

A2.4 Optimization variables

In the simulations, the following categories of optimization variables are adjusted by SuperOPF in the OPF computations:

- *Vm*: Bus voltage magnitudes.
- *Va*: Bus voltage phase angles.

- *Pg*: Generator real power outputs.
- *Qg*: Generator reactive power outputs.
- *t:* ULTC transformer tap ratios.
- *s*: phase shifters.
- *b*: switchable shunts.

A2.5 Stopping criteria

For the involved simulations, the stopping criteria for the OPF computation by BSI SuperOPF are specified as follows:

- The maximum allowable iterations: 500.
- The convergence tolerance for P-mismatches is 0.01MW.
- The convergence tolerance for Q-mismatches is 0.1MVar.
- The convergence tolerance for thermal limits is 0.01MVA.
- The convergence tolerance for voltage magnitude bounds is 1e-4 p.u.
- The convergence tolerance for shunt device bounds is 0.01MVar.
- The convergence tolerance for transformer tap ratio bounds is 1e-4.
- The convergence tolerance for phase shifter phase angle bounds is 1e-4 rad.

A3. Simulation Results

A3.1 CPFLOW Computation

In this simulation, in order to obtain power flow solutions under different loading conditions, BSI's voltage stability analysis (VSA) program is used to perform a CPFLOW computation on the test system. The "SDGE+CFE-BG-LOAD_INC" loading pattern is simulated, that is, loads are increased only in area 11 "SDGE-22" and power flow solutions are computed until the nose point of the P-V curves is reached, beyond which no power flow solutions exist.

Table A0-4: Loading conditions for simulation

Case	1	2	3	4	5	6	7	8
Load (MW)	76323.36	76489.11	77024.66	77541.53	78044.94	78532.81	78972.60	79052.42
Violations	#V: 41	#V: 41	#V: 37	#V: 42	#V: 49	#V: 49	#V: 180 #T: 1	#V: 215 #T: 1
Basecase system load margin: 2738.8MW. ("#V" for the number of voltage magnitude violations, "#T" for the number of thermal limit violations)								

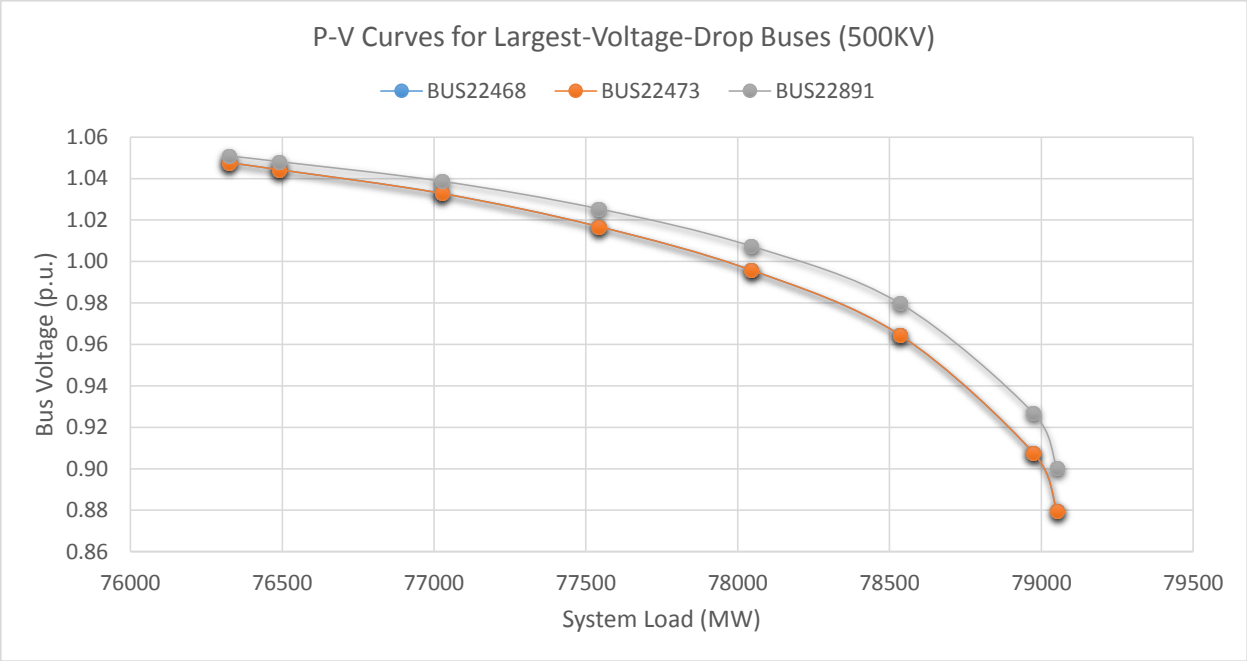

Figure A0-3: P-V curves for selected buses (500KV, voltage drop greater than 0.15p.u.)

There are eight points on the P-V curves, starting from the base load until the nose point, obtained by VSA CPFLOW computation, as summarized in Table A3-1 and depicted in Figure A3-1. These power flow solutions are used as the initial conditions for OPF computation. It needs to be noted that although these points correspond to power flow solutions under different loading conditions, they can still have violations, therefore are not feasible solutions to the OPF problem, as also shown in Table 3-1.

A3.2 Basecase Optimization under Different Loading Conditions

The first simulation is to use SuperOPF to perform system power loss and production cost minimization on the basecase system under different loading conditions.

Table A0-5: Basecase loss minimization under different loading conditions

Case	Load (MW)	PLoss0 (MW)	PLoss1 (MW)	Reduction	Iters	Time
1	76323.36	2672.63 (3.502%)	1420.40 (1.861%)	46.85%	77	7.95
2	76489.11	2684.16 (3.509%)	1423.96 (1.862%)	46.95%	149	15.47
3	77024.66	2726.84 (3.540%)	1438.40 (1.867%)	47.25%	96	10.07

4	77541.53	2784.84 (3.591%)	1456.76 (1.879%)	47.69%	82	8.51
5	78044.94	2859.73 (3.664%)	1479.10 (1.895%)	48.28%	45	4.67
6	78532.81	2957.29 (3.766%)	1526.84 (1.944%)	48.37%	84	8.69
7	78972.60	3091.82 (3.915%)	No OPF solution (problem infeasible)			
8	79052.42	3137.98 (3.969%)	No OPF solution (problem infeasible)			

The results on system power loss minimization are summarized in Table A3-2 and Figure A3-2. In the results,

- PLoss0: the CPFLOW solution losses and
- PLoss1: the OPF solution losses.

Following observations can be drawn from the results:

- The two largest loading conditions result infeasible OPF problems. We can have a visual inspection from Figure A3-1, which also provides some clue about this, since for these two largest loading conditions, in order to meet the demands, the selected bus voltage magnitudes have to drop below their lower bounds (0.95 p.u. for bus 22891, 0.9 p.u. for buses 22468 and 22473).
- The infeasibility of the two largest loading conditions is formally validated with our feasibility analysis engine. This engine transforms the task of finding feasible points to the OPF problem into the task of computing stable equilibrium points (SEPs) and stable equilibrium manifolds (SEM) in a tailored dynamical system. The findings is summarized in Table A3-3, which reveals that, for both loading conditions, there is no SEMs found that correspond to feasible regions, while only one null space SEP be found with non-zero energy value. The null space SEP is in fact the point in the search domain that is closest to be feasible.
- The SuperOPF solver can robustly compute the OPF solutions under all feasible loading conditions.
- SuperOPF can effectively reduce almost half system losses under all loading conditions, and the reduction rate tends to increase as system loads increase.
- The OPF system losses (percentage with respect to the system load) increase as system loads increase, but with lower rates than that of CPFLOW solutions. Both rates are higher than the increasing rate of the system total loads. In a word, such changes are nonlinear.

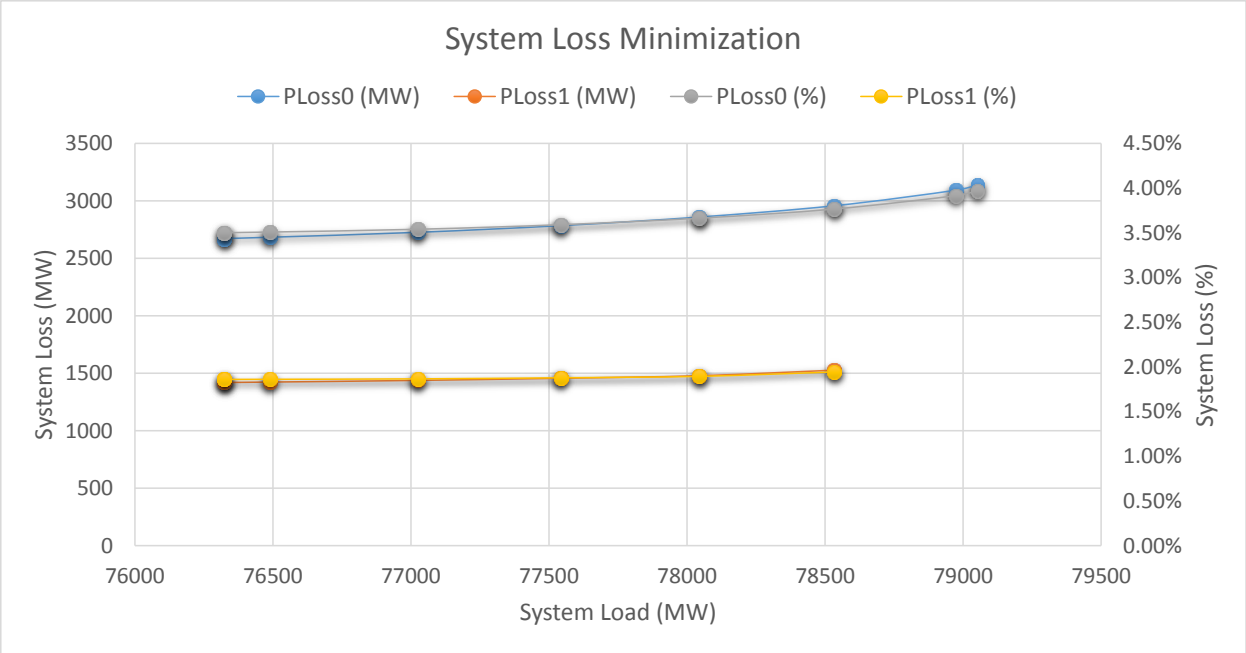

Figure A0-4: Basecase loss minimization under different loading conditions

Table A0-6: Infeasibility validation for the two largest loading conditions

Case	SEM	SEP	SEP Energy	Violations for SEP
7	None	1	2.92×10^{-4}	Six voltages with violations greater 0.001 p.u. ., which the largest being 0.0114 p.u.
8	None	1	3.91×10^{-4}	Seven voltages with violations greater 0.001 p.u., which the largest being 0.0124 p.u.

The results on system production cost minimization are summarized in Table A3-4, Table A3-5 and Figure A3-3. In the results,

- PCost0: the CPFLOW solution costs and
- PCost1: the OPF solution costs.

Following observations can be drawn from the results:

- Table A3-4 summarizes the convergence of the computation under different loading conditions. It can be seen that conventional IPM cannot converges for all loading conditions; more specifically, it failed to converge for four among six feasible cases. In contrast, for these non-convergent cases, our SuperOPF solution method can still successfully converge to the desired OPF solutions.
- Therefore, SuperOPF solver can still robustly compute the OPF solutions under all feasible loading conditions.
- As shown in Table A3-5, SuperOPF can effectively reduce more than 12% system production costs under all loading conditions. Although this is achieved on the synthetic

cost data, it is still reasonable to expect the significant economic impact brought by SuperOPF for real-life production cost data.

- As also shown in Table A3-5, the rate of OPF system production cost reduction (the costs of OPF solution with respect to that of the initial power flow solutions) tends to decrease as system loading condition becomes heavier.
- As shown in Figure A3-3, the change of the production costs is almost linear with respect to the change of system loads. This is because that the majority of the generators is assigned a linear cost, while only about 10% of the generators is assigned a piece-wise linear cost.

Table A0-7: Convergence for basecase cost minimization

Case	Load (MW)	IPM	SuperOPF
1	76323.36	Failed	Converged
2	76489.11	Converged	Converged
3	77024.66	Failed	Converged
4	77541.53	Failed	Converged
5	78044.94	Converged	Converged
6	78532.81	Failed	Converged
7	78972.60	No OPF solution (problem infeasible)	
8	79052.42	No OPF solution (problem infeasible)	

Table A0-8: Basecase cost minimization under different loading conditions

Case	Load (MW)	PCost0 ($/Hr)	PCost1 ($/Hr)	Reduction	Iters	Time
1	76323.36	8695662.83	7582236.18	12.80%	59	8.58
2	76489.11	8715101.45	7598383.37	12.81%	45	7.20
3	77024.66	8778607.18	7668672.15	12.64%	67	9.55
4	77541.53	8841738.16	7719517.58	12.69%	43	7.00
5	78044.94	8905250.95	7777127.93	12.67%	42	7.49
6	78532.81	8969524.78	7836365.40	12.63%	76	10.55

7	78972.60	9032534.30	No OPF solution (problem infeasible)
8	79052.42	9046363.55	No OPF solution (problem infeasible)

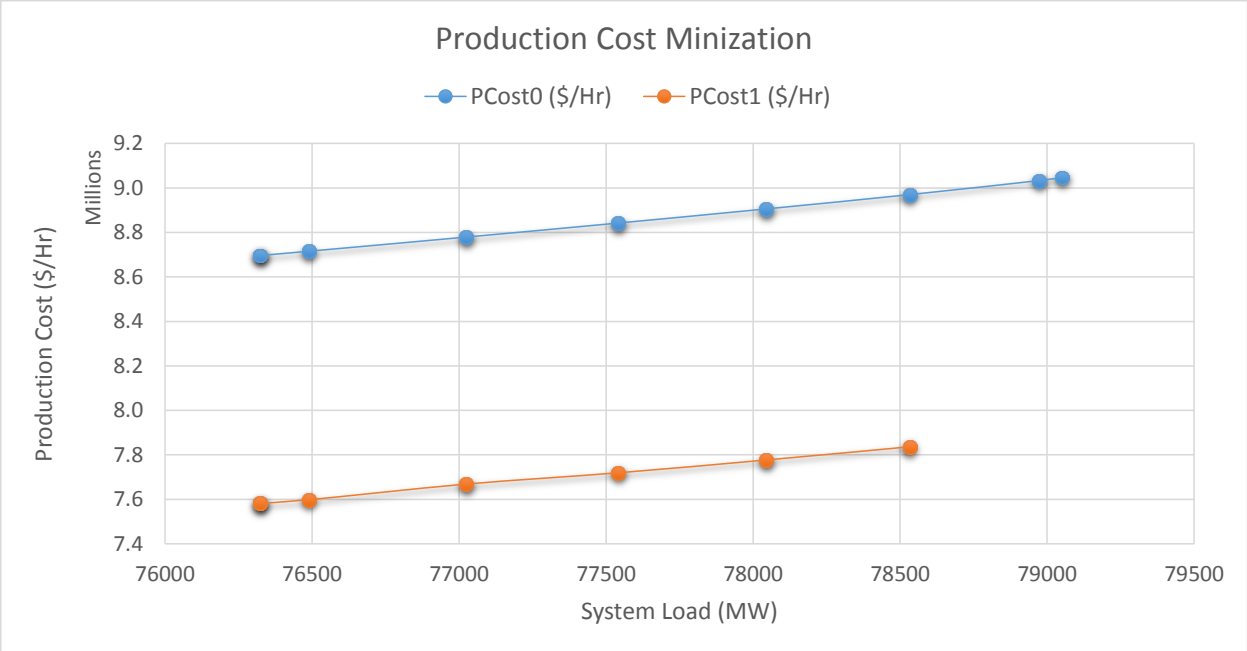

Figure A0-5: Basecase cost minimization under different loading conditions

A3.3 Worst Contingencies and Post-Contingency Optimization

In this simulation, "N-1" transmission line contingencies are first generated by BSI VSA program, then BSI VSA is used to estimate load margins for the post-contingency systems. Contingencies are ranked in terms of their margins and worst contingencies are identified as those ones with least load margins. There are two "N-1" transmission line contingencies identified by BSI VSA, which have zero load margins; in other words, these contingencies are insecure in that the system cannot support the system load demands should any of these contingences happen. The details of these two worst contingencies are summarized in Table A3-6.

Table A0-9: Worst "N-1" contingencies

Ctg ID	Details	Load Margin
0	Basecase	2738.8MW

558	DISCONNECT BRANCH FROM BUS 11217 TO BUS 11093 CKT 1 /* AFTON-LUNA 345.0 KV Line	0MW
2909	DISCONNECT BRANCH FROM BUS 34774 TO BUS 34776 CKT 1 /* MIDWAY-TAFT 115.0 KV Line	0MW

Table A0-10: Convergence for post-contingency optimization

Case	Load (MW)	IPM				SuperOPF
		Loss Minimization		Cost Minimization		
		Ctg_558	Ctg_2909	Ctg_558	Ctg_2909	
1	76323.36	Converged	Converged	Converged	Converged	Converged
2	76489.11	Converged	Failed	Converged	Converged	Converged
3	77024.66	Converged	Converged	Failed	Failed	Converged
4	77541.53	Converged	Converged	Converged	Converged	Converged
5	78044.94	Converged	Converged	Converged	Failed	Converged
6	78532.81	Failed	Failed	Failed	Converged	Converged

Table A3-7 summarizes the convergence of OPF computation for the post-contingency systems under different loading conditions. It can be seen that conventional IPM cannot converge for all post-contingency loading conditions; more specifically, it failed to converge for seven among 24 cases. In contrast, our SuperOPF solver is able to successfully converge to the desired OPF solutions for both worst contingencies under all loading conditions.

The results on post-contingency power loss minimization are summarized in Table A3-8 and Figure A3-4. In the results,

- PLoss1: the basecase OPF solution losses,
- PLoss2: the post-contingency-558 OPF solution losses, and
- PLoss3: the post-contingency-2909 OPF solution losses.

Following observations can be drawn from the results:

- SuperOPF can robustly compute the OPF solutions under all feasible loading conditions, even though the post-contingency systems are insecure. This is due to more controllable generations available for OPF computation, instead of the single slack generator for power flow computation (though other generations are changed before computation to support the load demand).

- Since only one transmission line is taken out in the "N-1" contingencies, its impact on the resulted post-contingency system losses is not significant. As shown in Table A3-8, the variations of the post-contingency OPF losses across are less than 2% with respect to the basecase OPF losses.
- It can also be observed that, contingencies not necessary always increase the OPF losses. As shown in Table A3-8, compared to the basecase system OPF losses shown in Table A3-2, contingency #558 consistently increases the post-contingency OPF losses under all loading conditions. In contrast, contingency #558 introduces almost not impact on the OPF losses for loading conditions 1 through 5; for the loading condition 6, it can result better loss reduction compared to the basecase OPF. This is related to another interesting research topic of optimal line switching for different purposes, such as system loss reduction and transfer capability improvement.

Table A0-11: Post-contingency loss minimization under different loading conditions

Case	Load (MW)	Ctg_558			Ctg_2909		
		PLoss2 (MW)	Iters	Time (s)	PLoss3 (MW)	Iters	Time (s)
1	76323.36	1446.84 (1.896%)	168	17.57	1420.50 (1.861%)	80	8.40
2	76489.11	1450.42 (1.896%)	160	17.12	1423.95 (1.862%)	83	12.86
3	77024.66	1465.40 (1.903%)	176	18.26	1438.36 (1.867%)	138	14.55
4	77541.53	1482.84 (1.912%)	81	8.34	1456.80 (1.879%)	107	11.56
5	78044.94	1505.67 (1.929%)	169	17.45	1479.10 (1.895%)	84	8.75
6	78532.81	1546.86 (1.970%)	101	14.33	1521.26 (1.937%)	50	9.34

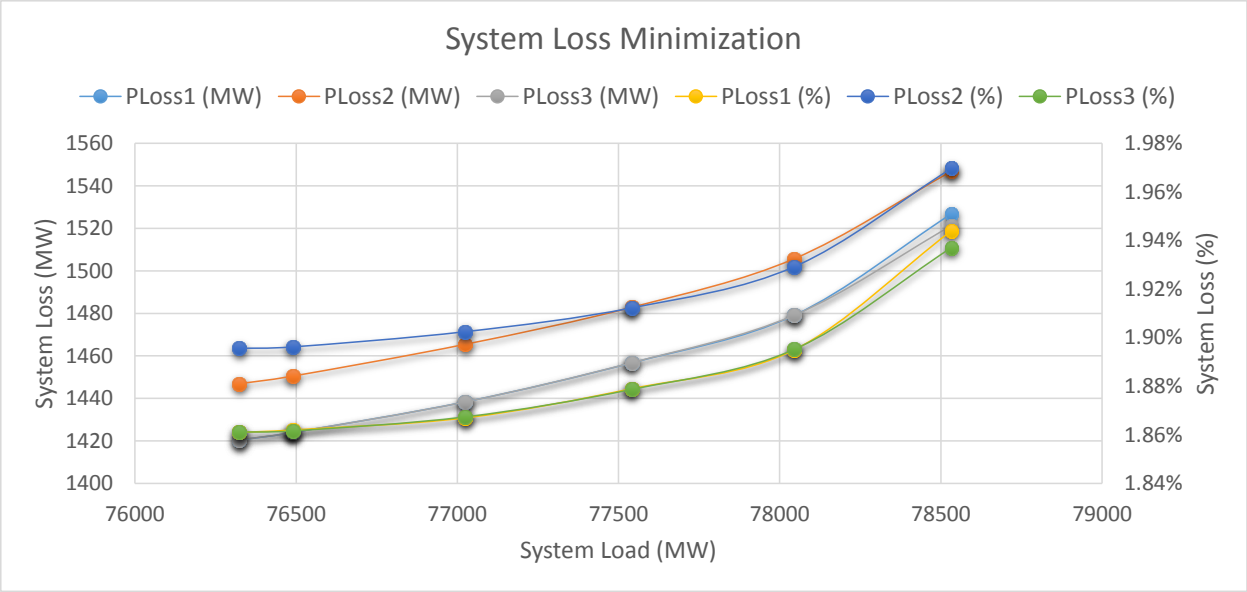

Figure A0-6: Post-contingency loss minimization under different loading conditions

The results on post-contingency production cost minimization are summarized in Table A3-9 and Figure A3-5. In the results,

- PCost1: the basecase OPF solution costs,
- PCost2: the post-contingency-558 OPF solution costs, and
- PCost3: the post-contingency-2909 OPF solution costs.

Similar observations can be drawn from the cost minimization results as from the above loss minimization results.

Table A0-12: Post-contingency cost minimization under different loading conditions

Case	Load (MW)	Ctg_558			Ctg_2909		
		PCost2 ($/Hr)	Iters	Time (s)	PCost3 ($/Hr)	Iters	Time (s)
1	76323.36	7582858.57	55	5.79	7582601.81	44	4.61
2	76489.11	7602631.16	66	6.95	7599915.84	42	4.40
3	77024.66	7662677.88	53	8.15	7659999.27	57	13.44
4	77541.53	7721382.9	40	4.25	7719793.49	55	5.92
5	78044.94	7777963.71	65	6.97	7775321.97	91	15.62
6	78532.81	7839068.25	55	8.36	7838036.41	78	8.40

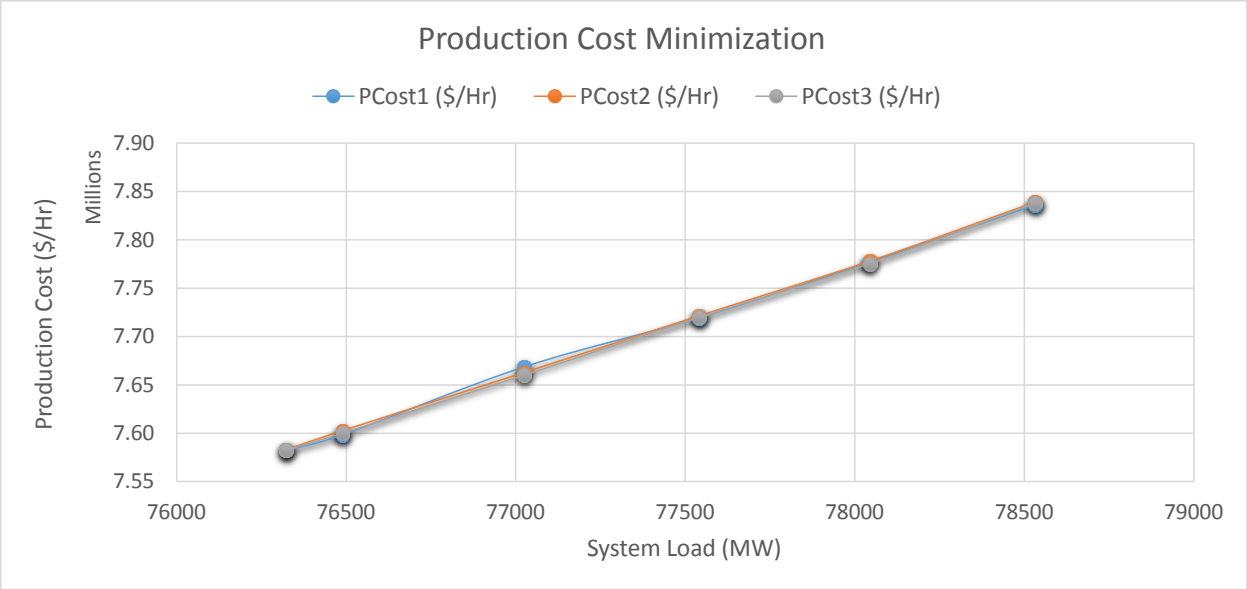

Figure A0-7: Post-contingency cost minimization under different loading conditions

A3.4 Base-case + Individual Contingency Co-optimization

In this simulation, SuperOPF is used to co-optimize the base case system and individual worst contingency.

Table A0-13: Convergence for "basecase + single-contingency" co-optimization

Case	Load (MW)	IPM				SuperOPF
		Loss Minimization		Cost Minimization		
		Ctg_558	Ctg_2909	Ctg_558	Ctg_2909	
1	76323.36	Converged	Failed	Failed	Failed	Converged
2	76489.11	Converged	Failed	Failed	Failed	Converged
3	77024.66	Converged	Failed	Converged	Failed	Converged
4	77541.53	Converged	Failed	Failed	Failed	Converged
5	78044.94	Converged	Converged	Converged	Converged	Converged
6	78532.81	Failed	Converged	Failed	Failed	Converged

Table A3-10 summarizes the convergence for the "basecase + single-contingency" co-optimization under different loading conditions. It can be seen that conventional IPM cannot converge for co-optimization under all loading conditions; more specifically, it failed to con-

verge for 14 among 24 cases. In contrast, our SuperOPF solution method has successfully converged to the desired OPF solutions for all contingencies under all loading conditions.

Table A0-14: "Basecase + single-contingency" co-optimization for loss minimization

Case	Load (MW)	Basecase + Ctg_558			Basecase + Ctg_2909		
		PLoss2 (MW)	Iters	Time (s)	PLoss3 (MW)	Iters	Time (s)
1	76323.36	1435.87 (1.881%)	63	14.86	1435.57 (1.881%)	123	37.63
2	76489.11	1439.39 (1.882%)	146	34.89	1438.14 (1.880%)	189	53.72
3	77024.66	1454.05 (1.888%)	225	52.94	1454.58 (1.888%)	145	44.62
4	77541.53	1472.60 (1.900%)	228	55.06	1472.51 (1.899%)	61	24.22
5	78044.94	1494.63 (1.915%)	123	28.71	1494.91 (1.915%)	111	22.32
6	78532.81	1540.30 (1.961%)	227	64.66	1537.25 (1.957%)	92	21.69

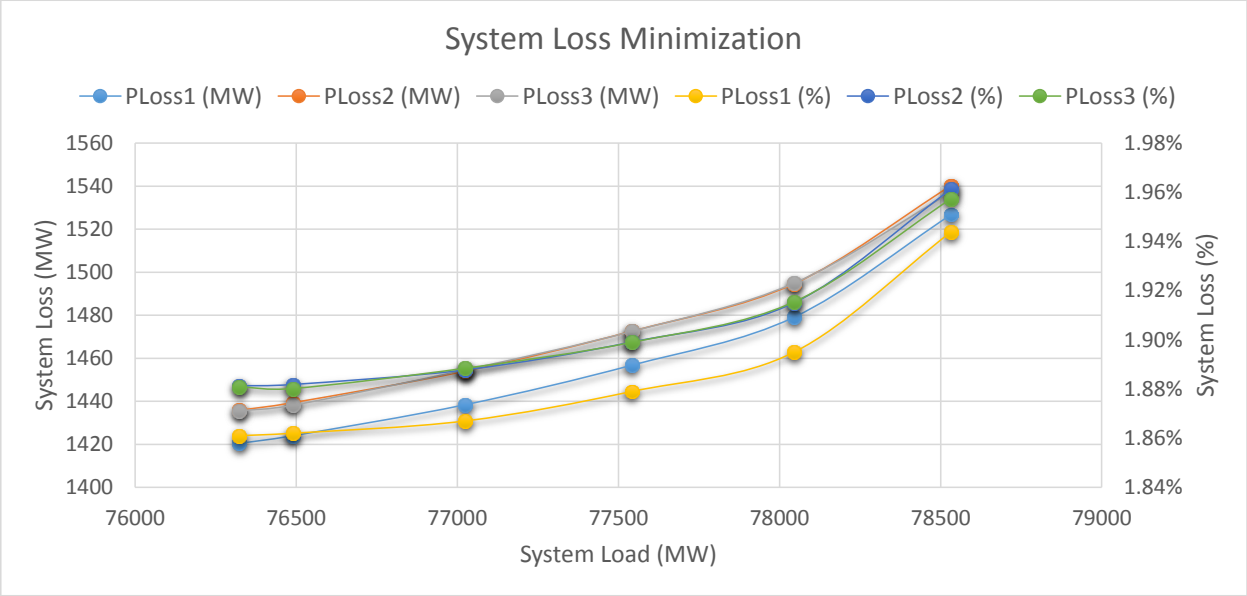

Figure A0-8: "Basecase + single-contingency" co-optimization for loss minimization

The results of co-optimization for power loss minimization are summarized in Table A3-11 and Figure A3-6. In the results,

- PLoss1: the basecase OPF solution losses,

- PLoss2: the "basecase + contingency-558" co-optimized OPF solution losses, and
- PLoss3: the "basecase + contingency-2909" co-optimized OPF solution losses.

Following observations can be drawn from the results:

- SuperOPF can robustly co-optimize the basecase system with worst contingency constraints under all feasible loading conditions, even though the contingencies are insecure.
- Since only one transmission line is taken out in the "N-1" contingencies, its impact on the resulted co-optimized system losses is also not significant. As shown in Table A3-11, the variations of the co-optimized OPF losses across are about 1% with respect to the basecase OPF losses.
- The differences between different co-optimized system losses are less than that between post-contingency minimized system losses.
- Considering the optimization problem size (the number of optimization variables and the number of constraints) is roughly doubled for the co-optimization problem as compared to the basecase OPF problem, the computational time is also roughly doubled (per iteration).
- Due to the increased problem complexity, the computation tends to require more iterations to converge to the co-optimized OPF solutions.

Table A0-15: "Basecase + single-contingency" co-optimization for cost minimization

Case	Load (MW)	Basecase + Ctg_558			Basecase + Ctg_2909		
		PCost2 ($/Hr)	Iters	Time (s)	PCost3 ($/Hr)	Iters	Time (s)
1	76323.36	7714212.64	63	31.45	7714114.04	82	36.20
2	76489.11	7732790.70	61	20.70	7732559.20	105	42.17
3	77024.66	7798172.14	149	35.47	7793811.69	62	31.38
4	77541.53	7851769.17	51	29.49	7851824.31	71	33.91
5	78044.94	7910018.53	142	34.21	7910470.52	81	19.36
6	78532.81	7970888.42	264	81.39	7969248.91	181	60.20

The results on post-contingency production cost minimization are summarized in Table A3-12 and Figure A3-7. In the results,

- PCost1: the basecase OPF solution costs,
- PCost2: the "basecase + contingency-558" co-optimized OPF solution costs, and
- PCost3: the "basecase + contingency-2909" co-optimized OPF solution costs.

Similar observations can be drawn from the co-optimized cost minimization results as from the above co-optimized loss minimization results.

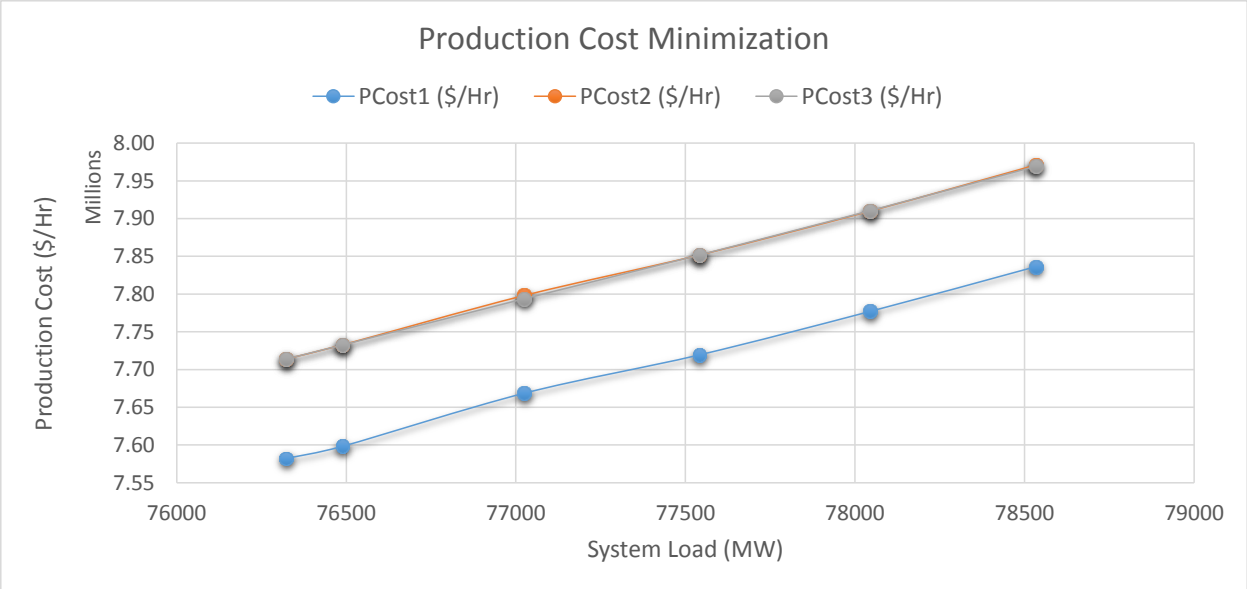

Figure A0-9: "Basecase + single-contingency" co-optimization for cost minimization

A3.5 Base-case + All Contingency Co-optimization

In this simulation, SuperOPF is used to co-optimize the base case system and both worst contingencies.

Table A3-13 summarizes the convergence for the "basecase + all-contingency" co-optimization under different loading conditions. Similarly, it can be seen that conventional IPM cannot converge for co-optimization under all loading conditions; more specifically, it failed to converge for eight among 12 cases. In contrast, our SuperOPF solution method is able to converge to the desired solutions for all loading conditions, for both loss minimization and cost minimization.

Table A0-16: Convergence for "basecase + all-contingency" co-optimization

Case	Load (MW)	IPM		SuperOPF
		Loss Minimization	Cost Minimization	
1	76323.36	Failed	Failed	Converged
2	76489.11	Converged	Failed	Converged
3	77024.66	Failed	Failed	Converged
4	77541.53	Failed	Failed	Converged
5	78044.94	Converged	Converged	Converged

6	78532.81	Converged	Failed	Converged

The results of co-optimization for power loss minimization are summarized in Table A3-14. In the results,

- PLoss1 corresponds to the basecase OPF solution losses,
- PLoss2 for the "basecase + contingency-558" co-optimized OPF solution losses, and
- PLoss3 for the "basecase + contingency-2909" co-optimized OPF solution losses.

Following observations can be drawn from the results:

- SuperOPF can still robustly co-optimize the basecase system with worst contingency constraints under all feasible loading conditions, even though the contingencies are insecure.
- Since only one transmission line is taken out in the "N-1" contingencies, its impact on the resulted co-optimized system losses is also not significant. As shown in Table A3-14, the variations of the co-optimized OPF losses across are about 1% with respect to the basecase OPF losses.
- The differences between different co-optimized system losses are less than that between post-contingency minimized system losses.
- Considering the optimization problem size (the number of optimization variables and the number of constraints) is roughly doubled for the co-optimization problem as compared to the basecase OPF problem, the computational time is also roughly doubled (per iteration).
- Due to the increased problem complexity, the computation tends to require more iterations to converge to the co-optimized OPF solutions.

Table A0-17: "Basecase + all-contingency" co-optimization

Case	Load (MW)	Loss Minimization			Cost Minimization		
		PLoss6 ($/Hr)	Iters	Time (s)	PCost6 ($/Hr)	Iters	Time (s)
1	76323.36	1449.96	215	134.73	7714284.52	84	60.41
2	76489.11	1453.26	173	70.16	7732869.31	89	43.80
3	77024.66	1468.05	133	64.52	7793250.29	87	79.41
4	77541.53	1486.65	118	72.98	7851992.34	186	134.71
5	78044.94	1515.52	237	123.66	7910274.56	77	26.90
6	78532.81	1553.22	69	33.69	7970107.54	303	169.59

Finally, for a better comparison, the results are condensed in two Figures. More specifically, a condensed summary is provide in Figure A3-8 for the results on loss minimization for all involved simulations, where

- PLoss1: the basecase OPF solution losses,
- PLoss2: the post-contingency-558 OPF solution losses,
- PLoss3: the post-contingency-2909 OPF solution losses,
- PLoss4: the "basecase + contingency-558" co-optimized OPF solution losses,
- PLoss5: the "basecase + contingency-2909" co-optimized OPF solution losses, and
- PLoss6: the "basecase + all-contingency" co-optimized OPF solution losses.

Similarly, a condensed summary is provide in Figure 3-9 for the results on cost minimization for all involved simulations, where

- PCost1: the basecase OPF solution costs,
- PCost2: the post-contingency-558 OPF solution costs,
- PCost3: the post-contingency-2909 OPF solution costs,
- PCost4: the "basecase + contingency-558" co-optimized OPF solution costs,
- PCost5: the "basecase + contingency-2909" co-optimized OPF solution costs, and
- PCost6: the "basecase + all-contingency" co-optimized OPF solution costs.

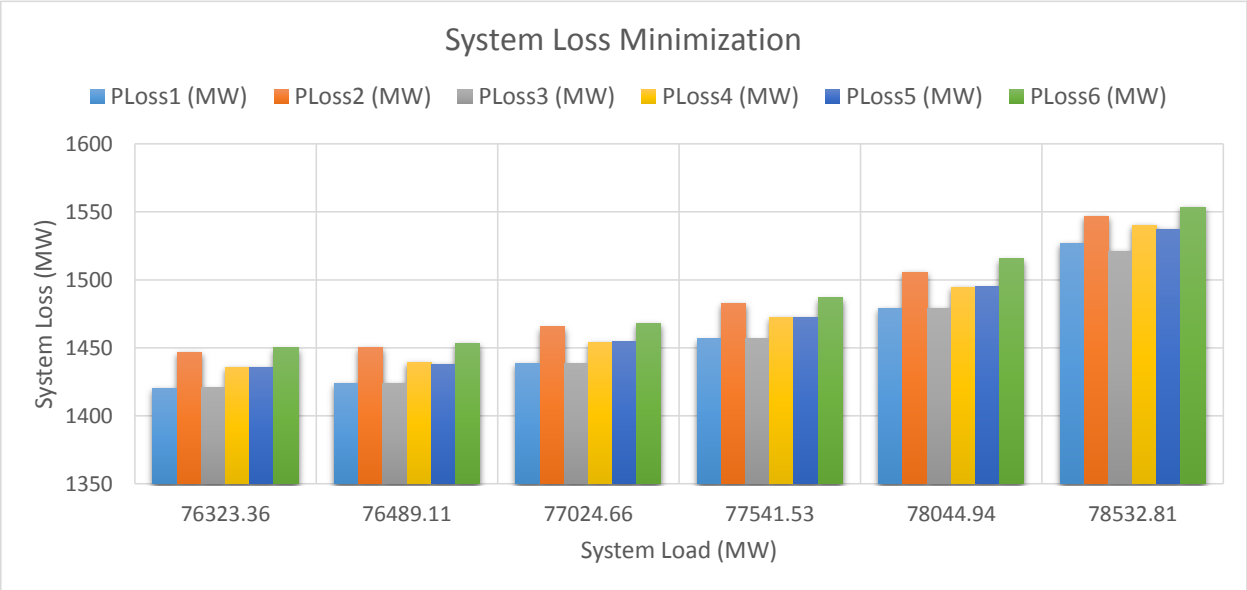

Figure A0-10: Summarized loss minimization results

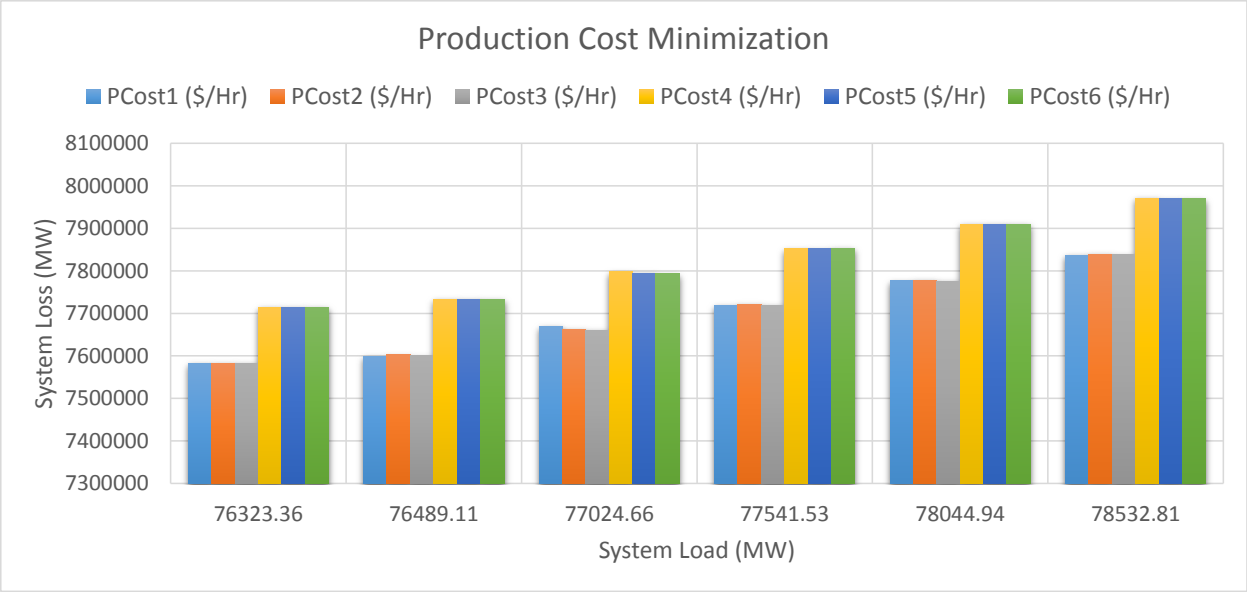

Figure A0-11: Summarized cost minimization results

A4. Summary

In this report, a new dataset for SuperOPF computation is created. Based on this dataset, following simulations have been carried out:

- SuperOPF computation on the basecase and post-contingency systems, and
- SuperOPF co-optimization for "basecase + single contingency" and "basecase + all contingency".

All simulations have been carried out for two OPF objectives, namely, system real power loss minimization and production cost minimization, and under different loading conditions.

The simulation results have shown that SuperOPF can robustly compute the OPF solutions for all the involved scenarios and under all feasible loading conditions, even though the post-contingency systems are insecure. Along with its comprehensive modeling capability, it is promising that SuperOPF can be a viable analysis tool for power industry.

References

[1] B. Borchers and J. E. Mitchell. "An improved branch and bound algorithm for mixed integer nonlinear programming", Comput. Oper. Res., 21(4):359–367, 1994.

[2] O. K. Gupta and A. Ravindran. "Branch and bound experiments in convex nonlinear integer programming", Manage. Sci., 31(12):1533–1546, 1985.

[3] A. M. Geoffrion. "Generalized benders decomposition", J. Optimiz. Theory App., 10(4):237–260, 1972.

[4] M. A. Duran and I. E. Grossmann. "An outer approximation algorithm for a class of mixed-integer nonlinear programs", Math. Program., 36(3):307–339, 1986.

[5] T. Westerlund, H. Skrifvars, I. Harjunkoski, and R. Porn. "An extended cutting plane method for a class of non-convex MINLP problems", Comput. Chem. Eng., 22(3):357–365, 1998.

[6] I. E. Grossmann and Z. Kravanja. "Mixed-integer nonlinear programming: a survey of algorithms and applications". In L. T. Biegler, T. F. Coleman, et al., editors, Large-Scale Optimization with Applications: Part II: Optimal Design and Control, pages 73–100. Springer Verlag, 1997.

[7] F. Capitanescu and L. Wehenkel. "Sensitivity-based approaches for han-dling discrete variables in optimal power flow computations", IEEE Trans. Power Syst., 25(4):1780–1789, 2010.

[8] W. T. Carson, Power System Voltage Stability, McGraw-Hill, Inc., New York, U.S.A. 1994.

[9] T. Van Cutsem, and C. D. Vournas, Voltage Stability of Electric Power Systems, Kluwer Academic Publishers, Boston, MA, U.S.A., 1998.

[10] Voltage Stability and Long-Term Stability Working Group (prepared by V. Ajjarapu and B. Lee), "Bibliography on Voltage Stability", IEEE Transactions on Power Systems, Vol. 13, No. 1, pp. 115-125, February 1998.

[11] I. Dobson and H. D. Chiang "Towards a Theory of Voltage Collapse in Electric Power Systems", *System and Control Letter*, Vol. 13, pp.253-262, 1989.

[12] V.A. Ajjarapu and B. Lee, "Bifurcation theory and its application to nonlinear dynamical phenomena in an electric power system", *IEEE Trans. on Power Systems,* Vol.7, No.1, pp.424-431,1992.

[13] H. D. Chiang, T. P. Conneen, and A. J. Flueck, "Bifurcations and Chaos in electric power systems: Numerical studies (Invited paper)", Journal of Franklin Institute 331B:1001-1036, 1995.

[14] H. D. Chiang, "Application of Bifurcation Analysis to Power Systems", Bifurcation Control, LNCIS 293, Springer-Verlag, G. Chen, D. J. Hill and X. Yu, (Eds.), pp. 1- 28, 2003.

[15] I. Dobson and L. Liu "Voltage Collapse Precipitated by the Immediate Change in Stability When Generator Reactive Power Limits Are Encountered" *IEEE Trans. Circuits Syst. I, Fundam. Theory Appl.*, Vol.39, No.9, pp. 762-766, 1992.

[16] C. A. Canizares, N. Mithiulananthan, A. Berizzi etc. "On the Linear Profile for the Prediction of Saddle Node and Limit-Induced Bifurcation Points in Power Systems," *IEEE Trans. on Circuits and Systems-I: Fundamental theory and applications*, Vol.50, No.12 , pp. 1588-1595, 2003.

[17] S. H. Li and H. D. Chiang, "Structure-induced Bifurcation in Large-Scale Electric Power Systems", *International Journal of Bifurcation and Chaos*, Vol.18, No.5, pp.1415-1424, 2008.

[18] C.W. Tang, M. Varghese, P. Varaiya,, and F.F. Wu, "Bifurcation, Chaos, and Voltage Collapse in Power Systems," *Proceedings of the IEEE*, Vol. 83, pp. 1484-1496, 1995.

[19] H. G. Kwatny, R. F. Fishl and C. O. Nwankpa, "Local bifurcation in power systems: Theory, computation, and application,". *Proceedings of the IEEE*, Vol. 83, pp. 1456-1483, 1995.

[20] H. D. Chiang, A. J. Flueck, K. S. Shah, and N. Bale, "CPFLOW: A practical tool for tracing power system steady state stationary behavior due to load and generation variations," *IEEE Trans. Power Syst.*, vol. 10, no. 2, pp. 623–634, May 1995.

[21] H. D. Chiang, C. S. Wand and A. J. Flueck, "Look-ahead Voltage and Load Margin Contingency Selection Functions for Large-Scale Power Systems", IEEE Trans. on Power Systems, Vol. 12, No. 1, Feb. 1997, pp. 173-179.

[22] J. Q. Zhao, H. D. Chiang, and H. Li, "Enhanced Look-Ahead Load Margin Estimation for Voltage Collapse Assessment", International Journal of Electrical Power and Energy Systems, Vol. 26, , pp. 431-438, 2004.

[23] J. Tong, "Real-time Transfer Limit Calculations", IEEE PES Winter Power meeting, 0-7803-6423-6, 2000

[24] H. Li, H. D. Chiang, and J. Tong, "An On-Line Tool for Voltage Stability Assessment and Control of Large-Scale Power Systems", Bulk Power Systems Dynamics and Control, August 2004, Cortina, Italy.

[25] H. D. Chiang, L. Jing, M. Varghese, S. Ghosh and H. Li, "Linear and Nonlinear Methods for Contingency Analysis in on-Line Voltage Security Assessment", IEEE PES Winter Power meeting, 978-1-4244-4241-6,, 2009.

[26] S. Greene, I. Dobson, and F. L. Alvarado, "Sensitivity of the loading margin to voltage collapse with respect to arbitrary parameters," IEEE Trans. on Power Systems, Vol. 12, No. 1, Feb. 1997, pp. 262-272.

[27] S. Greene, I. Dobson and F.L. Alvarado, "Contingency analysis for voltage collapse via

sensitivities from a single nose curve,'' IEEE Trans. on Power Systems. Vol. 14, No. 1, Feb. 1999, pp.232-240.

[28] H.D. Chiang and R. Jean-Jumeau, "Toward a practical performance index for predicting voltage collapse in electric power system". IEEE Trans. Power Systems. 10 1995, pp.584-592

[29] G. C. Ejebe, G. D. Irisarri, S. Mokhtari, O. Obadina, P. Ristanovic, and J. Tong, "Methods for contingency screening and ranking for voltage stability analysis of power systems", IEEE Trans. on Power Systems, Vol. 11, No. 1, Feb. 1996, pp. 350-356.

[30] A. J. Flueck, R. Gonella and J. R. Dondeti, "A New Power Sensitivity Method of Ranking Branch Outage Contingencies for Voltage Collapse", IEEE Trans. On Power Systems, Vol. 17, No. 2, May 2002.

[31] H. D. Chiang. Power system stability. In: Webster J.G. (Ed.) Wiley Encyclopedia of Electrical and Electronics Engineering. John Wiley & Sons, New York, 1999, pp. 104-137.

[32] E. Vaahedi, C. Fuchs, W. Xu, Y. Mansour, H. Hamadanizadeh, and G. K. Morison, "Voltage Stability Contingency Screening and Ranking", IEEE Trans. on Power Systems, vol. 14, No. 1, pp. 256-265, Feb. 1999.

[33] Z. Jia and B. Jeyasurya, "Contingency Ranking for On-line Voltage Stability Assessment", IEEE Trans. on Power Systems, Vol. 15, No. 3, pp. 1093-1097, Aug. 2000.

[34] J. A. Momoh, R. J. Koessler, M. S. Bond, B. Stott, D. Sun, A. Papalex-opoulos, and P. Ristanovic, "Challenges to optimal power flow", IEEE Trans. Power Syst., vol. 12, no. 1, pp. 444–455, Feb. 1997.

[35] B. Stott, O. Alsac, and A. J. Monticelli, "Security analysis and optimization", Proc. IEEE, vol. 75, no. 12, pp. 1623–1644, Dec. 1987.

[36] P. R. Gribik, D. Shirmohammadi, S. Hao, and C. L. Thomas, "Optimal power flow sensitivity analysis", IEEE Trans. Power Syst., vol. 5, no. 3, pp. 969–978, Aug. 1990.

[37] L. Liu, X. Wang, X. Ding, and H. Chen, "A robust approach to optimal power flow with discrete variables", IEEE Trans. Power Syst., vol. 24, no. 3, pp. 1182–1190, Aug. 2009.

[38] S. Y. Lin, Y. C. Ho, and C. H. Lin, "An ordinal optimization theory-based algorithm for solving optimal power flow problem with discrete control variables", IEEE Trans. Power Syst., vol. 19, no. 1, pp. 276–286, Feb. 2004.

[39] M. Liu, S. K. Tso, and Y. Cheng, "An extended nonlinear primal-dual interior-point algorithm for reactive power optimization of large-scale power systems with discrete control variables", IEEE Trans. Power Syst., vol. 17, no. 4, pp. 982–991, Nov. 2002.

[40] E. Liu, A. D. Papalexopoulos, and W. F. Tinney, "Discrete shunt controls in a Newton optimal power flow", IEEE Trans. Power Syst., vol. 7, no. 4, pp. 1509–1518, Nov. 1992.

[41] J.P. Paul, J.T. Leost, and J.M. Tesseron, "Survey of the secondary voltage control in France: present realization and investigations", IEEE Transactions on Power Systems, vol. 2, no.2, pp. 505-511, 1987.

[42] M. D. Ilic. "Secondary voltage control using pilot information", IEEE Transactions on Power Systems, vol.3, no.2, pp.660-668, 1988.

[43] P. Lagonotte, J. C. Sabonnadiere, J.Y. Leost, J.P. Paul. "Structural analysis of the electrical system: application to secondary voltage control in France", IEEE Transactions on Power Systems, vol.4, no.2, pp.479-486, 1989.

[44] S. Corsi, M. Pozzi, C. Sabelli, et al. "The coordinated automatic voltage control of the Italian transmission grid - Part I: reasons of the choice and overview of the consolidated hierarchical system", IEEE Transactions on Power Systems, vol.19, no.4, pp.1723-1732, 2004.

[45] S. Corsi, M. Pozzi, M. Sforna, et al. "The coordinated automatic voltage control of the Italian transmission grid- Part II: control apparatuses and field performance of the consolidated hierarchical system", IEEE Transactions on Power Systems, vol.19, no.4, pp.1733-1741, 2004.

[46] Q. L. Guo, H. B. Sun, B. M. Zhang, and W. C. Wu, "Power network partitioning based on clustering analysis in Mvar control space," Automation of Electric Power Systems, vol.29, no.10, pp.36-40,2005.

[47] Q. L. Guo, H. B. Sun, B. M. Zhang, W. C. Wu, and Qin Li, "Study on coordinated secondary voltage control," Automation of Electric Power Systems, vol.29, no.23, pp.19-24, 2005.

[48] Q. L. Guo, H. B. Sun, B. M. Zhang, W. C. Wu, B. Wang, Z. H. Li, and Lei Tang, "Coordination of continuous variables and discrete variables in automatic voltage control part two coordinated voltage control among power plants and substations," Automation of Electric Power Systems, vol.32, no.9, pp.65-68, 2008.

[49] H. B. Sun, Q. L. Guo, B. M. Zhang, W. C. Wu, and J. Z. Tong, "Development and applications of system-wide automatic voltage control system in China," in Proc. 2009 IEEE Power & Energy Society General Meeting, pp. 1-5.

[50] Q. L. Guo, H. B. Sun, J. Z. Tong, M. Y. Zhang, B. Wang, and B. M. Zhang, "Study of system-wide Automatic Voltage Control on PJM system," in Proc. 2010 IEEE Power & Energy Society General Meeting, pp. 1-6.

[51] D. Denzel, K.W. Edwin, F.R. Graf, et al. "Optimal power flow and its real time application at the RWE energy control centre", in Proc. 1988 CIGRE, paper 39-19,Paris, France.

[52] F. R. Graf, "Real time application of an optimal power flow algorithm for reactive power allocation of the RWE energy control center," in Proc. 1993 IEE Colloquium on International Practices in Reactive Power Control, pp.7/1 - 7/4.

[53] D. Q. Gan, R. J. Thomas, and R. Zimmerman, "Stability-constrained optimal power flow", IEEE Transactions on Power Systems, 15(2):535-540, 2000.

[54] K. M. Kodsi and C. A. Canizares, "Application of a Stability-Constrained Optimal Power Flow to Tuning of Oscillation Controls in Competitive Electricity Markets", IEEE Transactions on Power Systems, 22(4):1944-1954, 2007.

[55] J. Kubokawa, R. Inoue, and H. Sasaki, "A solution of optimal power flow with voltage stability constraints", In Proc. Intl. Conf. Power System Tech. (PowerCon'00), vol. 2, pp:625-630, 2000.

[56] W. D. Rosehart, "Effect of detailed power system models in traditional and voltage-stability-constrained optimal power-flow problems", IEEE Transactions on Power Systems, 18(1):27-35, 2003.

[57] E. Vaahedi, Y. Mansour, et al, "Dynamic security constrained optimal power flow/VAr planning", IEEE Transactions on Power Systems, 16(1):38-43, 2001.

[58] H. C. Song, "Reactive reserve-based contingency constrained optimal power flow (RCCOPF) for enhancement of voltage stability margins", IEEE Transactions on Power Systems, 18(4):1538-1546, 2003.

[59] F. Milano, C. A. Cañizares, A. J. Conejo, "Sensitivity-based security-constrained OPF market clearing model", IEEE Transactions on Power Systems, 20(4):2051-2060, 2005.

[60] W.J. Zhang, F. X. Li, L. M. Tolbert, "Review of Reactive Power Planning: Objectives, Constraints, and Algorithms" IEEE Transactions on Power Systems, 22(4):2177-2186, 2007.

[61] E. Vaahedi, J. P. Tamby, et al, "Large scale voltage stability constrained optimal VAr planning and voltage stability applications using existing OPF/optimal VAr planning tools", IEEE Transactions on Power Systems, 14(1):65-74, 1999.

[62] Y. Yuan, J. Kubokawa, and H. Sasaki, "A solution of optimal power flow with multicontingency transient stability constraints" IEEE Transactions on Power Systems, 18(3):1094-1102, 2003.

[63] R. A. Jabr, N. Martins, B. C. Pal, and S. H. Karaki, "Contingency Constrained VAr Planning Using Penalty Successive Conic Programming", IEEE Transactions on Power Systems, 27(3):545-553, 2012.

[64] B. Cova, N. Losignore, P. Marannino, and M. Montagna, "Contingency constrained optimal reactive power flow procedures for voltage control in planning and operation", IEEE Transactions on Power Systems, 10(2):602-608, 1995.

[65] J. Z. Zhao, B. M. Zhang, and H. D. Chiang, "An Optimal Power Flow Model and Approach with Static Voltage Stability Constraints", In Proc. IEEE/PES'05, pp. 1-6, 2005.

[66] F. Bouhafs, M. Mackay, and M. Merabti, "Links to the future: Communication requirements and challenges in the smart grid", IEEE Power Energy Mag. 10(1): 24–28, 2012.

[67] Department of Energy, "The smart grid: An introduction", URL: http://energy.gov/oe/downloads/smart-grid-introduction.

[68] D. R. Baker, "Brown signs law requiring 33% renewable energy", San Francisco Chronicle, April 12, 2011.

[69] Wikipedia, "Solar power in the United States", URL: http://en.wikipedia.org/wiki/Solar_power_in_the_United_ States.

[70] S. Zhen and P. Jirutitijaroen, "Latin Hypercube Sampling Techniques for Power Systems Reliability Analysis with Renewable Energy Sources", IEEE Trans. Power Syst., 26(4):2066–2073, 2011.

[71] H. Yu, C. Y. Chung, K. P. Wong, H. W. Lee, and J. H. Zhang, "Probabilistic Load Flow Evaluation with Hybrid Latin Hypercube Sampling and Cholesky Decomposition", IEEE Trans. Power Syst., 24(2):661–667, 2009.

[72] M. Aien, M. Fotuh-Firuzabad, and F. Aminifar, "Probabilistic Load Flow in Correlated Uncertain Environment Using Unscented Transformation", IEEE Trans. Power Syst., 27(4):2233–2241, 2012.

[73] B. Borchers and J. E. Mitchell. "An improved branch and bound algorithm for mixed integer nonlinear programming", Comput. Oper. Res., 21(4):359–367, 1994.

[74] O. K. Gupta and A. Ravindran. "Branch and bound experiments in convex nonlinear integer programming", Manage. Sci., 31(12):1533–1546, 1985.

[75] A. M. Geoffrion. "Generalized benders decomposition", J. Optimiz. Theory App., 10(4):237–260, 1972.

[76] M. A. Duran and I. E. Grossmann. "An outer approximation algorithm for a class of mixed-integer nonlinear programs", Math. Program., 36(3):307–339, 1986.

[77] T. Westerlund, H. Skrifvars, I. Harjunkoski, and R. Porn. "An extended cutting plane method for a class of non-convex MINLP problems", Comput. Chem. Eng., 22(3):357–365, 1998.

[78] I. E. Grossmann and Z. Kravanja. "Mixed-integer nonlinear programming: a survey of algorithms and applications". In L. T. Biegler, T. F. Coleman, et al., editors, Large-Scale Optimization with Applications: Part II: Optimal Design and Control, pages 73–100. Springer Verlag, 1997.

[79] F. Capitanescu and L. Wehenkel. "Sensitivity-based approaches for handling discrete variables in optimal power flow computations", IEEE Trans. Power Syst., 25(4):1780–1789, 2010.

[80] J. Chen, T. Mount, J. Thorp, and R. Thomas, "Location-based scheduling and pricing for energy and reserve: a responsive reserve market proposal," Decision Support Systems, vol. 40, no. 3, pp. 563–577, October 2005.

[81] C. Murillo-S´anchez, R. Zimmerman, C. Anderson, and R. Thomas, "A stochastic, contingency-based securit-constrained optimal power flow for the procurement of energy and distributed reserve," Decision Support Systems (under review).

[82] J. Condren, T. Gedra, and P. Damrongkulkamjorn, "Optimal power flow with expected security costs," IEEE Trans. Power Syst., vol. 21, no. 2, pp. 541–547, May 2006.

[83] F. Bouffard and F. Galiana, "Stochastic security for operations planning with significant wind power generation," IEEE Trans. Power Syst., vol. 23, no. 2, pp. 306–316, May 2008.

[84] P. Meibom, R. Barth, B. Hasche, H. Brand, C. Weber, and M. O'Malley, "Stochastic optimization model to study the operational impacts of high wind penetrations in ireland," IEEE Trans. Power Syst., vol. 26, no. 3, pp. 1367–1379, August 2011.

[85] E. Denny and M. O'Malley, "Wind generation, power system operation, and emissions reduction," IEEE Trans. Power Syst., vol. 21, no. 1, pp. 341–347, February 2006.

[86] A. Papavasiliou, S. Oren, and R. O'Neill, "Reserve requirements for wind power integration: A scenario-based stochastic programming framework," IEEE Trans. Power Syst., vol. 26, no. 4, pp. 2197–2206,November 2011.

[87] H. Oh, "Optimal planning to include storage devices in power systems," IEEE Trans. Power Syst., vol. 26, no. 3, p. 1118, August 2011.

[88] M. Lange, "On the uncertainty of wind power predictions–analysis of the forecast accuracy and statistical distribution of errors," Journal of Solar Energy Engineering, vol. 127, no. 2, p. 177, 2005.

[89] B. Hodge and M. Milligan, "Wind power forecasting error distributions over multiple timescales," in Power and Energy Society General Meeting, IEEE, Ed. IEEE, 2011.

[90] California ISO, "Locational marginal pricing (LMP): basics of nodal price calculation", CRR Educational Class #2, December 6-8, 2005.

[91] California ISO, "Market optimization details", Technical Bulletin 2009-06-05, June 16,2009.